COPPE
Instituto Alberto Luiz Coimbra de Pós-Graduação e Pesquisa de Engenharia
UFRJ

HIGH PERFORMANCE VOLTAGE CONTROL FOR THREE-PHASE UPS INVERTER

Jorge Eliécer Caicedo Castaño

Dissertação de Mestrado apresentada ao Programa de Pós-graduação em Engenharia Elétrica, COPPE, da Universidade Federal do Rio de Janeiro, como parte dos requisitos necessários à obtenção do título de Mestre em Engenharia Elétrica.

Orientador: Mauricio Aredes

Rio de Janeiro

Dezembro de 2014

HIGH PERFORMANCE VOLTAGE CONTROL FOR THREE-PHASE UPS INVERTER

Jorge Eliécer Caicedo Castaño

DISSERTAÇÃO SUBMETIDA AO CORPO DOCENTE DO INSTITUTO ALBERTO LUIZ COIMBRA DE PÓS-GRADUAÇÃO E PESQUISA DE ENGENHARIA (COPPE) DA UNIVERSIDADE FEDERAL DO RIO DE JANEIRO COMO PARTE DOS REQUISITOS NECESSÁRIOS PARA A OBTENÇÃO DO GRAU DE MESTRE EM CIÊNCIAS EM ENGENHARIA ELÉTRICA.

Examinada por:

_____

Prof. Mauricio Aredes, Dr.-Ing.

_____

Prof. Luís Guilherme Barbosa Rolim, Dr.-Ing.

_____

Prof. Guilherme Gonçalves Sotelo, D.Sc.

RIO DE JANEIRO, RJ - BRASIL

DEZEMBRO DE 2014

Castaño, Jorge Eliécer Caicedo

High Performance Voltage Control for Three-phase UPS Inverter / Jorge Eliécer Caicedo Castaño. – Rio de Janeiro: UFRJ/COPPE, 2014.

XIII, 115 p.: il.; 29,7 cm.

Orientador: Mauricio Aredes

Dissertação (mestrado) – UFRJ/ COPPE/ Programa de Engenharia Elétrica, 2014.

Referências Bibliográficas: p. 84-88.

1. Three-phase UPS Inverter. 2. Synchronous Voltage Control. 3. Stationary Voltage Control. I. Aredes, Mauricio. II. Universidade Federal do Rio de Janeiro, COPPE, Programa de Engenharia Elétrica. III. Título.

Acknowledgments

Many thanks to Dr. Mauricio for his advices and support through these years in Brazil.

Many thanks to my colleagues in the Laboratory of Power Electronics and Medium Voltage Applications (LEMT), for their technical discussions and continuous support.

To my family and wife, for all their care and outstanding support, THANKS! This work and all accomplishments in my life will be especially dedicated to you.

Resumo da Dissertação apresentada à COPPE/UFRJ como parte dos requisitos necessários para a obtenção do grau de Mestre em Ciências (M.Sc.)

CONTROLE DE TENSÃO DE ALTO DESEMPENHO PARA INVERSORES TRIFÁSICOS DE FONTES ININTERRUPTAS DE ENERGIA

Jorge Eliécer Caicedo Castaño

Dezembro/2014

Orientador: Mauricio Aredes

Programa: Engenharia Elétrica

Este trabalho apresenta uma estratégia de controle de tensão aplicada em inversores trifásicos de Fontes Ininterruptas de Energia (*Uninterruptible Power Supply*, UPS). As caraterísticas principais da estratégia proposta são: Erro zero em regime permanente na frequência fundamental, imunidade aos distúrbios das cargas desequilibradas e compensação harmônica seletiva. Duas topologias (eixos de referência síncrono e estacionário) são apresentadas e comparadas. O comportamento dinâmico obtido nas simulações e ensaios experimentais, num protótipo de 5kVA, validam as abordagens teóricas propostas, assim como os modelos matemáticos introduzidos nesse estudo. Os resultados experimentais observados corroboram com os resultados previstos analiticamente, apresentando alto desempenho na resposta dinâmica quando comparado ao mínimo requerido pelas normas internacionais (IEEE e IEC).

Abstract of Dissertation presented to COPPE/UFRJ as a partial fulfillment of the requirements for the degree of Master of Science (M.Sc.)

HIGH PERFORMANCE VOLTAGE CONTROL FOR THREE-PHASE UPS INVERTER

Jorge Eliécer Caicedo Castaño

December/2014

Advisor: Mauricio Aredes

Department: Electrical Engineering

This work proposes a voltage control strategy applied to three-phase UPS inverter. Main characteristics are: zero steady state error for the fundamental frequency, immunity to load unbalance and selective harmonic compensation. The fundamental-frequency control was performed in stationary and synchronous frames. These topologies will be analyzed and compared. Results obtained in simulations and experiments confirm theoretical approaches and mathematical models presented along this document. In addition, results shows a high performance dynamic response compared to the requirements set by standards such as IEEE and IEC.

Index

Figure Index

Chapter 1 - Introduction

This chapter presents a general approach to objectives that motivated this research. It is also introduced a description of each chapter and document organization.

This work proposes a new control strategy in order to provide a high performance behavior in output voltage of three-phase UPS inverters. There were taking into account several restrictions, such as international standards and industrial requirements. Thus, in order to guarantee and excellent performance and at the same time ensure suitable implementations on industrial equipments.

A wide research in the state of art of these kind of controllers were performed. Using this information, a brief resume is presented in this work, making a simple classification which provide to reader a quickly and organized way to know previous works, different control proposes, its main features and results.

The proposed control strategy is presented in two different approaches (synchronous and stationary references plane). A deeply analyses and performance comparison are included in this work. In addition, some theoretical discussions were also performed such as mathematical models, simplified electrical representations and methodologies to calculation of controller parameters. Those theoretical analysis were validated through simulation and experimental results. The excellent performances achieve by proposed control strategy were presented at the International Conference and Exhibition on Power Electronics, Intelligent Motion, Renewable Energy and Energy Management, 2014.

Below are presented some reasons that had impulsed this research as well as principal objectives and how this work will be presented to the reader.

1.1. Problem identification

The Main objective of Uninterruptable Power Supplies (UPS) is to ensure a power backup to critical loads/processes. Besides this feature they are also used to support sensitive load such as telecommunications, medical or manufacturing equipment where high power quality is required. This high quality has to be ensured by the inverter stage, which must ideally provide a perfect sinusoidal voltage waveform with a constant magnitude value regardless of the load connected to its output.

Similar high performance aspects are also expected on UPS input, where power quality must be ensured on the connection point with electrical network. In addition, merge of new complex and sensitive process or technologies force to a continuous improvement of UPS systems. Several technical norms and international standards have

been published, describing very strict requirements for such systems. Furthermore, industrial applications have become more demanding.

Another important aspect is the system complexity. Through improvement of powerful digital systems, new functionalities are increased to conventional UPS equipment's. For instance: inclusion of measurement modules, Human-Machine Interfaces (HMI), communication modules, smart protections, among others.

Manufacturers also demand suitable implementations, in which compact hardware and flexible configuration features represent an advance from the economic point of view.

Motivation

The above features present a restricted scenario, where high power quality is demanded but at the same time low computational cost is encourage, i.e., the aim is to create a digital control system in which several functions are included but, at the same time fast dynamic performance is expected.

Different approaches have been proposed to pursue such demands. Nevertheless, continuous development of technology and control theories could represent an interesting background. Also, high performance expectations in UPS output could demand studies and implementations of several new concepts, applicable to some other power electronics areas as well.

1.2. Objectives

The aim of this document is to achieve a suitable voltage control scheme applied to inverter stage of an UPS system. This control strategy must accomplish the high performance expectations demanded by international standards, as well as industrial applications.

Theoretical discussions are expected to support a methodology to calculate the controller parameters. In addition, simulation and experimental results must validate the effectiveness of the proposed control strategy and confirm theoretical approaches.

1.3. Description of the Following Chapters

This document is divided in 4 principal parts: i) introduction to UPS inverter problems, ii) development of two control strategies to achieve high performance voltage control, iii) comparison between the proposed strategies and iv) conclusions of the main contributions. In addition, three appendices with mathematical concepts and development process of mathematical models are presented. Following a brief description of each chapter.

In chapter 2, it will be presented an introduction to UPS systems, focusing on the inverter stage and loads´ features. International standards will be studied in order to obtain specific control requirements. It also included a review of inverter voltage for UPS inverters.

In chapter 3, it will be presented a control strategy to solve each drawback introduced to voltage waveform due to disturbance of current load. Its main features are: Dual control loop in fundamental frequency based on synchronous PI controllers, resonant harmonic compensators and a current output filter capacitor feedback loop. The mathematical model, theoretical analysis, simulation and experimental results will be presented. Contributions to this chapter were published and presented at the international conference [1].

In chapter 4, it will be presented a control strategy that can offer a dynamic behavior similar to the strategy on Chapter 3. However, it is proposed replacing the synchronous PI by Stationary P+Resonant controllers. The plant's mathematical modeling and a detailed analysis of behavior in a closed-loop system will be discussed.

In chapter 5, it will be performed a comparison between voltage control topologies presented in Chapters 3 and 4. This chapter allows identifying which is the most suitable strategy for implementation of an output voltage controller of a three-phase UPS inverter.

Chapter 6 presents a summary of major contributions of this document and some suggestions for development of future work.

Appendix A, displays mathematics postulations taken to the Clarke and Park transformations used in this document.

Appendix B and C, develop the mathematical expressions presented in chapters 3 and 4 respectively.

Chapter 2 - Background and Review of previous Research

In this chapter, it will be presented an introduction to UPS systems. It focuses on inverter stage and loads' features/disturbances. International standards will be studied in order to obtain specific control requirements. Finally a review of inverter voltage control will be presented.

UPS systems involve different functional blocks, providing robust and flexible power supply for critical loads. In this way, it is important to understand principal features of these blocks before dealing with UPS inverter control. These aspects include internal and external elements which restrict the normal operation of the inverter stage. Below, the inverter topology used in this work, as well as the different loads, will be described.

UPS Scheme

Despite several UPS topologies reported in literature, Figure 2-1 present a high level UPS block diagram used in this work. Main aspects of this UPS topology are: i) the load has two options to be directly powered, ii) DC power for the inverter stage is controlled on a rectifier stage, iii) the load is an external agent for the UPS system, being in principle, an unknown factor for the inverter controller.

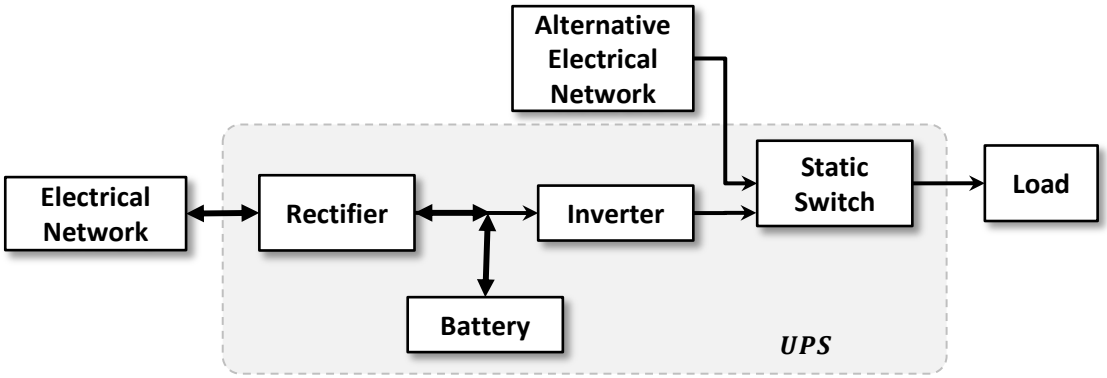

Figure 2-1. High level UPS block diagram.

As mentioned in chapter 1, the main purpose of this study is to achieve a high power quality on inverter stage, thus a three-phase inverter circuit topology is shown in Figure 2-2. Principal aspects of this circuit topology are found to be:

- DC voltage. From the inverter stage point of view, DC power can be considered perfectly controlled by the rectifier stage. In this way, it could be represented as a battery bank.
- DC/AC converter. This block describes a three-phase two level converter that will be triggered with a SPWM scheme.
- LC output filter. This second order low-pass filter is added to eliminate high switching frequency from the DC/AC converter.
- Output transformer. This block has several functions: i) offers a galvanic isolation for the load, ii) increases synthesized voltage from the DC/AC

converter to load voltage rating, iii) its leak impedance is used as part of the output filter, iv) provides a neutral point to connect single phase loads. In addition, the transformer topology can be used to reduce load imbalance effects, e.g. zig-zag topologies help to equilibrate the current demanded by an unbalanced load.

- Static switch. This component allows fast electrical switching between the alternative source and the voltage synthesized by the inverter.

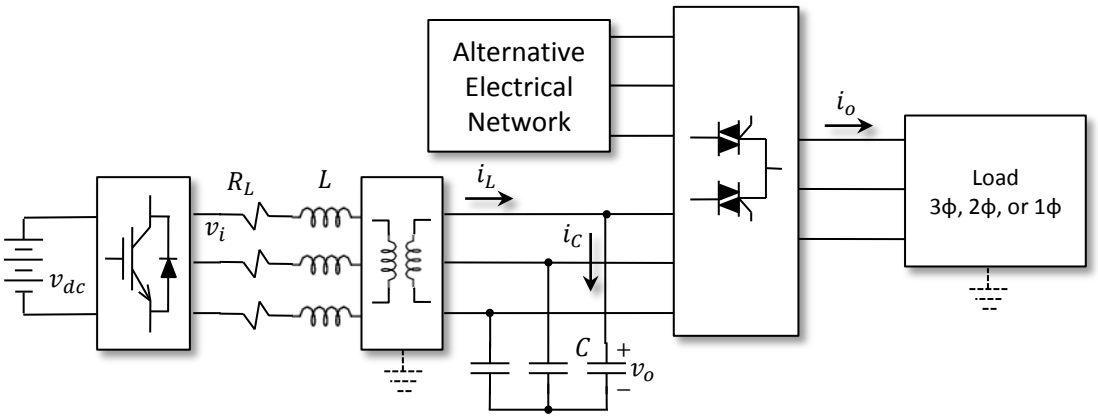

Figure 2-2.Inverter circuit topology.

2.1. UPS Loads

As mentioned before, the load is an unknown factor for the UPS inverter stage. Nevertheless, there are limited types of options and its principal characteristics and disturbances on the voltage waveform can be studied. The UPS load options are summarized in two main categories (linear and nonlinear loads). Figure 2-3 shows different connection options for linear-loads, where $\boldsymbol{Z_n}$ represents load impedance. This could be: pure-resistive, or inductive/capacitive in series or parallel connection.

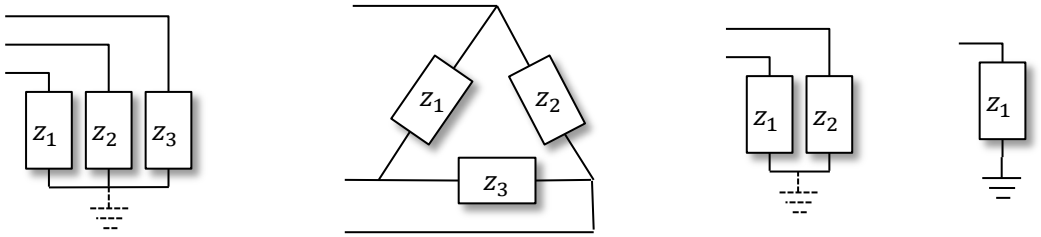

a) b) c) d)

--------- optional

Figure 2-3.Test linear loads, a)Three-phase (start connection), b) Three-phase delta connection, c) Two-phase, d) Single-phase.

2.1.1. Load Connection disturbances

The connection and disconnection of loads represent a great disturbance for voltage waveform magnitude. Figure 2-4 presents the effects of a three-phase linear load when connected to a non-controlled three-phase inverter. This disturbance occur regardless of the three-phase connection (see Figure 2-3a or b).

Voltage sag shown in Figure 2-4 will be mathematically explained later on chapters 3 and 4.

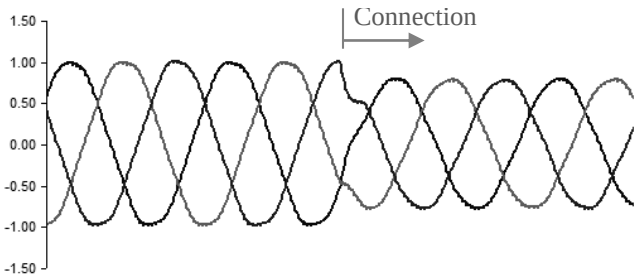

Figure 2-4. Voltage sag due to connection of a three-phase linear load.

2.1.2. Unbalanced Load Disturbances

An unbalanced load produces some imbalance on voltage output and at the same time introduce some harmonic pollution. Figure 2-5 shows these drawbacks produced by a two-phase linear load. It could be noted in Figure 2-5b that the 3rd harmonic is the biggest pollution introduced by this kind of load. These effects also appear when single-phase loads are connected into a non-controlled three-phase inverter.

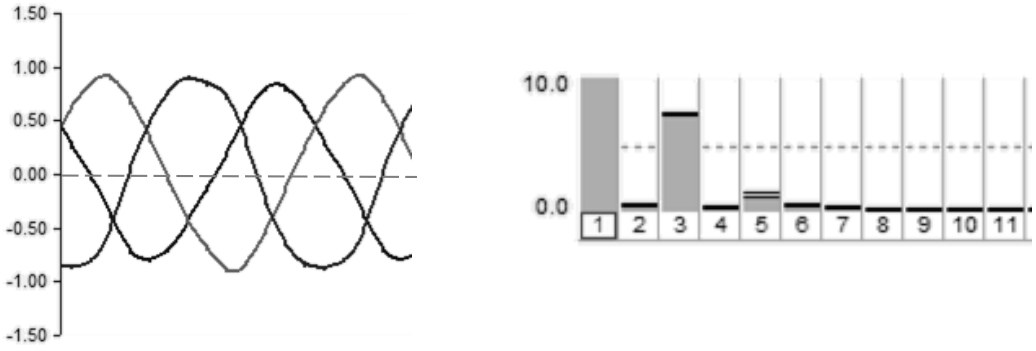

a) b)

Figure 2-5. Distortion due to connection of a two-phase linear load, a) voltage waveform, b) harmonic spectrum.

2.1.1. Nonlinear loads disturbances

Nonlinear loads are shown in Figure 2-6, where nonlinear inductive and capacitive loads are presented in their three-phase form. Nonlinear behavior is represented by a diode rectifier block, but could be an SCR or TRIAC as well. In these cases normally an inductance is added in series to minimize input $^{di}/_{dt}$.

A Nonlinear load represents a large harmonic pollution for UPS inverter. This highly distorted current significantly affects the output-voltage waveform. In addition, the capacitive nonlinear load produces a large current peak at connection when the capacitor is discharged. Pre-charge schemes are usually implemented to avoid that as shown in Figure 2-6c, allowing the capacitor to be charged through a limited current. Effects of a three-phase nonlinear load (Figure 2-6b) are presented in Figure 2-7.

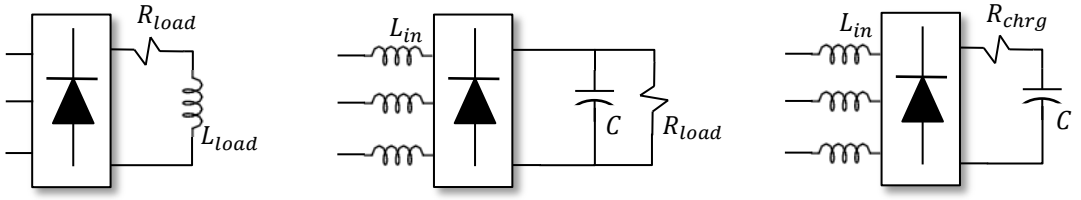

a) b) c)

Figure 2-6.Non-linear loads, a) Inductive type, b) Capacitive type, c) Capacitive pre-charge circuit.

Note: Nonlinear loads presented in Figure 2-6 can be applied to single and two-phase schemes as well.

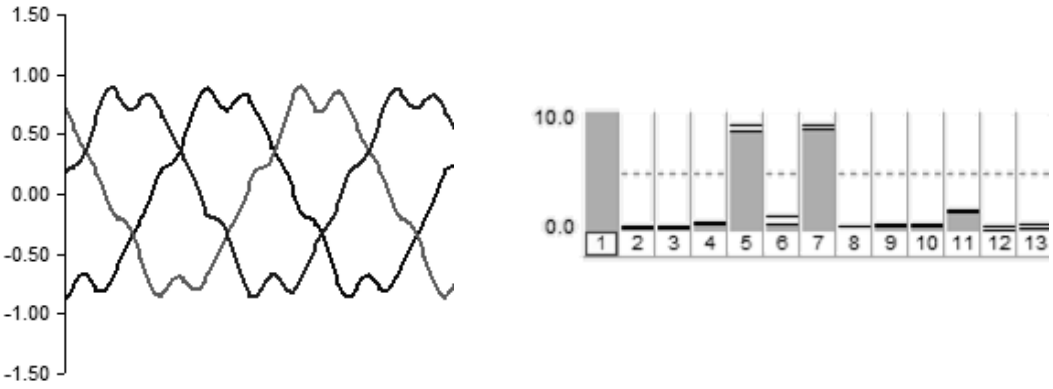

a) b)

Figure 2-7. Distortion due to connection off a capacitive three-phase nonlinear load, a) voltage waveform, b) harmonic spectrum.

2.2. Output-Voltage Constraints in UPS inverters

UPS systems are widely studied equipments and their principal behaviors are defined by some international standards such as IEEE and IEC. Limits or constraints established by these standards will be highlighted in this chapter as control requirements. This section presents a summary of the principal features on IEEE519-1992 and IEC62040-3 standards, focusing on inverter behavior characteristics. In addition, there will be considered some specifications required by industrial manufactures and clients as well.

Note: the aim of this section is not to create a technical standard guide or explanation. Following descriptions are principal dynamic aspects covered by these international standards, and it will considered in this work as UPS inverter voltage control requirements.

2.2.1. Transient Dynamics

Transients' dynamics on inverters voltage control for UPS systems are specified in detail by IEC62040-3 standard. Figure 2-8 shows the over and under-voltage transients limit allowed in the output voltage of an UPS inverter, when a connection or disconnection of a rate power load occur [2], i.e., the control topology must stabilize in less than 100ms with up to 30% overshoot.

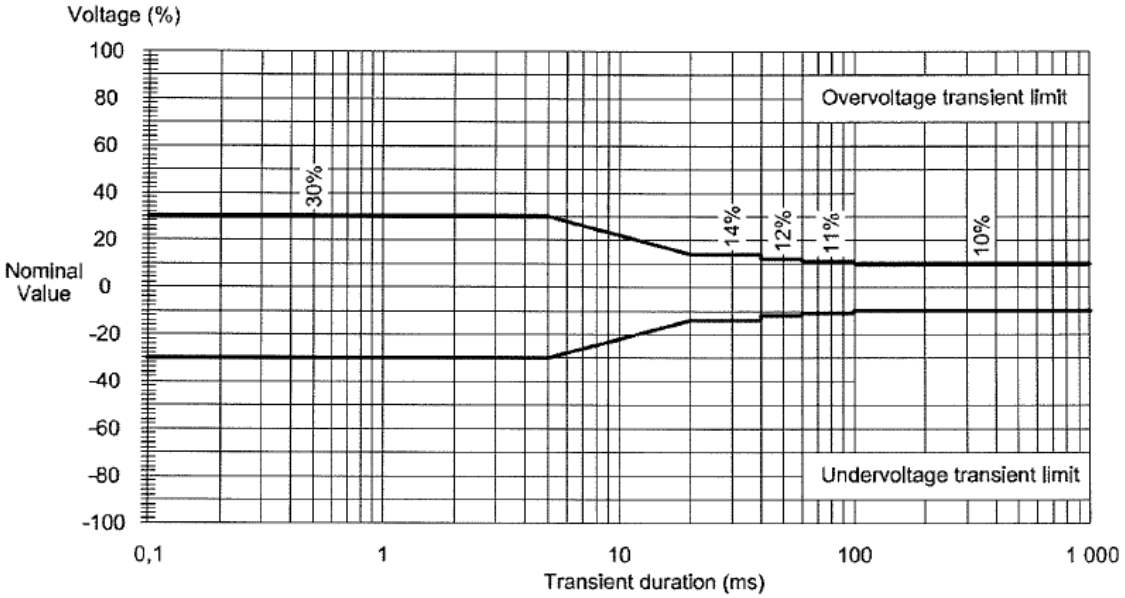

Figure 2-8. Transient dynamic restrictions.

2.2.2. Frequency Behavior

Frequency behavior of inverter output voltage is specified in both IEEE519 and IEC62040-3 standards. These constraints are especially important when a nonlinear load is connected to UPS inverter. In the following section, the main requirements for the voltage controller performance are described.

Total Harmonic Distortion

Table 2-1 presents the THD allowed on the international standards and some technical Norms. These THD limits are expected in steady-state conditions.

Table 2-1. THD limits.

	THD Limits
***IEC* 62040 – 3**	8%
***IEEE* 519**	5%
N-2760	3% (linear) 5% (non-Linear)

Note: N-2760 is a technical norm who defines the UPS specifications' demanded by the Brazilian multinational energy corporation PETROBRAS.

Individual Harmonic behavior

The maximum value for each harmonic is also specified by IEEE519 and IEC62040-3 standards. Figure 2-9 resumes the first 21st harmonic magnitude constraints. These harmonic values represent percent RMS value of fundamental-frequency component.

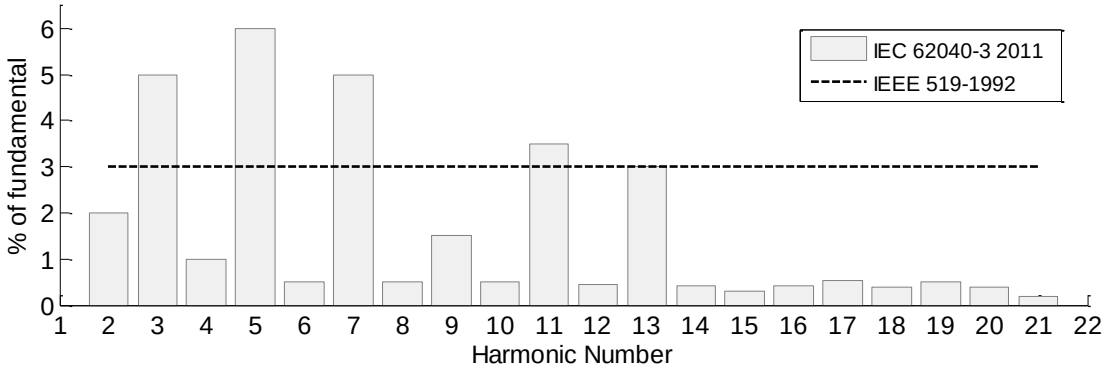

Figure 2-9. Harmonic limits.

2.2.3. Synchronization

Transfer static-switch shown in Figure 2-2 demands synchronization between alternative electrical network and voltage synthesized by UPS inverter. This in order to ensure fast load power transfer.

Frequency variations are expected in some industrial applications. Especially, where weak electrical networks are formed by variant electrical sources such as, wind and solar powered plants. In addition, connection and disconnection of parallel backup system can produce large frequency variations. Table 2-2 presents some synchronization constraints, based in some manufacture specifications to attend critical frequency variations, i.e. the inverter output-voltage should be synchronized with alternative electrical network as long as the frequency value falls within the specification shown in Table 2-2.

Table 2-2. Synchronization requirements.

Constrain	Specification
Frequency span	2% frequency rate (IEC62040-3) 5% frequency rate (N-2760)
Frequency slew-rate	1Hz/s (N-2760)

Note: frequency slew rate shown in Table 2-2 represents the maximum allowed variation rate in frequency value, i.e. maximum $^{d\omega}/_{dt}$ *in whish the inverter should synchronize with the alternative electrical network.*

2.2.4. Computational Effort

Computational effort is not an important factor from the international standards point of view. Nevertheless, as can be seen in Figure 2-1 UPS system involves different functional block, which implies several control loops (rectifier control, battery charge, inverter and rectifier synchronization, etc…). In addition there are others features offered by UPS equipment such as: measurement, protections, Human-Machine Interface, communication modules, among others. Thus encourage to consider computational effort as an important constraint for each functional block, in order to achieve a suitable DSP implementation, i.e., low computational effort will be considered as a fundamental feature for inverter control strategies evaluation.

2.3. UPS Inverter Voltage Control review

This section's aim is to present a brief introduction of some control schemes used in output voltage control for UPS inverters. To facilitate presentation, they were classified under 5 principal categories, as follows:

2.3.1. Classic Control Schemes

Classic Control Schemes are based on output-feedback control theory. This kind of controllers has been used since early XX century. Normally used for linear time-Invariant Systems (LTI). Nevertheless, through the need to control sinusoidal signals, it has been evolved with some theoretical analysis which allows accomplish for these kind of applications.

RMS Control

RMS schemes for UPS inverter control achieve tracking reference magnitude. Nevertheless, this kind of controller presents a noticeably slow response under load step changes (several cycles of the output waveform). In addition, nonlinear loads could greatly distort their output voltage waveform.

RMS scheme are normally applied to fundamental–frequency control in UPS inverter. While another strategy is used on with harmonic distortion and imbalance, e.g. in [3] RMS topology was proposed for fundamental-frequency control. At the same time a selective FFT algorithm was implemented for harmonic compensation. Thus achieving a THD=2.24%. In [4] a fundamental RMS control is combined with a multi-loop state-space based model control. In this case the UPS inverter under nonlinear load got a THD=3.8%.

Instantaneous Multi-Loop Stationary Control

Using additional voltage feed-forward loops and high gain values it is possible to handle sinusoidal waveforms in LTI controllers. This results in controlled system with almost zero steady-state error. In addition, involving current feedback loop it is possible to decrease significantly inverter-output impedance. Thus achieving good performance, especially on nonlinear loads.

Studying the physical system of UPS inverter shown in Figure 2-2, it was noted that the mathematical model of the LC filter was directly analogous to a DC motor model. Therefore it is possible to implement well known control techniques for this kind of system. This principle is show in [5], where several state-space model-based controllers for UPS inverters are deeply analyzed.

More recently, P+Resonant controller was implemented to an UPS inverter control in [6]. This kind of controller ensures elimination of steady-state error by inclusion of a P+Resonant on the fundamental-frequency. Transient responses were improved by adding a PID controller with capacitor-current feedback, thus achieving a THD = 1.49% under nonlinear load and an excellent transients response.

Note: LTI controllers can handle near to zero steady-state error for sinusoidal signal by using high gain values, but this gets the controlled system near to instability [5].

Instantaneous Multi-Loop Synchronous Control

Synchronous reference frame controllers ensures zero steady-state error for sinusoidal waveforms. At the same time it is possible to use multiples SRF on specific harmonic frequency. This concept was implemented in [7], reducing significantly voltage THD and ensuring zero steady-state error.

2.3.2. Predictive Control

This kind of control topology has many classes of controllers that have been found in many power electronics applications [3]. Those controllers use system models to predict the future behavior of controlled variables. Allowing to obtain optimal actuation according to a predefined optimization criterion [8]. Usually they provide a very fast dynamic response and constraints as well nonlinearities can be easily included.

Deadbeat Controllers (DB)

DB controllers are able to reduce state variables error to zero in a finite number of sampling steps. Usually giving the fastest dynamic response for digital implementation [3]. Nevertheless, despite fairly good dynamic response of DB controllers, their steady-state performance is largely dependent on the accuracy of system modelling. Which will negatively impact their performance under parameter variations.

A deadbeat control application on UPS inverter is presented in [9], using disturbance observer in order to reduce model mismatches. This control strategy presents a THD=4.1% under nonlinear capacitive load.

In [10] a DB was combined with a repetitive controller achieving a better performance on steady-state, a THD=1.44% was obtained in this case. (*Repetitive-control concept it will be explained later in this chapter).*

Model Predictive-Based Control

Model Predictive Control (MPC), uses a model of the system to predict specific variable states on a limited horizon of time, then a cost function is used as criterion to select the optimal future actions [8] [11]. This kind of controller allows include constraints and nonlinearities in the design stage of the controller. On the other hand, this topology involves several computational costs and presents a variable switching frequency scheme.

In case of voltage control for UPS inverters, there are some proposals using this type of controllers. In [12] a model reference controller (MCR) was used to obtain the desire plant dynamic, whereas a repetitive control minimize periodic distortions. This approach achieved a THD=2.01% under nonlinear load.

In [13] a synchronous reference dq frame internal-model-based controller was proposed. A predictive PD compensator was also included, getting an excellent performance with THD =1%.

2.3.3. Learning and Adaptative Control Schemes

The principle of Learning control schemes are based on the fact that almost all AC loads exhibits cyclic behavior. Thus allowing conceive a control strategy which updates its action using last cycle information. This improve steady-state behavior of the system, but their dynamic performance is weak [6]. Therefore, they are normally accompanied by a controller with faster dynamic response [3].

Repetitive Control

Repetitive control theory provides an alternative to minimize periodic errors that occur in a dynamic system. The repetitive action improves steady-state response of control system when reference signal and disturbances are periodic [14]. Several

approach of this kind of control has been proposed for voltage control in UPS inverters. There are normally in hybrid control schemes, some implementations examples of this technique are found to be:

- Discrete-time plug-in repetitive control plus servo controller [15].
- Deadbeat, plus repetitive control [10].
- One-sample-ahead predictive controller plus repetitive integral action [14].
- Tracking controller plus repetitive controller [16].
- Self-tuning repetitive controller with adaptative parameter tuner [17].

Iterative Learning Control

Iterative learning control (ILC) is a set of methods that iteratively adjust the control command as the control task is repeated, with the aim of converging to zero tracking error. These schemes accomplish this task without full knowledge of the system [3]. In [18] two proposals (direct and hybrid) Iterative Learning control were implemented on a UPS inverter. Obtaining a THD = 1.65% under nonlinear load.

Neural Networks Controllers

Neural Network (NN) is an interconnection of a number of artificial neurons that simulates a biological brain system. It has the ability to approximate an arbitrary function mapping and can achieve a higher degree of fault tolerance [19]. In addition, it is possible to performed training stage by simulations, thus reduce the computational effort on the implementation stage. A voltage control applied to single-phase UPS inverter was proposed in [19]. Getting a THD = 2.4% under nonlinear loads.

B-Spline Network

Unlike the feed-forward NNs, there is no nonlinear function in the proposed B-spline network, which reduces the stress of computation. Inverter voltage control based on B-spline network was proposed in [20]. In addition a PD controller was added to improve transients response and harmonic rejection, getting a THD=1.47% under nonlinear loads.

Neuro fuzzy

In [20] an integration of the Artificial Neural Network (ANN) and Fuzzy-Logic (FL) is proposed to output voltage control in a three-phase UPS inverter. This neuro-fuzzy inference system (ANFIS) can function to provide more accurate solutions under different operating conditions and nonlinear loads. Simulation result presented in [20] gets a THD=1%. Nevertheless, experimental results presents in this paper did not reported THD value.

2.3.4. Nonlinear Control Schemes

Hysteresis Control

Several hysteresis-type controllers have been presented for UPS inverter control. Although these controllers present great transients response, it can suffer from relatively high and variable switching frequencies.

Sliding Mode Control

This method alters the dynamics of a nonlinear system by application of a discontinuous control signal, i.e. forcing the system to "slide" along a cross-section of system's normal behavior. Using this scheme a three-phase inverter voltage control is proposed in [21], where large uncertainty in parameters and external perturbations were included. Despise robustness features presented by this proposal, dynamic response and THD behavior wasn't enough to be considered as high performance.

2.3.5. Optimization Method

H_∞ Method

H∞ method finds the controller who solves a mathematical optimization problem. H∞ techniques have the advantage over classical control techniques in that they are readily applicable to problems involving multivariate systems with cross-coupling between channels. That's why it could be considered as a suitable option to perform a voltage control for UPS inverters.

In [22] a H∞ method was used on a system based on resonant controllers to ensure tracking of sinusoidal reference signals and to reject harmonic disturbances from the load. Some restrictions were added to the control strategy such as: i) limited precision and

dynamic range of data representation in the DSP; ii) delay from the digital implementation of the control law; iii) limitation on the amplitude of the control signal. Thus achieved a THD = 0.98% and an excellent transients responses as well.

Note: H∞ method is known to provide optimal performances but frequently at the high cost of prohibitively large control gains [22].

2.4. Partial Conclusions

- Load effects, IEEE519 and IEC62040-3 standards were analyzed in order to obtain control requirements for UPS inverters.
- Was presented a brief review of voltage control schemes applied to UPS inverters. Thus allow to identify:
  - Hybrid control strategies are strongly suggested in order to achieve high performance in both transient response and frequency behavior, i.e. uses more than one control theory to attend the control requirements.
  - Current feedback loops involving output filter are used in several control proposal in order to decrease inverter output impedance.
  - Several mathematical approaches proposed by authors uses load current as a system disturbance, in order to evaluate the control effectiveness.
  - Digital controllers, mathematical model base methods and predictive control presented good performances. Nevertheless they exhibit strong relation with system physical parameters.

Chapter 3 - Synchronous Double Frame Voltage Control with Selective Harmonic Compensation

In this chapter it will be presented a control strategy to solve each of the drawbacks introduced to voltage waveform due to disturbance of current load. Its main features are: Dual control loop in fundamental frequency based on synchronous PI controllers, resonant harmonic compensators and a feedback loop of the capacitor current of the output filter. The mathematical model, theoretical analysis, simulation and experimental results of the control strategy will be presented. Obainted results confirm the feasibility of implementing the proposed control strategy. Detailed development of mathematical expressions presented in this chapter are shown on appendix B.

3.1. Control Topology Overview

The proposed control topology presented in this chapter was designed analyzing problems due to different loads in the waveform on output voltage of the inverter. The control topology is based on different widely-studied techniques and theories, applied to solve each problem (voltage drop, imbalance and harmonic pollution), in order to achieve high performance expectations presented on Chapter 2. Figure 3-1 shows a general diagram of the topology proposed in this chapter.

Proposed control strategy main aspects:

- Positive and Negative- voltage control "P&N Control". Which regulates the fundamental-frequency component.
- Resonant harmonic compensation "Series and Parallel HC". Used to minimize the harmonic pollution.
- Capacitor-current feedback. Which minimize the inverter output impedance.

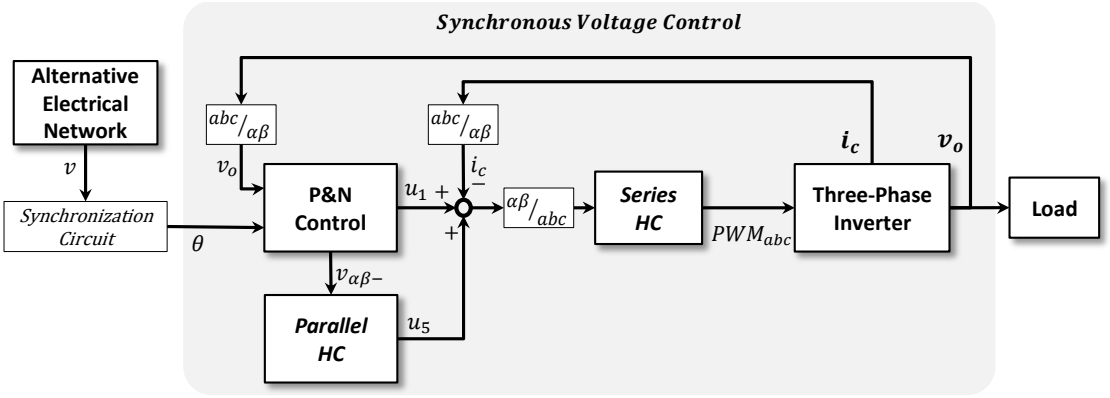

Figure 3-1. General block diagram of the proposed synchronous control topology.

3.1.1. Fundamental-Frequency Voltage Control in Synchronous Reference Frame

The main goal of P&N control block in Figure 3-1 is ensuring a constant magnitude on voltage vectors $\boldsymbol{V_a}$, $\boldsymbol{V_b}$ and $\boldsymbol{V_c}$, against perturbances caused when connecting or disconnecting any load. For unbalanced two-phase or single-phase loads, this block must also ensure reduction or elimination of fundamental negative-sequence component.

P&N Synchronous voltage control

The idea of using a double control loop (positive and negative-sequence) has been proposed and widely discussed on issues such as: synchronization of converters on unbalanced networks [23] [24] [25], current control in grid connected converters [26] [27] [28], voltage control in AC power supplies [7], among others. Analyzing the characteristics of these proposals it can be conclude that: i) Positive-sequence control can ensure zero error in magnitude of voltage vectors. And ii) providing a zero reference in negative-sequence controller would be possible to eliminate consequences of unbalanced loads.

The outline of a PI controller on a synchronous reference axis (SRF) is adopted in this chapter in order to ensure zero steady-state error for fundamental frequency.

As expressed in Chapter 2, UPS inverter must operate under variable system frequency. Thereby the information of frequency and phase will be provided to the park's transformation blocks as an input coming from a synchronization circuit (PLL.). Thus allowing the controller adapts to frequency variations. Figure 3-2 presents a detailed diagram of the proposed dual voltage control loop for the fundamental frequency.

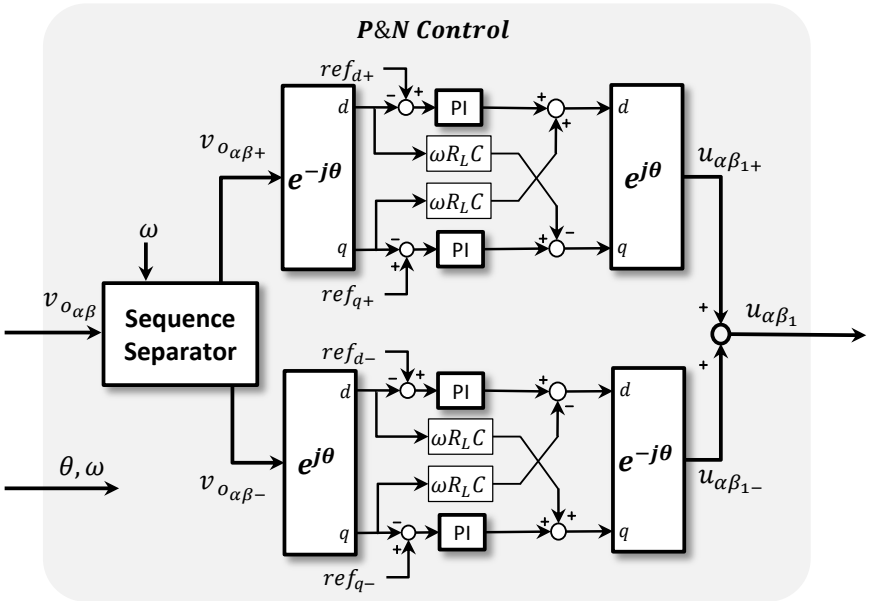

Figure 3-2. Detailed block diagram of proposed fundamental-frequency controller.

As reported in [23] there is a strong relation between control efforts on each of the control loops (Positive and Negative-sequences). There are two option to avoid that:

- Understanding the cross-coupling and integrating decoupling loops between sequences [23] [26].
- Use a scheme based on an electrical sequence separation [29] [30] [25].

The modular approach presented in the second option, can facilitate theoretical analysis and mathematical model calculations. For that reason that alternative will be adopted in this work.

Sequence Separator

At early 30's Lyon extended the use of the Fortescue's symmetrical components to time-domain [31]. More recently, P. Rodriguez used this method to realize a positive-sequence calculator as an essential part of a new high-performance PLL [32]. The positive-sequence component can be determined in terms of alpha-beta variables as

$$\begin{bmatrix} v_{\alpha+} \\ v_{\beta+} \end{bmatrix} = \frac{1}{2}\begin{bmatrix} 1 & -q \\ q & 1 \end{bmatrix}\begin{bmatrix} v_{\alpha} \\ v_{\beta} \end{bmatrix} \quad , \tag{3.1}$$

where:

$$q = e^{-j\frac{\pi}{2}} = -j \quad .$$

In a similar way, the negative-sequence component is found to be

$$\begin{bmatrix} v_{\alpha-} \\ v_{\beta-} \end{bmatrix} = \frac{1}{2}\begin{bmatrix} 1 & q \\ -q & 1 \end{bmatrix}\begin{bmatrix} v_{\alpha} \\ v_{\beta} \end{bmatrix} \quad . \tag{3.2}$$

There are different techniques to implement the "q" operator used in (3.1) and (3.2). As mentioned in the chapter 2, an UPS inverter must operate under variable system frequency. This requirement restricts the number of possible solutions implementing the "q" operator. A simple solution is using two second-order generalized integrators for quadrature-signals generation, generally known as DSOGI-QSG [32].

Above concepts of symmetrical components in time-domain and DSOGI-QSG are combined to create a sequence separator as shown in Figure 3-3. The control block identified as SOGI-QSG is detailed in Figure 3-4.

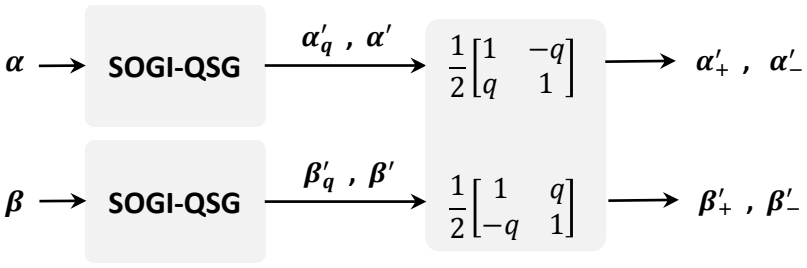

Figure 3-3. Block diagram of sequences separator based on DSOGI-QSG.

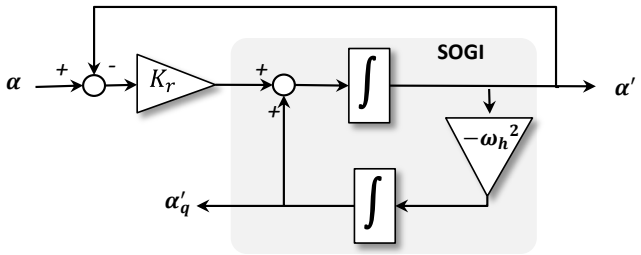

Figure 3-4. SOGI-QSG Block diagram.

Transfer functions of DSOGI-QSG presented in [32] are found to be

$$\frac{v'_{(s)}}{v_{(s)}} = \frac{k\omega s}{s^2+k\omega s+\omega^2} \quad \text{and} \tag{3.3}$$

$$\frac{qv'_{(s)}}{v_{(s)}} = \frac{k\omega^2}{s^2+k\omega s+\omega^2} \quad , \tag{3.4}$$

where, ω is resonance frequency and k is the damping factor. A value of $k = \sqrt{2}$ is suggested in [32] to achieve a critical-damped response.

Synchronization Circuit

As presented in chapter 2, estimation of frequency and phase its necessary due to the possibility of having an inverter output voltage synchronized with an alternative network. A common way suggested by authors is using a Phase Locked Loop (PLL). A comprehensive study and comparison of several types of PLL's is presented in [33]. This study shows that a simple SRF-PLL meets the requirements presented in Chapter 2. Figure 3-5 presents a general block diagram of this PLL.

A dynamic analysis of this PLL based on the instantaneous power theory is presented in [34]. Internal PLL parameters can be calculated based on dynamic characteristics desired for "ωt". Mathematical relationship presented in [34] is found to be

$$K_i = \omega_n^2 \quad \text{and} \tag{3.5}$$

$$K_p = \frac{\xi}{2K_i} \quad , \tag{3.6}$$

where K_p and K_i are the proportional and integral parameters of internal PI controller respectively, while ω_n and ξ are the frequency pass-band and damping factor of desired dynamic response of PLL respectively.

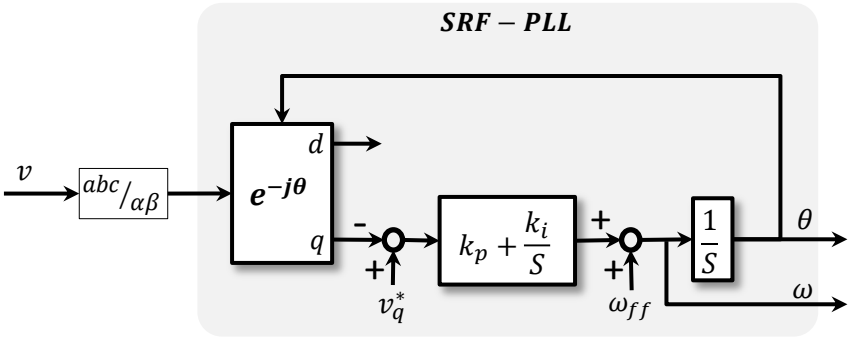

Figure 3-5.PLL block diagram.

3.1.1. Current feedback loop

As shown in the Figure 3-1, a capacitor current feedback loop was included into the proposed control strategy. This current information can reduce significantly the output impedance of the UPS inverter [5]. Improving in this way the voltage-control performance, especially to nonlinear loads. A comparison between this two current loops is performed in [6] showing that capacitor information has more advantages compared to inductor information current. Effects of this feedback on the proposed control strategy will be detailed on chapter 4.

3.1.2. Voltage Harmonic Compensation

Unbalance, non-linear loads and three-phase inverter topology itself produce some harmonics pollution. Considering this and to meet international standards, the proposed strategy control includes a scheme of harmonic compensators.

Many authors recommend using resonant harmonic compensators in parallel with fundamental-frequency controller as an efficient method for selective compensation of each harmonic [35] [36] [37] [38] [39]. Another advantage in this type of harmonics compensator is that it doesn't significantly affects the dynamics of fundamental-frequency controller [40]. These behaviors are not only flexible and modular, but facilitate theoretical analysis to calculate controller parameters.

Resonant Harmonic compensator (HC) is a topology based on cosine model of Laplace transformation. When used in a closed control loop adds to system an infinite gain at a specified resonance frequency, ensuring zero steady-state error, i.e. if there is any harmonic component of same frequency than HC internal frequency, the control-effort increases its response as necessary to eliminate it.

Transfer function of resonant HC is found to be

$$HC_{(S)} = \frac{K_h S}{S^2+\omega_h^2} \quad , \tag{3.7}$$

Where, K_h and ω_h represent the gain and resonance frequency respectively. As described in [41], is possible to represent this expression as two first order equations. Figure 3-6 shows HC implementation diagram.

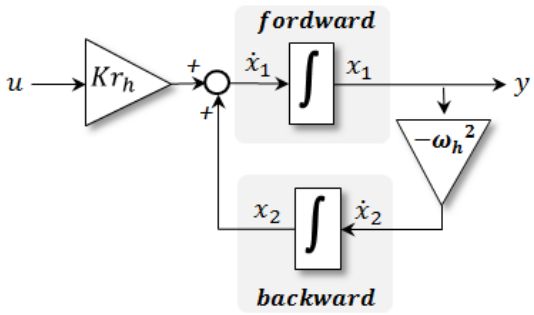

Figure 3-6. Resonant HC block diagram.

Series Harmonic Compensation

As presented in chapter 2 unbalanced load introduces 3rd harmonic. However, trough research it was experimentally demonstrated that conventional parallel HC configuration doesn´t effectively reduces 3rd harmonic. On the other hand, when placed in series whit fundamental frequency controller it could successfully compensate this harmonic. Figure 3-1 shows this proposed 3rd harmonic compensator as "series HC" block. Figure 3-7 shows in detail the internal topology of this block.

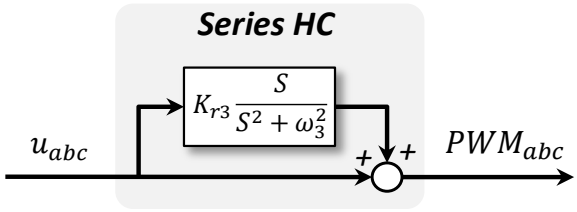

Figure 3-7. Proposed series harmonic-compensator block diagram.

Note: U_{abc} signal, represents the control effort of the fundamental-frequency controller.

Parallel Harmonic Compensator

Nonlinear load introduces into the voltage waveform some harmonic content. As presented in chapter 2 the most representative distortion is given by 5th and 7th harmonics. Usually, parallel harmonic compensation schemes achieve the reduction of this harmonic pollution. Nevertheless when capacitor current feedback is used in control topology (see Figure 3-1), this kind of HC becomes instable in closed loop. This fact was experimentally observed through this work.

The proposed solution adopted in this work was the implementation of parallel HC scheme but using just the negative sequence information from output voltage. In order to improve the signal-noise ratio of the 5th harmonic. At the same time it was a natural choice due to 5th harmonic normally has negative component nature.

It will be shown later in this chapter that just 5th harmonic compensation is enough to keep THD value within the international standards. That's why 7th harmonic will not be compensated in order to reduce the computational cost of the proposed control strategy.

3.1.3. Double Synchronous Voltage Control with Selective Harmonic Compensator and Capacitor Current Feedback Topology

Using information presented above, Figure 3-8 shows a detailed diagram of the proposed voltage-control strategy for UPS inverter.

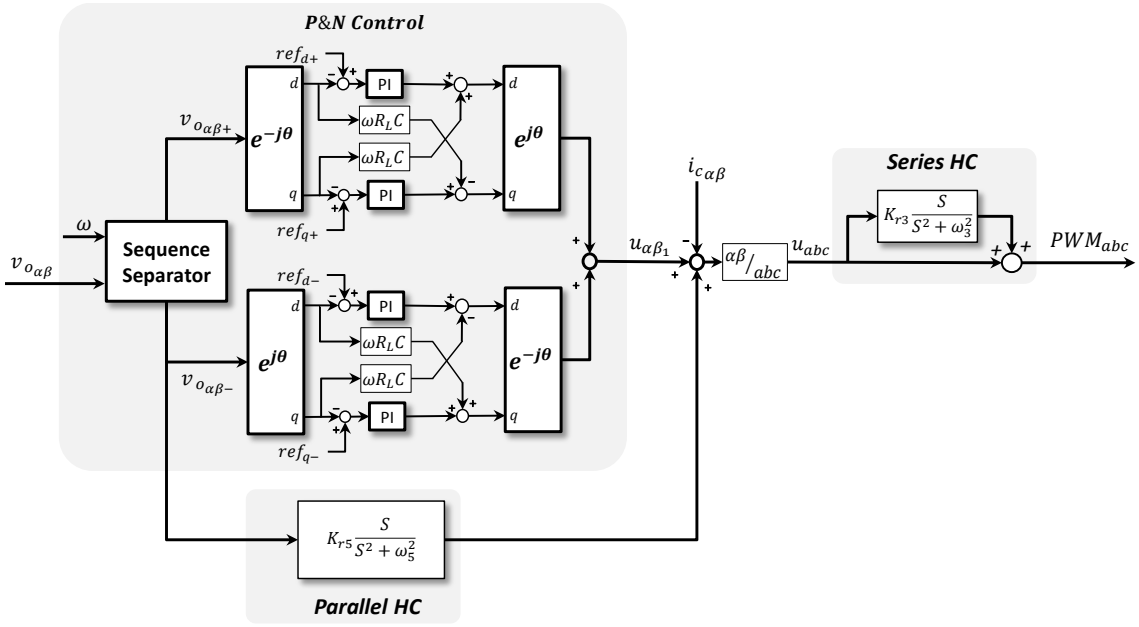

Figure 3-8. Proposed synchronous control topology detailed block diagram.

3.2. Theoretical Analysis and Mathematical Modeling

Representing the dynamics of all plant´s component can be an arduous task and the results can lead to very complex models. Hence, reduced models based on approximations are encouraged to obtain mathematical expressions that are suitable for performing theoretical analysis. UPS inverter has several components and dynamics that can be expressed in an approximate way and some others that can be ignored at all. Detailed descriptions of approaches taken in this chapter are presented below.

3.2.1. Analytical Approaches

It's necessary to identify the main components of UPS inverter that significantly affect output-voltage dynamic. Which is the control objective or "variable of interest". Following, are analytical approaches and theoretical assumptions, taken into account to build an equivalent circuit, as shown in Figure 3-9 and a mathematical model in (3.13):

- Output transformer will be described using the equivalent simplified electrical model, i.e. magnetization circuit, hysteresis and saturation of the core will be ignored.
- Inductance leak and resistance of transformer will be grouped on the secondary side using equivalent windings ratio [13].

- Inductance leak of transformer will be considered as output filter inductor.
- Transformer windings ratio will be included as gain in transfer function.
- DC/AC converter will be modeled only as a fundamental-frequency source with variable magnitude, i.e. nonlinear and dead-time effects will be omitted [5].
- DC voltage Dynamics of inverter will not be included in model.
- Resistance, capacitance and inductance magnitudes of output filter will be considered as constants.
- ω will be considered constant, i.e. frequency variation ($\Delta\omega$) is small enough compared with its nominal value.
- The resistance of the output filter capacitor will be ignored.
- Load current will be modeled as a system perturbation [5] [6] [42] [27].
- First-order derivatives of couplings terms in (3.8), (3.9), (3.10) and (3.11) will be ignored as shown in Figure 3-8.

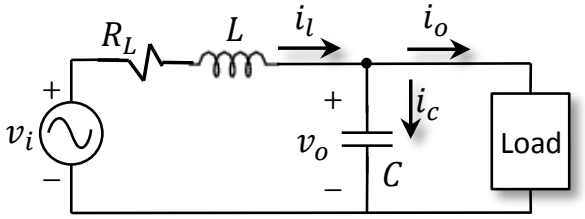

Figure 3-9. Per phase equivalent UPS inverter circuit.

Figure 3-9 shows an equivalent electrical representation for each phase of the inverter, where:

- "v_i" is the synthesized fundamental-frequency magnitude in each phase of the inverter.
- "R_L" and "L" represents the resistance and inductance value of output filter, respectively.
- "C" is the output-filter capacitance value.
- "i_L", "i_C" and "i_o" represents instantaneous currents flowing in each phase through inductor, capacitor and load, respectively.
- "v_o" represents instantaneous output voltage in each phase of the inverter.

3.2.2. Mathematical Modeling

Temporal representation of UPS inverter dynamics in synchronous reference plane, for both positive and negative sequence can be achieved by a voltage and current analysis on circuit shown in Figure 3-9. These dynamic representations are given by

$$v_{id+} = LC\frac{d^2v_{od+}}{dt^2} + R_LC\frac{dv_{od+}}{dt} + (1-\omega^2LC)v_{od_+} + L\frac{di_{od_+}}{dt} + R_Li_{od_+} - 2\omega LC\frac{dv_{oq+}}{dt} - \omega R_LCv_{oq_+} - \omega Li_{oq_+} \quad , \tag{3.8}$$

$$v_{iq+} = LC\frac{d^2v_{oq+}}{dt^2} + R_LC\frac{dv_{oq+}}{dt} + (1-\omega^2LC)v_{oq+} + L\frac{di_{oq+}}{dt} + R_Li_{oq+} + 2\omega LC\frac{dv_{od+}}{dt} + \omega R_LCv_{od+} + \omega Li_{od_+} \quad , \tag{3.9}$$

$$v_{id-} = LC\frac{d^2v_{od-}}{dt^2} + R_LC\frac{dv_{od-}}{dt} + (1-\omega^2LC)v_{od_-} + L\frac{di_{od-}}{dt} + R_Li_{od_-} + 2\omega LC\frac{dv_{oq-}}{dt} + \omega R_LCv_{oq_-} + \omega Li_{oq_-} \quad , \tag{3.10}$$

$$v_{iq-} = LC\frac{d^2v_{oq-}}{dt^2} + R_LC\frac{dv_{oq-}}{dt} + (1-\omega^2LC)v_{oq_-} + L\frac{di_{oq-}}{dt} + R_Li_{oq_-} - 2\omega LC\frac{dv_{od-}}{dt} - \omega R_LCv_{od_-} - \omega Li_{od_-} \quad . \tag{3.11}$$

Where:

- "V_{i_d}" and "V_{i_q}" represents voltage synthesized by the converter in "*d*" and "*q*" components respectively.
- "V_{od}" and "V_{oq}" represents voltage in the output filter in "*d*" and "*q*" component respectively.
- "ω" is the reference-axes angular frequency.
- The symbols "X_+" and "X_-" represents positive and negative-sequence components respectively.

Highlighted part in (3.8), (3.9), (3.10) and (3.11) indicates the existence of cross-couplings terms between reference axes “d” and “q”. This can be ignored during the mathematical modeling due to decoupling inner loops in control topology as shown in Figure 3-8. Thus a single transfer function is enough to describe the behavior of output voltage.

Without coupling terms, voltage dynamic information is the same as shown in (3.8), (3.9), (3.10) and (3.11). Using the Laplace transform in above temporal expression is found to be

$$V_{in} = LCS^2V_{on} + R_LCSV_{on} + (1 - \omega^2LC)V_{0n} \ , \tag{3.12}$$

where $n = \{d_+ \quad q_+ \quad d_- \quad q_-\}$.

The objective of mathematical modeling is to obtain dynamics of the system (transformer + output filter + capacitor current feedback). Henceforth, known as “plant.”

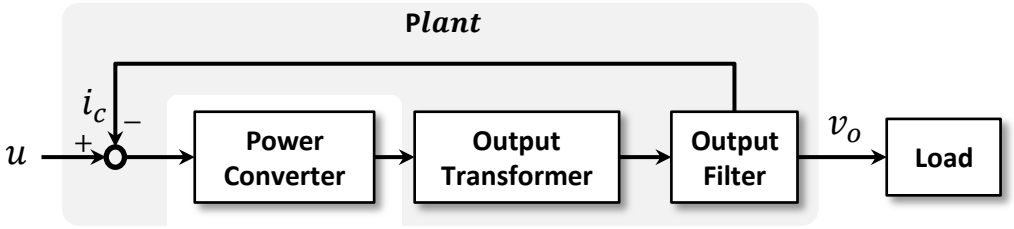

Figure 3-10. Proposed mathematical block diagram.

It is possible to understand the main characteristics and calculate the appropriate control parameters by knowing dynamic behavior of the plant. Transforming the natural dynamics of the plant, into a dynamic that satisfies all the requirements imposed by international standards. All of this within the allowed margins of control-effort and ensuring system stability.

The transfer function of the highlighted area of Figure 3-10 is giving:

$$G(s) = G_{V_o}(s) - G_{I_o}(s) \ , \tag{3.13}$$

where,

$$G_{V_o}(s) = \frac{V_o}{U} = \frac{K_{inv}}{LCS^2+(R_L+K_o)CS+(1-\omega^2LC)} \ , \tag{3.14}$$

$$G_{I_o}(s) = \frac{V_o}{I_o} = \frac{LS+R_L}{LCS^2+(R_L+K_o)CS+(1-\omega^2LC)} \ , \tag{3.15}$$

$$K_{inv} = K_o K_{trans} \ , \tag{3.16}$$

$$K_o = \frac{V_{dc_{pu}}}{2} \tag{3.17}$$

and:

- $G_{V_o}(s)$ Represents transfer function of output-voltage in relation to control efforts.
- $G_{I_o}(s)$ Represents the transfer function of output-voltage in relation to disturbance caused by load current.
- "U" represents control-effort.
- "K_{trans}" represents transformer winding ratio.
- "$V_{dc_{pu}}$" represents magnitude of DC-voltage link, expressed in per unit value.
- "K_o" represents gain of DC/AC converter.
- "K_{inv}" represents system output gain (converter + transformer).

3.2.3. Controller calculation

Using information from mathematical model presented above it is possible to analytically obtain parameters for fundamental-frequency controllers. The aim of this methodology is to achieve a controlled system, which satisfies specifications of international standards, and some design criteria as well. Constraints and design criteria are listed below:

- Control-effort value must remain within ±1 to avoid over-modulation of the inverter. (*Linear operating range of inverter*).
- System dynamics should respond in less than 100ms. (*IEC standard*).
- Broad gain-margin (GM> 6dB) [41]. Guarantees control-loop stability against not considered changes in model gain. One of the most important in the case of a UPS inverter is the DC-voltage variations. Which have direct relation to DC-AC converter gain, as shown in (3.17). (*System stability*).

- Wide phase margin (PM> 30°) [41]. Guarantees control-loop stability against additional not considered delays coming from model approaches, conditioning circuits and sensors. (*System stability*).
- System dynamics must have none overshoot (*Design criteria*).

Temporal and frequency behaviors of open-loop model presented in Figure 3-11 doesn´t meet the above requirements. Henceforth a PI controller block was added into proposed voltage-control topology.

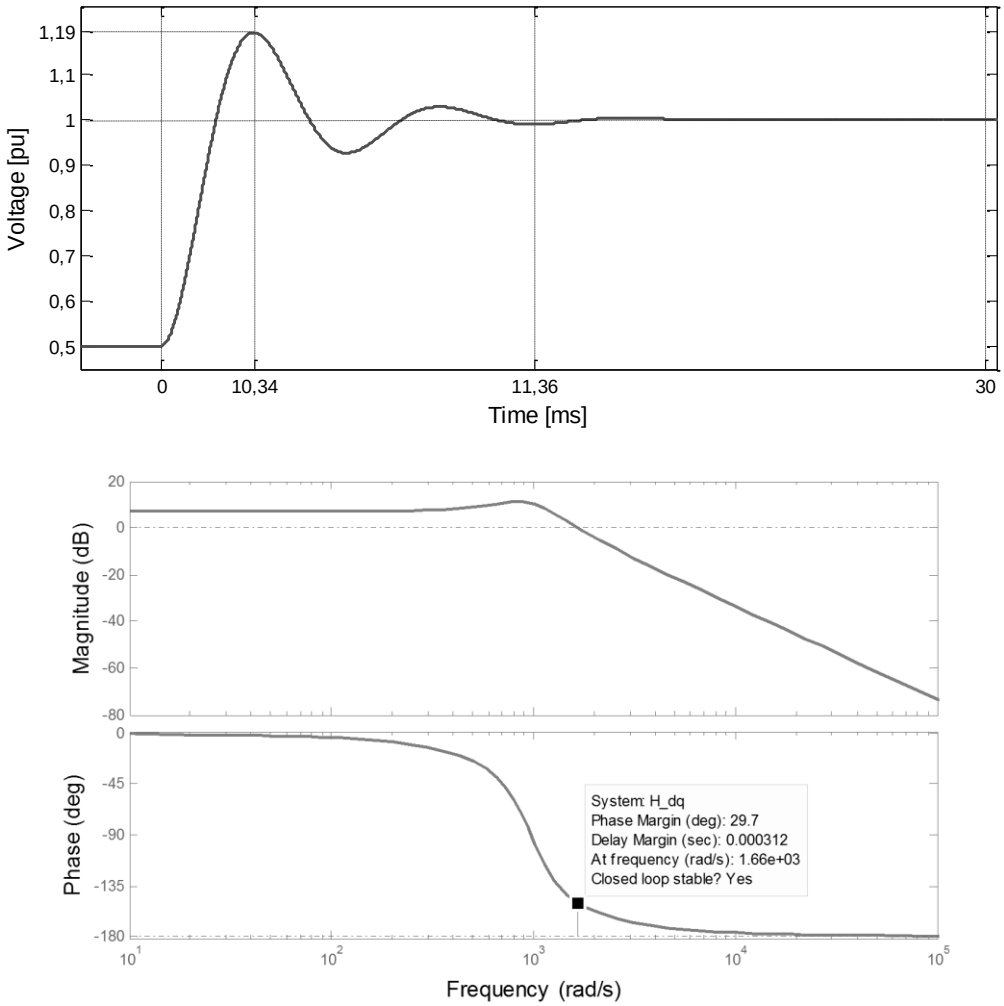

Figure 3-11 Plant behavior, a) step response, b) Bode diagram.

Fundamental-component Controller

Closed-loop system in synchronous reference plain is described by:

$$H(s) = H_{V_o}(s) - H_{I_o}(s) \quad , \tag{3.18}$$

where

$$H_{V_o}(S) = \frac{V_o}{V_o^*} = \frac{K_{inv}G_{PI_{(S)}}}{LCS^2+(R_L+K_o)CS+\left(1-\omega^2 LC+K_o G_{PI_{(S)}}\right)} \quad , \tag{3.19}$$

$$H_{I_o}(S) = \frac{V_o}{I_{on}} = \frac{(LS+R_L)}{LCS^2+(R_L+K_o)CS+\left(1-\omega^2 LC+K_o G_{PI_{(S)}}\right)} \quad , \tag{3.20}$$

$$\text{And } G_{PI_{(S)}} = \frac{K_p S+K_i}{S} \quad . \tag{3.21}$$

"K_p" and "K_i" represents proportional and integral controller gains respectively.

The effect introduced by controller and closed loop are found to be in (3.18). It is important to note that disturbance dynamic is directly affected by controller action as shown in (3.20), i.e. Controller action affects the value of inverter-output impedance. Therefore, the controlled system is less sensitive to load connection [26].

"Robust response time tuning algorithm" offered by Matlab was the most suitable option to calculate parameters of fundamental-frequency controller, given specifications and design criteria outlined at beginning of this section. This method tuning the PI gains to achieve a good balance between performance and robustness. Temporal behavior of controlled system is shown in Figure 3-12, while Figure 3-13 shows the frequency behavior. The controlled-system characteristics are found in Table 3-1. Results exhibit the capability of a tuned controller to ensure the system into the imposed requirements.

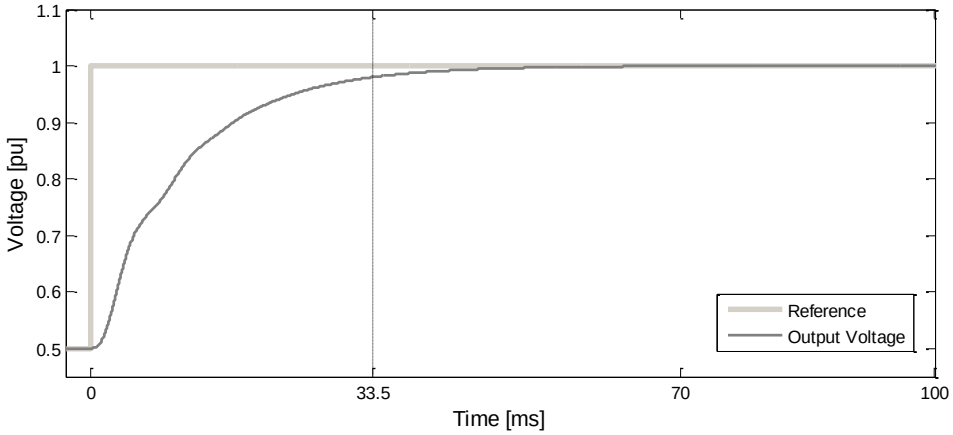

Figure 3-12. Step response of tuned PI controller under reference change.

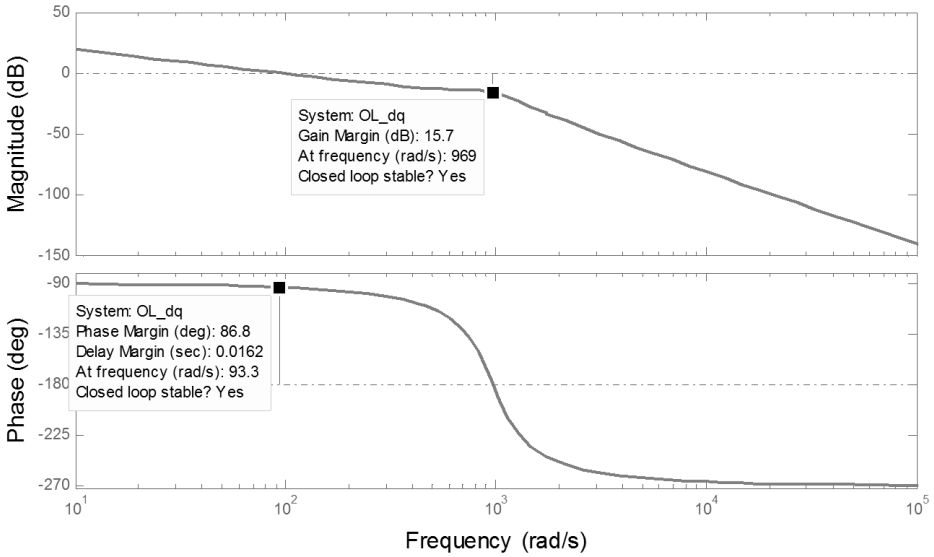

Figure 3-13. Bode diagram of close-loop behavior with tuned PI controller.

Closed-loop bode diagram shown in Figure 3-13 is a system approximation around the angular frequency of synchronous reference. Higher and lower frequencies may vary from the actual plant behavior. To avoid bringing instability to real system it is important to give a wide stability range in the theoretical calculations.

Table 3-1. Resume of the close loop behavior of the mathematical model.

Item	Value
K_p	0
K_i	50.93
Phase Margin	86.8°
Gain Margin	15.7dB
settling time	33.5ms
Over-shoot	0%
Maximum control effort	0.51

Harmonic compensation

Resonant compensator does not significantly affect the dynamic of the fundamental-frequency controller [35]. Another important feature is a highly selectivity, so they can be treated as independent blocks. Compensator gain does not significantly affect other compensating dynamic. A deeper explanation of these HC blocks will be presented in Chapter 4.

This document does not propose calculation of gain values of HC blocks. Instead, values adjustment can be carried out in both simulation and experiment. An initial value of 0 is assigned to each HC gains and gradually will be increased. This adjustment is perform by observing the magnitude of each harmonic in frequency spectrum.

3.3. Simulation Results

Proposed simulation in this paper has as main objective to provide a rapid prototyping system for control strategies in order to validate theoretical hypotheses. Also, it is possible to test the discrete form of control topology before code is implemented in DSP.

Transient electromagnetic Simulator PSCAD was the selected tool to perform theoretical validation. This software offers a fixed step simulation, with properties of interpolation in power switching transitions. In addition, it offers a dynamic interface that facilitates analysis and comparison on different waveforms.

In general, there are two ways to perform control algorithms made during theoretical discussions: The first one is using generic blocks offered in PSCAD and setting a very fast simulation time, considering it as an approximation of continuous-time control. The second way is using the ability of PSCAD to communicate with source code in C. This allows discrete time approximation of proposed control topology.

Figure 3-14 shows electrical circuit of simulated three-phase inverter using a breaker set to configure different types of loads. Values in this simulation represent a very close approximation of those used in a real prototype. Table 3-2 summaries parameter values used in simulation.

Note: Voltage-battery dynamic won't be considered during simulation stage.

Table 3-2. Simulated parameters.

parameter	Value
$\boldsymbol{K_p}$	1e-5
$\boldsymbol{K_i}$	50.93
$\boldsymbol{K_{r3}}$	150
$\boldsymbol{K_{r5}}$	300

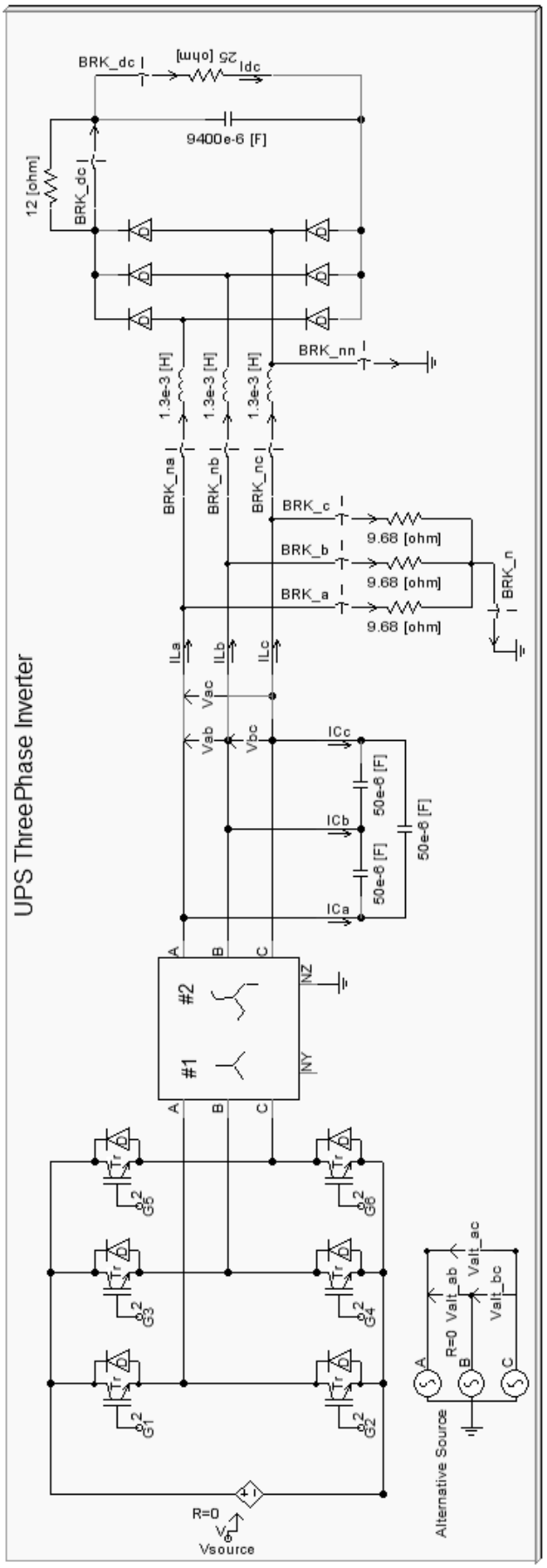

Figure 3-14. Three-phase inverter simulated circuit.

3.3.1. Continuous Time Domain

As discussed in last section, one part of the simulation stage was dedicated to emulate a control topology in continuous time. This represents the most appropriated way to validate theoretical discussions, since there were carried out in continuous domain. The importance of this simulation is to assess effectiveness of proposed topology without considering effects of discrete approximations.

It is possible to neglect effects of discretization control blocks performed by simulator if a fast integration period is set. An integration period 97 times faster than sampling period was used in this simulation.

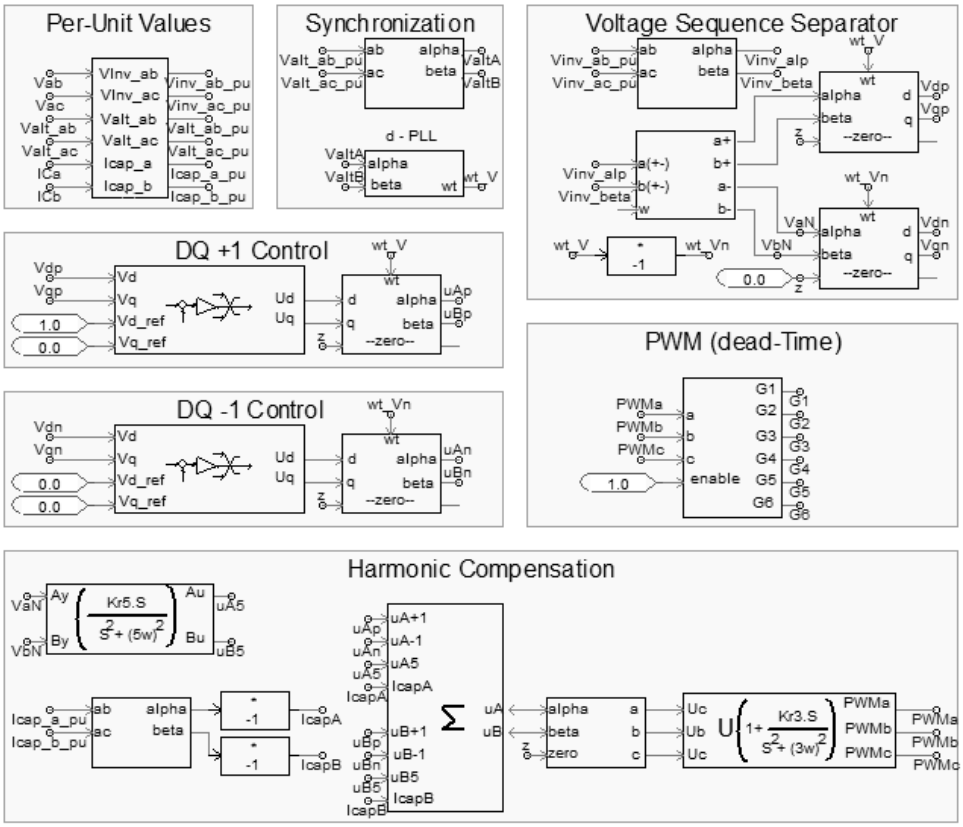

Figure 3-15. Simulated synchronous voltage control using PSCAD functional blocks.

Figure 3-15 shows a block diagram with main modules of simulated controller. In addition to control blocks and signal conditioning, there are dead-time blocks on trigger signals. On the other hand, positive/negative sequences, were built using parallel type PI controllers. Finally, HC blocks were simulated using second order transfer functions.

The instantaneous behavior of inverter output-voltage is shown in Figure 3-16. Instead of comparing sinusoidal waves, magnitude of alpha-beta vector was chosen, this magnitude is given by

$$\left|\overrightarrow{v_{\alpha\beta}}\right| = \sqrt{{v_\alpha}^2 + {v_\beta}^2} \quad . \tag{3.22}$$

Figure 3-16 shows that controlled system responds without overshoot and stabilizes at a time of approximately 30ms. This shows great similarity to expected settling time (33.5ms).

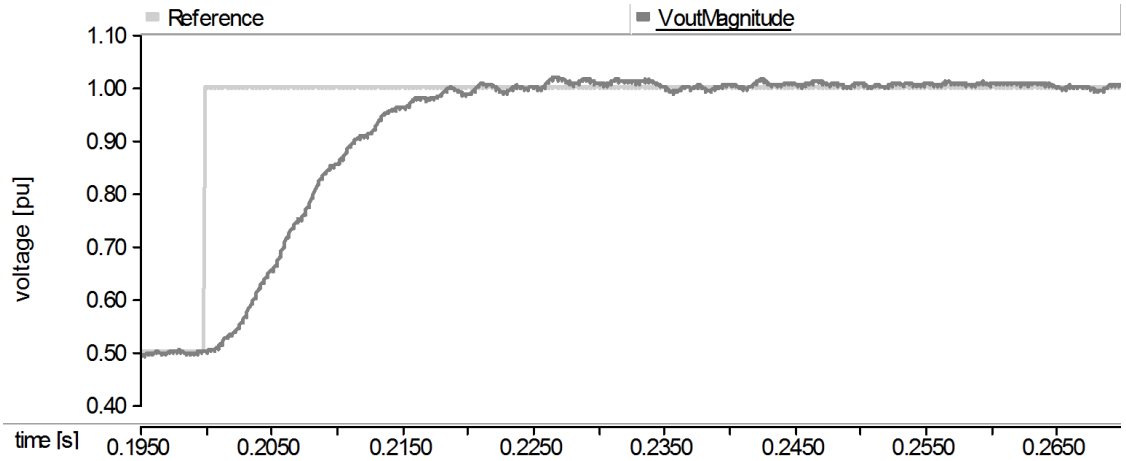

Figure 3-16. Synchronous voltage control response on reference step (simulation).

Results shown in Figure 3-16 are very close to expected results. However, changing reference magnitude is not a relevant scenario in voltage control of UPS inverters. Therefore, primary analysis should be assessing output-voltage behavior on connections with different kind of load (Figure 3-17, Figure 3-22, Figure 3-23 and Figure 3-24).

Figure 3-17 shows the response of controller to connection and disconnection of nominal three-phase load. In this scenario the system successfully retrieves the magnitude of output voltage without overshooting and settling time of 30ms approximately. This is an expected result as presented in (3.20), dynamics of disturbance is the same as output-voltage dynamic (3.19).

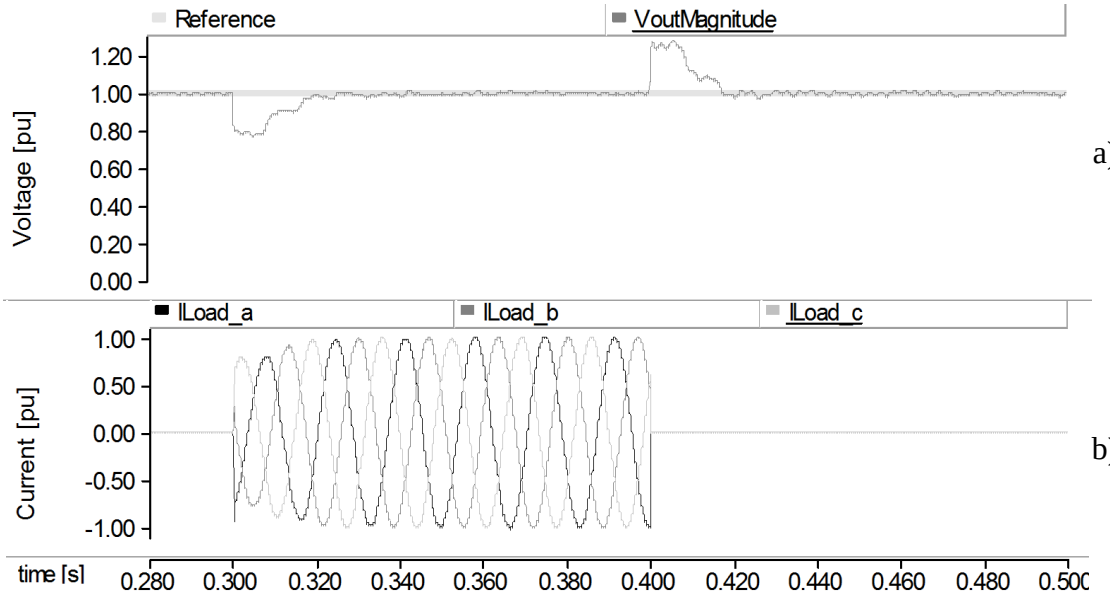

Figure 3-17. Synchronous voltage control response on connection and disconnection of a three-phase linear load (simulation), a) Reference and output voltage, b) load currents.

3.3.2. Discrete Time Domain

The final goal of this controller is to be implemented in a DSP system as mentioned in chapter 2. Thus, discretization of all control blocks is a necessary task that can be performed using several types of mathematical approximations. This process can introduce quantization errors and delays to the system. To avoid those issues, simulation tools can be used to test discrete codes and algorithms.

Hardware in the Loop (HIL) is usually adopted to perform discrete code evaluation. However, this option involves a communication protocol between DSP and simulator, which significantly decreases simulation speed. This work proposes an alternative system to improve simulation time.

Hardware in the Loop Alternative Option

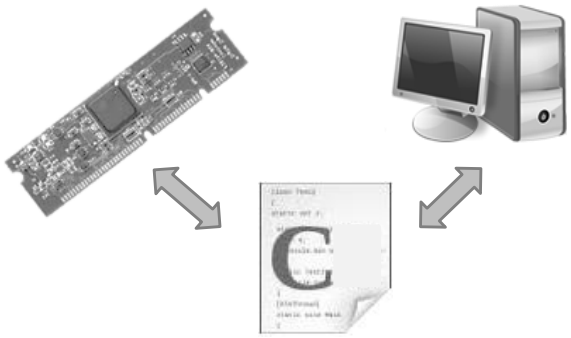

Figure 3-18. Double function of proposed program code structure.

Using high-level programing languages such as *C* and *C++* makes it possible to conceive a structured programming, separating peripherals configuration and control algorithms. This allows using the same tested code in simulation and real prototype.

The Figure 3-19 shows the flowchart of proposed programming structure. Highlighted area shows the common code for both simulation and implementation in DSP. This highlighted area represents 70% of program code. Figure 3-20 shows simulation blocks used in PSCAD for discrete approximation of proposed controller. In this case C language and GNU Fortran compiler were used.

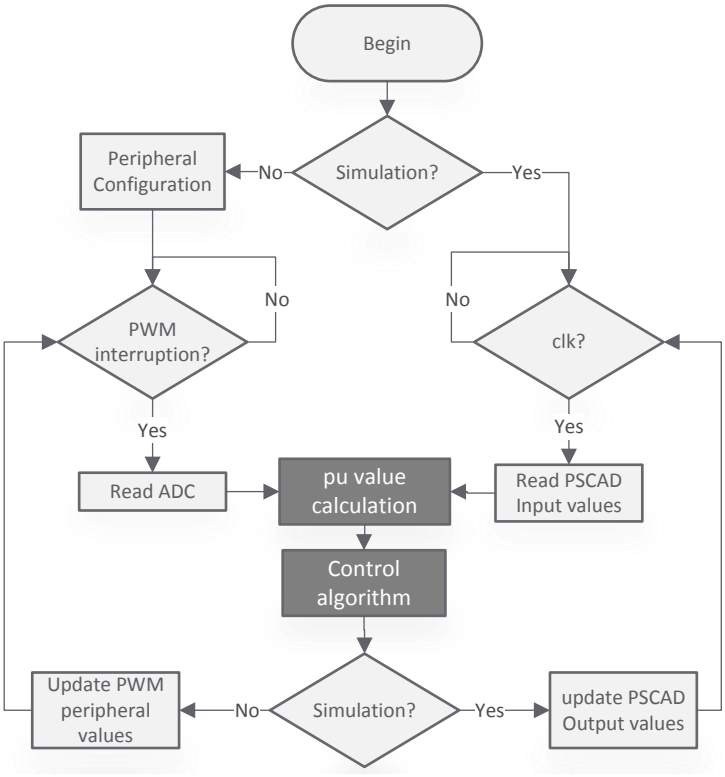

Figure 3-19. Proposed program structure flowchart.

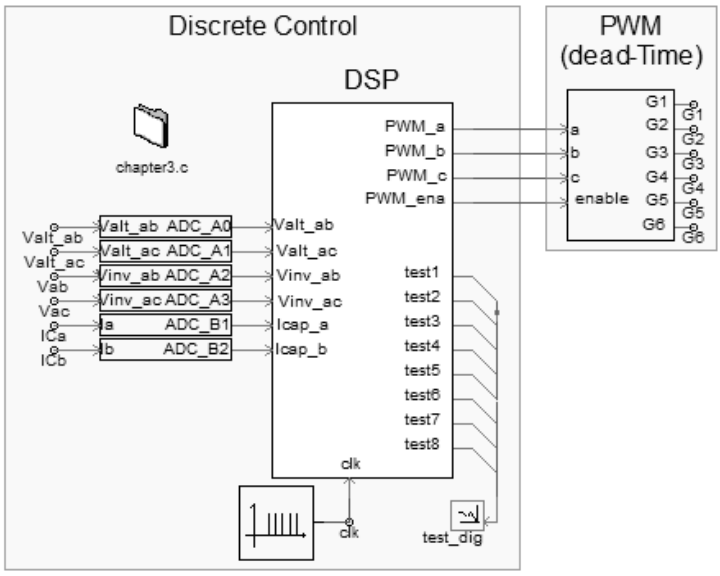

Figure 3-20. Simulated discrete synchronous voltage control using PSCAD interacting with C code.

Control Behavior of the Proposed Discrete Approximation

Figure 3-21 presents the instantaneous open-loop behavior of output-voltage magnitude. Thus it is possible to observe effects of different loads on wave forms.

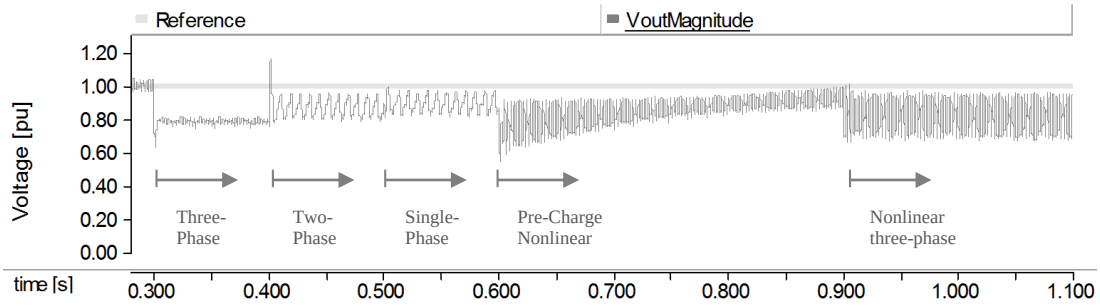

Figure 3-21. Instantaneous behavior of three-phase inverter in open loop (simulated output voltage).

Behavior of synchronous controller with different kind of loads is presented in Figure 3-22. Proposed controller retrieves voltage value back to its reference value in unbalanced loads cases. Nevertheless, plant behavior now seems to describe an underdamped dynamic. However, a more detailed analysis shows that exhibited oscillations corresponds to twice electrical-network frequency, which means negative-sequence component as seen in Figure 3-22d. In addition, oscillation only exists during time it takes negative-sequence controller to eliminate such disturbance as shown in Figure 3-22a.

Figure 3-22c shows dynamics of positive-sequence component, which behaves according to theoretical calculation. Figure 3-22d shows dynamic behavior of negative-

sequence controller, which does not have a similar dynamic compared to the one established by theoretical calculations. This difference is due to small value of negative-sequence magnitude. This turns signal to noise ratio as a major disturbance to control system. However, negative sequence controller is able to reach voltage reference in less than 100ms with an overshoot lower than 10%, which is within requirements set by IEC and IEEE standards.

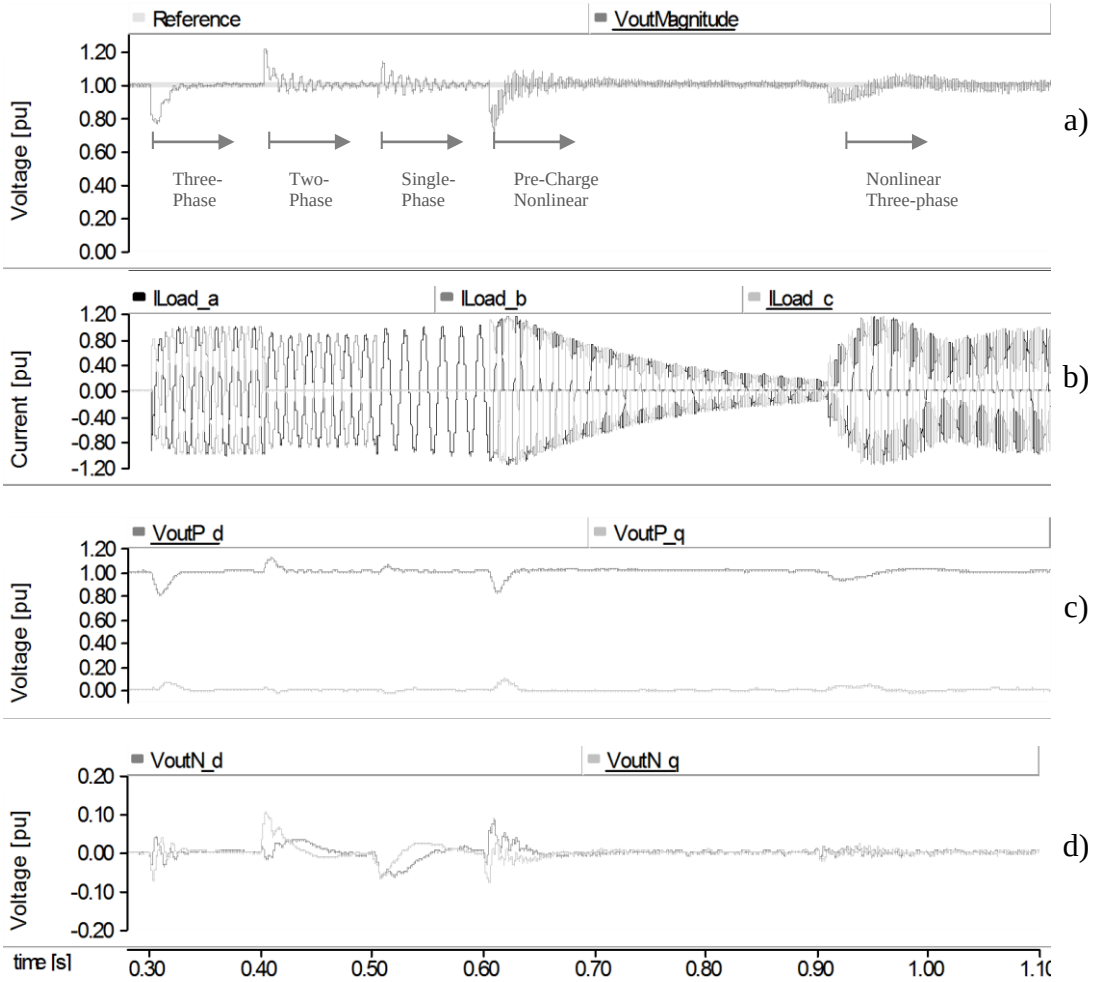

Figure 3-22. Three-phase inverter instantaneous behavior with synchronous voltage control (simulation), a) Output voltage, b) Load current, c) Positive-sequence output voltage, d) Negative-sequence output voltage.

The Figure 3-23 shows output-voltage harmonics spectrum using different types of loads. Nonlinear load represents the worst case scenario for harmonic pollution. However a proposed synchronous controller regulates harmonics values according to IEC and IEEE standards as shown in Figure 3-23e.

Transient behavior of total harmonic distortion (THD), is not mentioned by international standards. However is possible to observe through simulation the instantaneous value of THD variable as shown in Figure 3-24, the proposed synchronous controller achieves regulating value of harmonic distortion in less than 100ms.

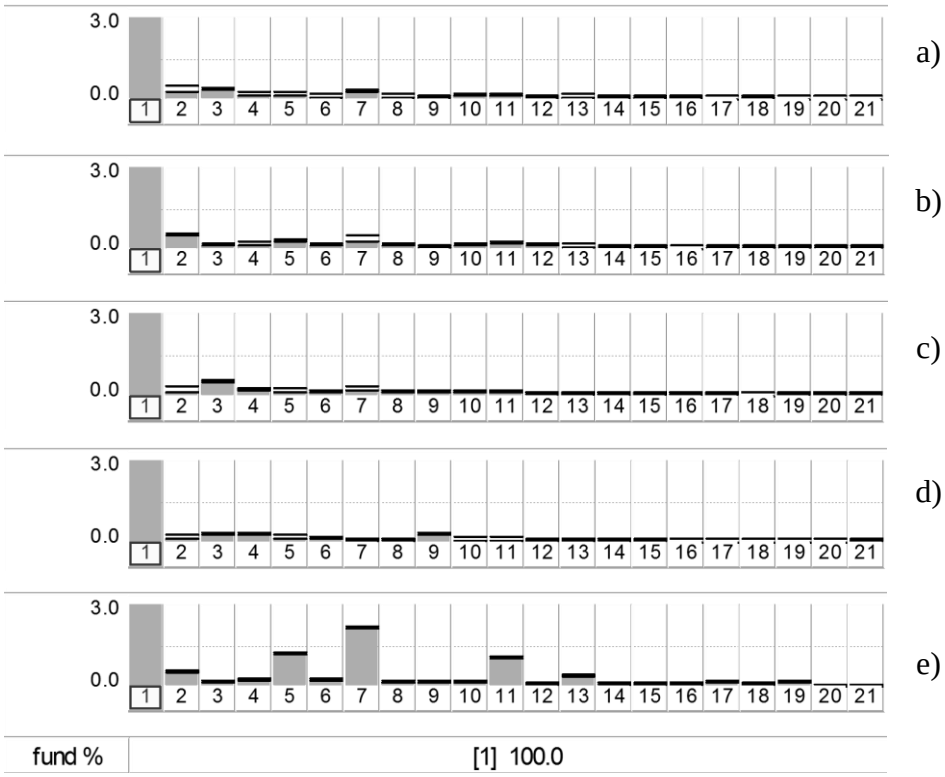

Figure 3-23. Output-voltage harmonic spectrum with synchronous voltage control (simulation), a) none-Load, b) Three-phase linear load, c) Two-phase linear load, d) single-phase linear load, e) Three-phase none-linear load.

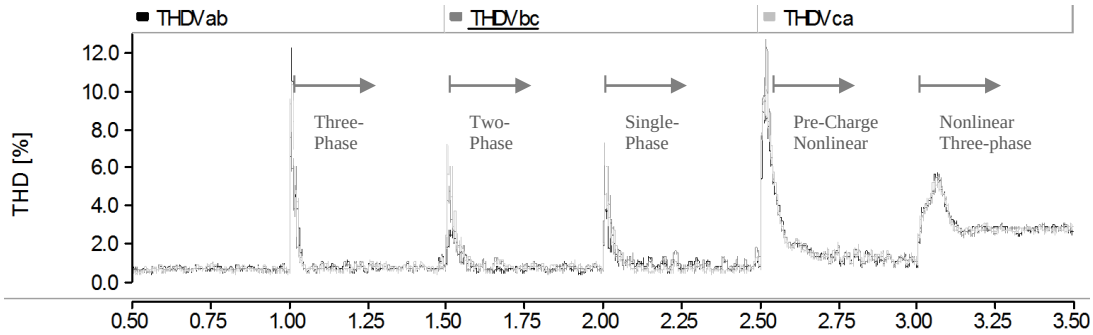

Figure 3-24. Harmonic compensators transient response, output voltage THD.

Results obtained in simulations denote that theoretical analysis is consistent through tests. This means discretization of control blocks successfully achieves continuous-time analysis.

3.5. Experimental Confirmation

Experimental validation scenario

- 3.6kVA prototype of three-phase inverter.
- Control system was implemented in DSP "Concerto F28M35H52c" chip from Texas Instrument.
- Data collection and measurement of electrical variables was performed using an oscilloscope "Tektronix TPS2024", and a power quality meter "ION7650".
- DEBUG tools provided by "Code Composer Studio V6.0.1" were used to capture some internal measurements on DSP.

Main features of prototype are summarized in Table 2-1.

Table 3-3]. Prototype setup.

Item	Value
$\boldsymbol{Power}$	3.6kVA
Switching frequency	5kHz
Input voltage (DC)	130V
Output Voltage (AC)	$220V_{RMS}$
Output frequency	$60Hz$
$\boldsymbol{K_p}$	0.000001
$\boldsymbol{K_i}$	50.93
$\boldsymbol{K_{r3}}$	10
$\boldsymbol{K_{r5}}$	100

Reference voltage step

Figure 3-25 shows vector magnitude of alpha-beta component (3.20). This value is calculated online and accumulated as a vector in the DSP. This figure shows that controlled system behaves according to results specified by design criteria, i.e. no overshoot and settling time of approximately 30ms. This result validates theoretical method of controller parameters calculation. In addition it shows strong similarity to results presented by simulations.

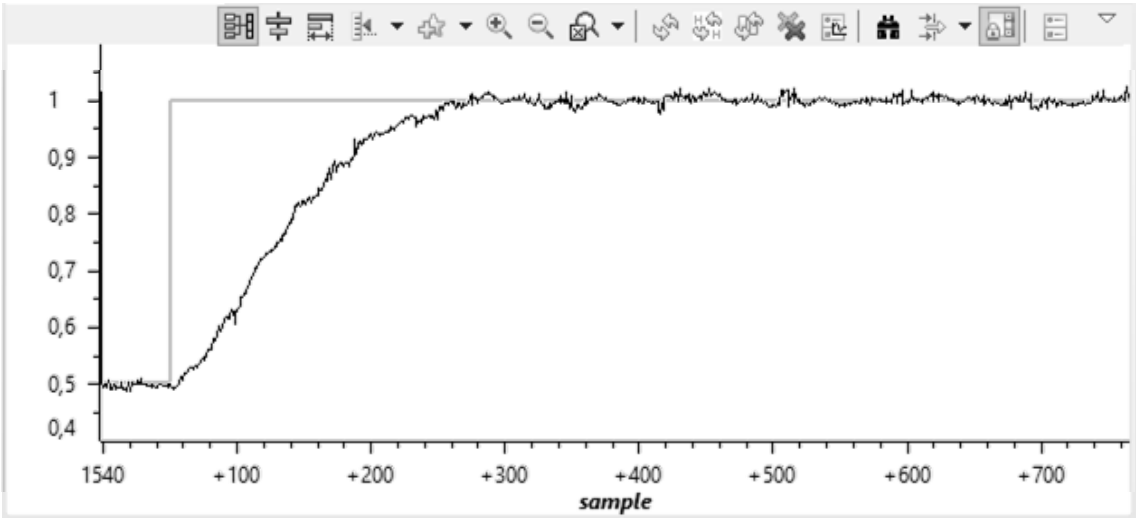

Figure 3-25. Synchronous voltage control response on reference step.

Connection and Disconnection of Nominal Load

Figure 3-26 shows Inverter Behavior to connection and disconnection on linear and balanced three-phase load. This experimental results show that proposed fundamental-frequency control rejects load perturbations within calculated dynamic criteria.

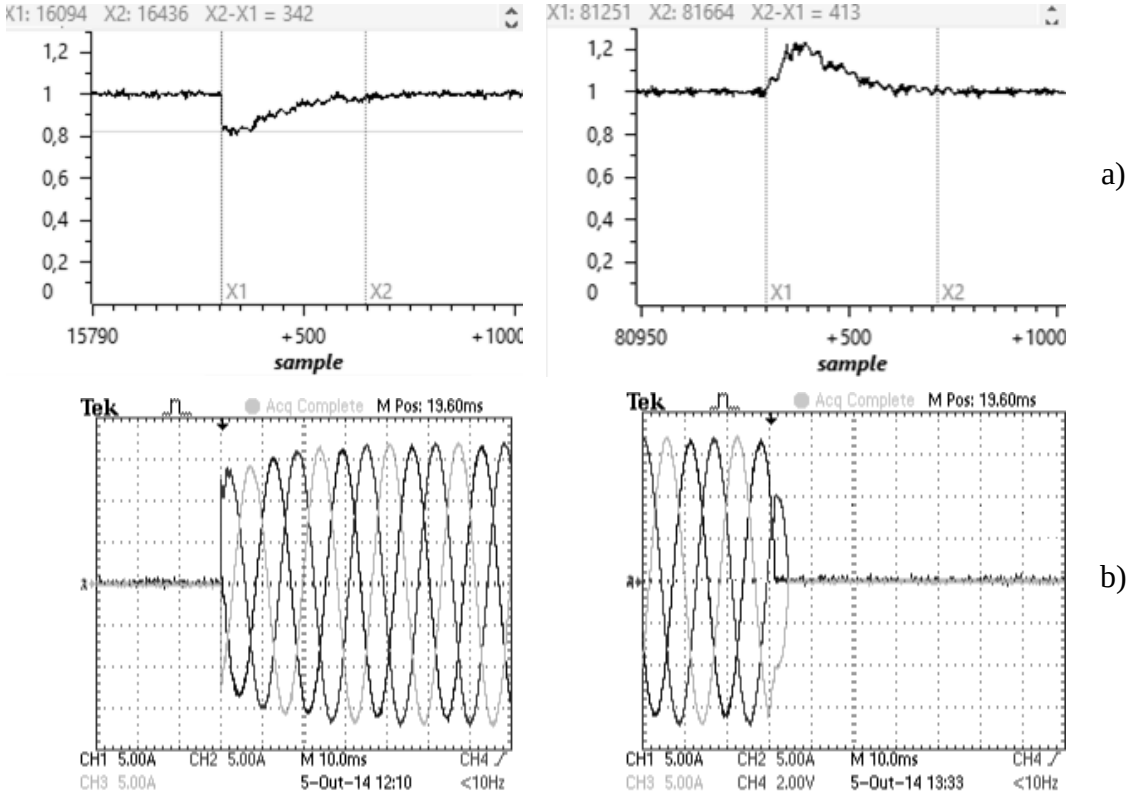

Figure 3-26. Synchronous voltage control response on connection and disconnection of a three-phase linear load, a) output voltage magnitude, b) load currents.

Unbalanced Load

In order to analyze the behavior under unbalanced load a two-phase linear load was connected on the inverter output. This load represents 66% of the inverter nominal power. Figure 3-27a presents the instantaneous alpha-beta vector magnitude. It is possible to see on this figure that none second harmonics are present. It means that the controller effectively eliminated the negative sequence component.

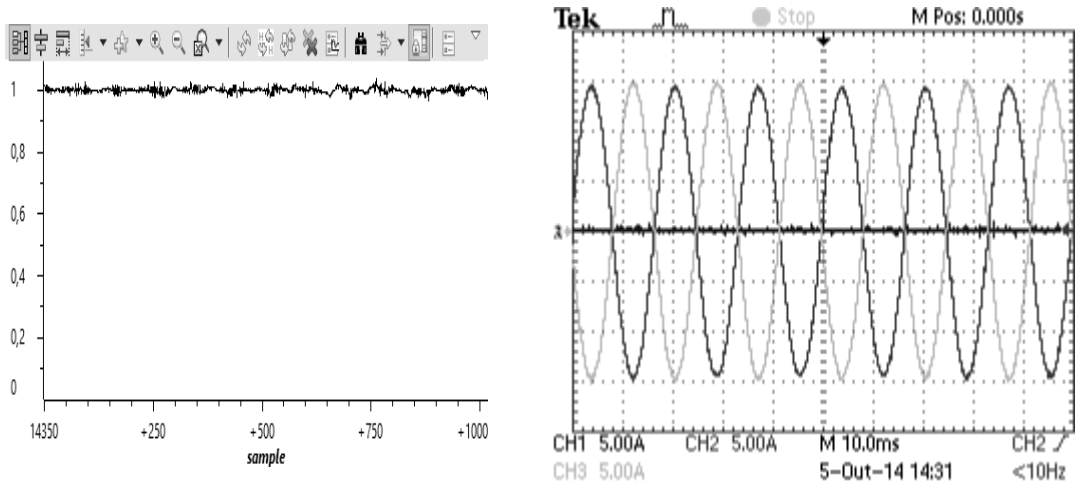

a) b)

Figure 3-27. Synchronous voltage control with unbalance linear load, a) output voltage magnitude, b) load currents.

Despise of result shown in Figure 3-27 it is interesting to present how significant is the contribution of controller to get this results. That's why Figure 3-28 presents a comparison of inverter behavior under unbalanced load when controller is turn on and off. It is important to mention that only *P&N control* and *Series HC* blocks where used in this test. It means that 5 harmonics will be in open loop.

Figure 3-28a shows that unbalanced load affects significantly the inverter voltage when control is turned off, i.e. voltage amplitude decrease on those phases where load are connected. Also phase angle is shifted more than 6° of the ideal 120°. On the other hand, when controller is turned on, an almost perfect balanced voltage appears in Figure 3-28b.

The effects of the proposed series HC tuned for 3rd harmonics is presented in Figure 3-28c and Figure 3-28d. where it is possible to see how 3rd harmonic is completely eliminated when controller is turned on.

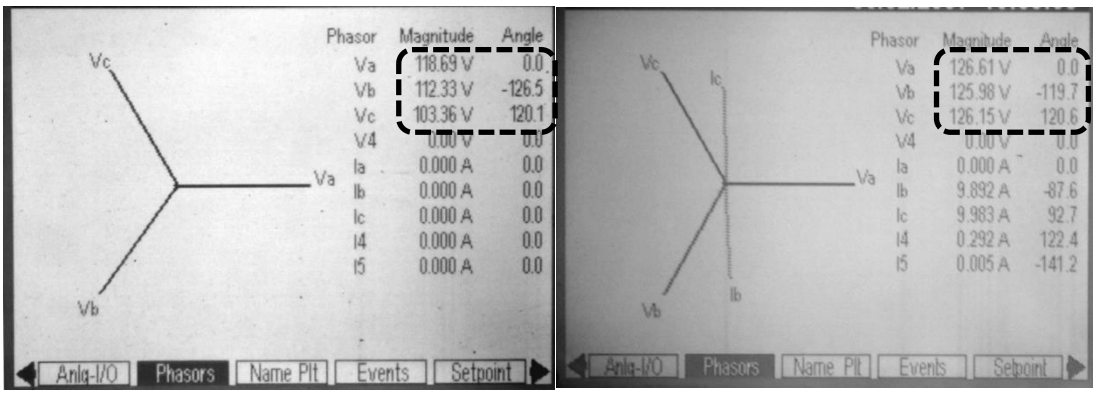

b) c)

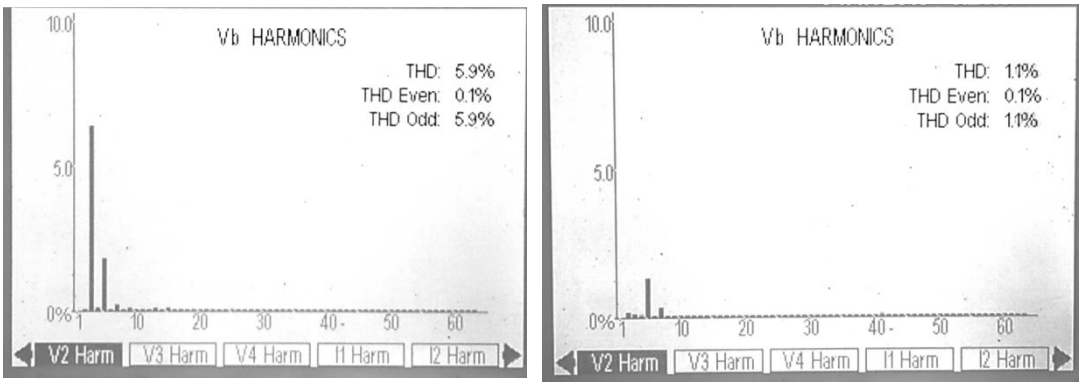

c) d)

Figure 3-28. Controller contribution under unbalanced load a) Phasor diagram (Off), b) Phasor diagram (On), c) Harmonic spectrum (Off), d) Harmonic spectrum (On).

Nonlinear Load

As mentioned in chapter 2. Rectifier with output capacitor is a nonlinear load which represents the biggest challenge to control system for an UPS inverter. Figure 3-29a shows the voltage waveform when this type of load is connected. The output voltage THD in this case is 2.6% which is below than specified by the IEC and IEEE standards.

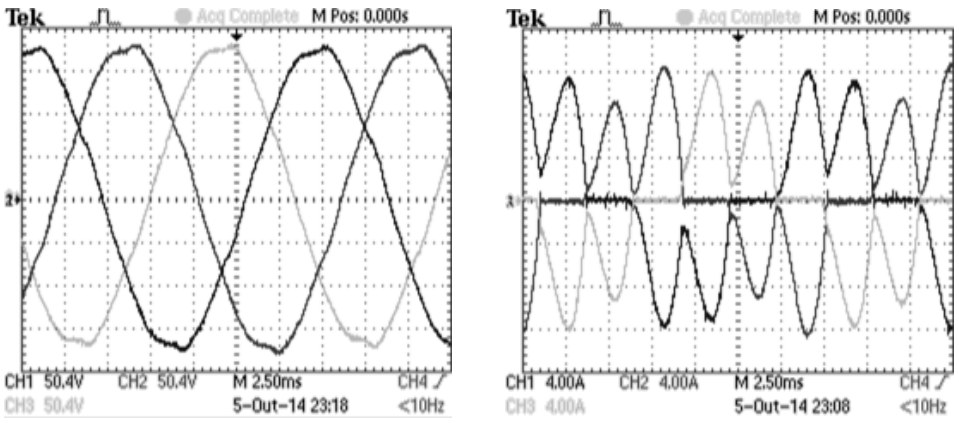

a) b)

Figure 3-29. Synchronous voltage control with none-linear load, a) output voltage, b) load currents, c) voltage harmonic spectrum. d) Voltage and current THD.

As performed in last section, it is interesting to observe the contribution of the parallel HC block to reduce 5th harmonic. For this reason Figure 3-30 shows a comparison of harmonic spectrum when parallel HC block is turned on and off. It is possible to observe that 5th harmonic is reduced almost 73%. It´s worth mentioning that 7th harmonic increases when controller is turned on but still accomplish IEC and IEEE restrictions. That's why proposed control topology doesn´t include any harmonic compensation tuned in 7th harmonic.

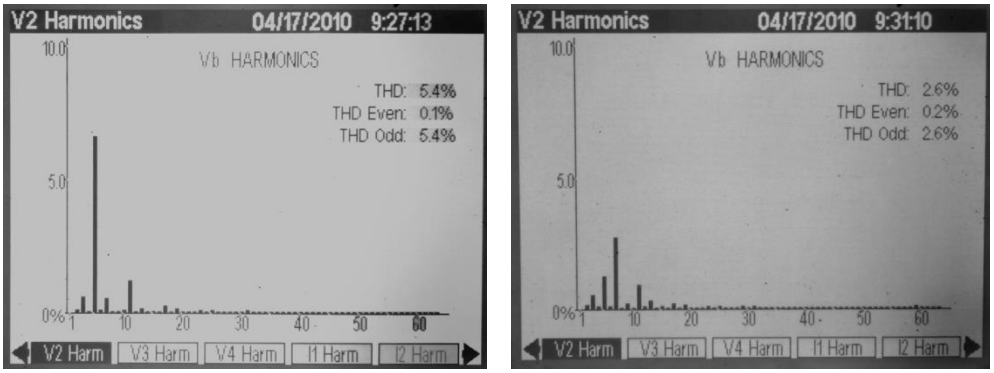

a) b)

Figure 3-30. Controller contribution under nonlinear load a) Harmonic spectrum (controller Off), b) Harmonic spectrum (controller On).

3.6. Partial conclusions

- Calculated parameters for fundamental frequency controller were successfully established with expected dynamic. A response with a 19.1% error in settling time was achieved.
- Inverter output voltage remains balanced despite the connection of an extremely unbalanced load.
- HC in the proposed topology gets the harmonic magnitudes significantly below from requirements imposed by the IEC and IEEE standards.
- There is a large difference in values of harmonic compensating gains between simulation and experimental results.
- Although voltage derivatives and current terms were ignored in decoupling loops, results show no significant impact of the inverter behavior (compared with theoretical analysis).

- Dynamics of positive sequence voltage behaves according to theoretical calculation of controller parameters.
- Dynamics of negative sequence voltage does not present a similar dynamic to theoretical calculated. However, negative sequence controller is able to reach voltage reference in less than 100ms with an overshoot lower than 10%, which is within requirements set by IEC and IEEE standards.

Contributions to this chapter were published and presented at the international conference [1].

Chapter 4 - Stationary Voltage Control with P+ Resonant Controller and Selective Harmonic Compensation

In this chapter a control strategy that can offer a dynamic behavior similar to strategy on Chapter 3 will be presented. However, said strategy is proposed by replacing the synchronous PI by Stationary P+Resonant controllers thus, giving an extra advantage by working all control blocks in the same reference axis. This allows the mathematical modeling of the plant and a detailed analysis of the closed-loop behavior of the system.

The experimental and simulation results demonstrate the effectiveness of the proposed strategy. Detailed development of the mathematical expressions presented in this chapter are shown on appendix C.

4.1. Control Topology Overview

The control strategy proposed in this chapter as in previous chapters, is based on solving each problem presented in the behavior of the output voltage caused by the connection of different types of loads. As seen in Figure 4-1, the resonant compensators and the capacitor feedback current was preserved from the proposal presented in Chapter 3. The fundamental frequency control has been redesigned using a Resonant Proportional controller in alpha-beta stationary axis. Thus achieving zero steady-state error for tracking sinusoidal reference signal [43] [44] [45] [35]. A detailed analysis of stationary fundamental-frequency voltage control will be presented below.

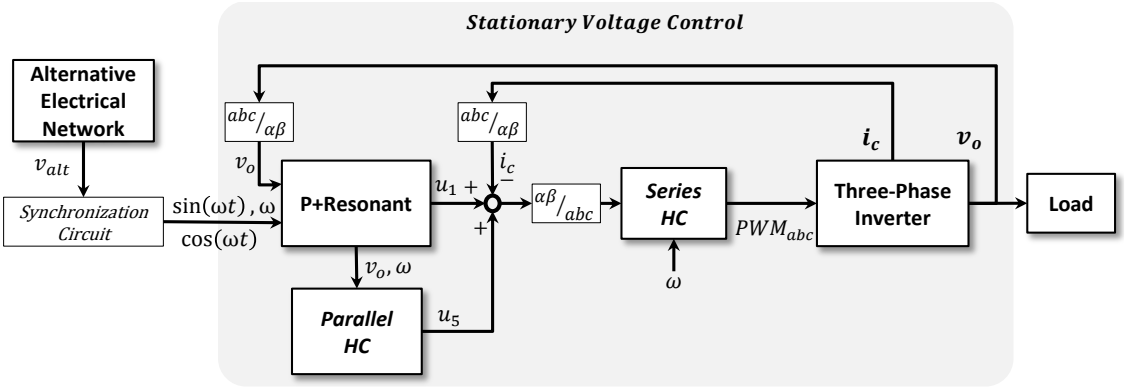

Figure 4-1. Proposed stationary control strategy high-level block diagram.

4.1.1. Stationary P+Resonant Voltage Control

The main goal of the fundamental-frequency controller is to ensure constant amplitude in the output-voltage signal and a reduction or elimination of the negative-sequence component caused by the connection of unbalanced loads as well. Reference signals and voltage measurement are sinusoidal waveforms, representing an instantaneous time varying magnitude. Classical control systems (LTI) do not have an adequate response for these kind of signals and do not allow zero steady-state error [40]. In addition, when they are forced to track sinusoidal references, they normally use large gain values that may lead the system to instability [5] [40].

Problems presented above can be solved using control systems in synchronized reference axes as shown in Chapter 3. However, as presented in [44] [46] [43] [47] [48] [45] [35] [40] [37], it is possible to conceive a system with infinite gain in a specific frequency using sine or cosine model of Laplace transform, as seen in (4.1) and (4.2)

respectively, i.e. it is possible to emulate the behavior that provides an integrator in a constant signal, with sinusoidal type entries, thus ensuring zero steady-state error for an input signal whose frequency is equal to the resonance frequency of the controller. Henceforth the resonant proportional controller will be called as P+Resonant. The Laplace form is found to be

$$F_{(S)} = \frac{\omega}{s^2+\omega^2} \quad , \tag{4.1}$$

and

$$F_{(S)} = \frac{S}{s^2+\omega^2} \quad . \tag{4.2}$$

Cosine form (4.2) is preferred since absence of zero at S = 0 in (4.1) causes a relatively slow response [44], further enhances system stability [39]. The transfer function of the P+Resonant controller is found to be

$$C_{(S)} = K_1 + \frac{k_2 S}{s^2+\omega^2} \quad , \tag{4.3}$$

Where:

- ω is the resonant frequency.
- k_1 and k_2 are the proportional and integral gains.

There is a relation between synchronous PI controller shown in Chapter 3 and P+Resonant controller [47] [48]. Transfer function of P+Resonant controller including this relationship is given by

$$C_{(S)} = K_p + \frac{2k_i S}{s^2+\omega^2} \quad . \tag{4.4}$$

P+Resonant controller in alpha-beta stationary axes replaces the two synchronous PI controllers, which compensate positive and negative sequences [38]. Furthermore, it is possible to treat each axis independently, since they don't have cross-coupling [40]. Given the characteristics described above it is possible to include P+Resonant as the fundamental frequency controller in voltage control strategy for three-phase UPS inverter. Figure 4-2 presents a block diagram of scheme used and Figure 4-3 presents the frequency response.

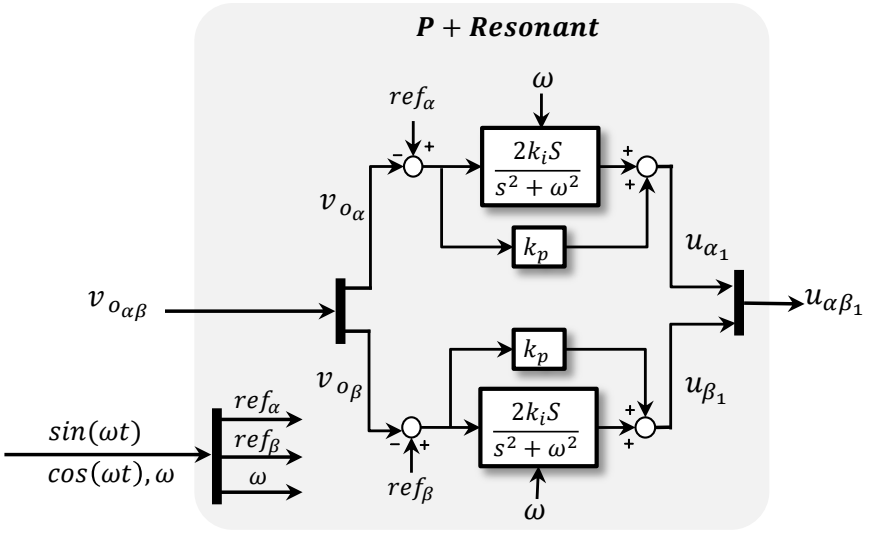

Figure 4-2. Proposed fundamental stationary voltage controller detailed block diagram.

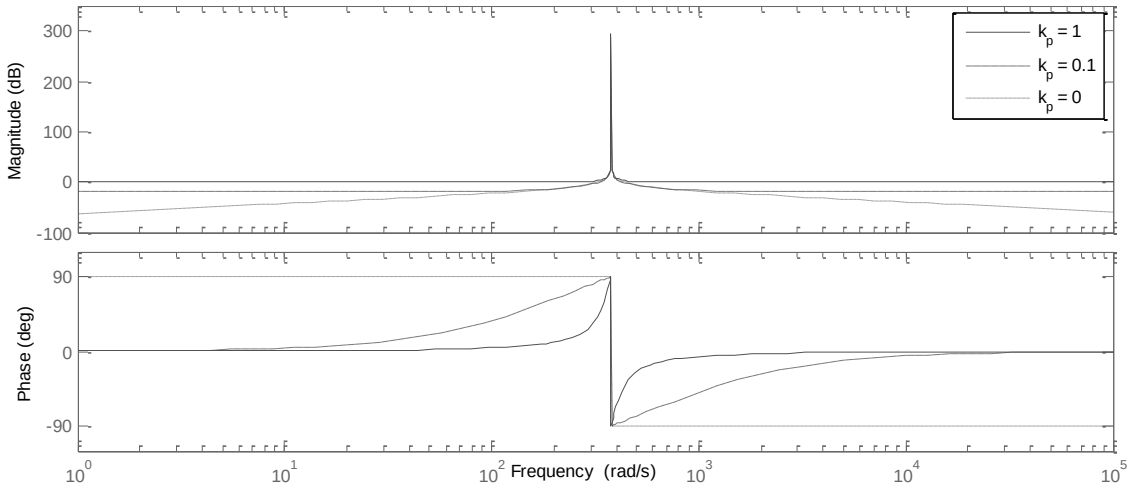

Figure 4-3. P+Resonant controller frequency behavior.

Discrete implementation

The transfer function of P+Resonant controller shown in (4.4) which describes a second-order system with a dominant frequency ω. It can be approximated in discrete time by several methods such as: zero-order hold, first-order hold, forward Euler, backward Euler, Tustin, Tustin With prewarping, zero-pole matching and invariant impulse, among others.

Each of these methods can lead to different effects, such as displacement of poles and zeros, i.e. the shift in resonance frequency can reduce controller effectiveness to ensure zero steady-state error.

A detailed analysis of these approximation techniques used in resonant controllers are performed in [39] .Which points that the most suitable discrete representation of

P+Resonant controller is achieved when expressing transfer function(4.4), as an iteration of two first order transfer functions. In addition, it is encouraged to use two different methods of approximation (forward-Euler and Backward-Euler), as presented in Figure 4-4. Difference equation is given by

$$\begin{cases} y_{(n)} = 2k_i T_s u_{(n-1)} + T_s v_{(n-1)} + y_{(n-1)} + k_p u_{(n)} \\ v_{(n)} = -\omega^2 T_s y_{(n)} + v_{(n-1)} \end{cases}, \qquad (4.5)$$

where:

- $\boldsymbol{T_s}$ represents sample period.
- $\boldsymbol{y}$ and $\boldsymbol{u}$ are output and input respectively.
- $(\boldsymbol{n})$ and $(\boldsymbol{n-1})$ represents current and previous sample respectively.
- $\boldsymbol{\omega}$ represents controller resonance frequency.

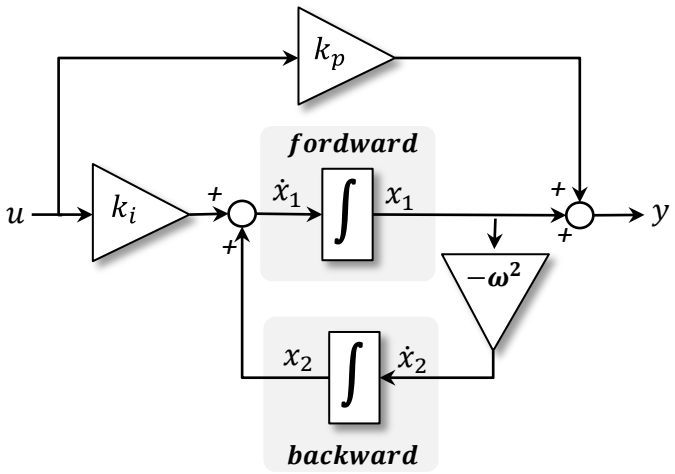

Figure 4-4. P+Resonant controller block diagram.

4.1.1. Stationary Voltage Control with Selective Harmonic Compensator and Capacitor Current Feedback Topology

Based on information presented above it is possible to construct a control strategy using the P + Resonant controller in alpha-beta reference axes, and applied to handle output voltage of a three-phase UPS inverter. The harmonic compensators (series/parallel) and capacitor feedback current have the same characteristics as described in Chapter 3. Figure 4-5 presents a detailed block diagram of proposed control topology.

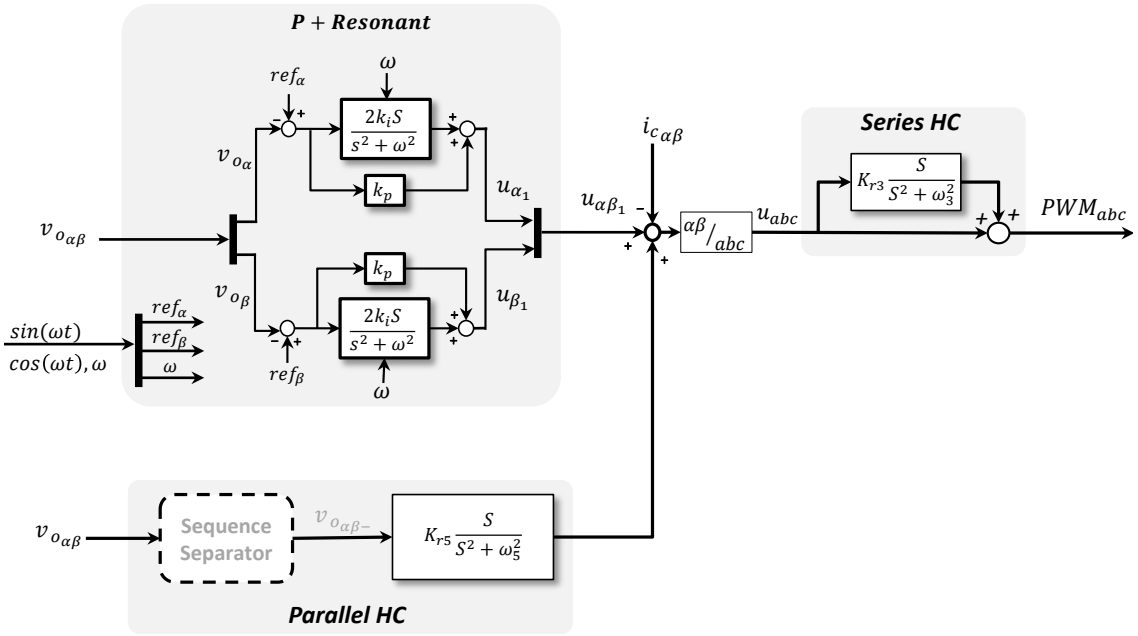

Figure 4-5. Proposed stationary voltage control topology detailed block diagram.

. Figure 4-5 presents a diagram where in "parallel HC block" was incorporated in a component sequence separator block in the input of HC. The purpose of this block is to only use the information of the negative sequence for removal of the 5th harmonic. Improving the Signal Noise Ratio (SNR), i.e., from the viewpoint of the 5th harmonic, the positive sequence of fundamental component represents a magnitude hundreds of times greater than amplitude of interest.

An additional advantage of using resonant controllers within the proposed control topology is that now, the whole system is in the same reference axis. This facilitates theoretical analysis, especially interaction between fundamental-frequency controller and HC blocks.

Below a detailed analysis of open and closed-loop model of the proposed control strategy are presented.

4.2. Mathematical Modeling and Theoretical Analysis

As mentioned in previous chapter, the main idea of this section is to perform a mathematical description of the output voltage behavior. To perform this analysis an approach described in Section 3.2.1 will be used. It is possible to obtain the mathematical model of the system relative to the stationary alpha-beta axes using the per-phase

equivalent circuit shown in Figure 3-9. In addition a detailed study of the closed loop system can be achieved.

4.2.1. Mathematical Modeling

It is possible to find temporal representation of UPS inverter dynamics in stationary reference plane. This can be done performing a voltage and current analysis in per-phase equivalent circuit, and then using Clarke transformations. The expression is found to be

$$v_{in} = LC\frac{d^2v_{on}}{dt^2} + R_LC\frac{dv_{on}}{dt} + v_{on} + L\frac{di_{on}}{dt} + R_Li_{on} \quad , \tag{4.6}$$

where $n = \{\alpha_+ \quad \beta_+ \quad \alpha_- \quad \beta_-\}$

and:

- "v_{in}" represents synthesized voltage by DC/AC converter (system input).
- "V_{on}" represents output filter voltage. (system output).
- Expressions "x_+" and "x_-" represents positive and negative-sequence components respectively.

Using Laplace transform in (4.6) is possible to find transfer function of inverter output voltage as shown in (4.7). Figure 4-6, presents poles and zeros diagram of this mathematical model. An effect of load current on inverter output voltage in (4.7). Can be observed. This effect describes voltage sag when there is a current demanded by load. The open-loop transfer function is found to be

$$V_o = G_{vo}(s)V_o^* - G_{io}(s)I_o \quad , \tag{4.7}$$

where

$$G_{vo}(s) = \frac{K_{inv}}{(LCS^2+RCS+1)} \tag{4.8}$$

and

$$G_{io}(s) = \frac{(R+LS)}{(LCS^2+RCS+1)} \quad . \tag{4.9}$$

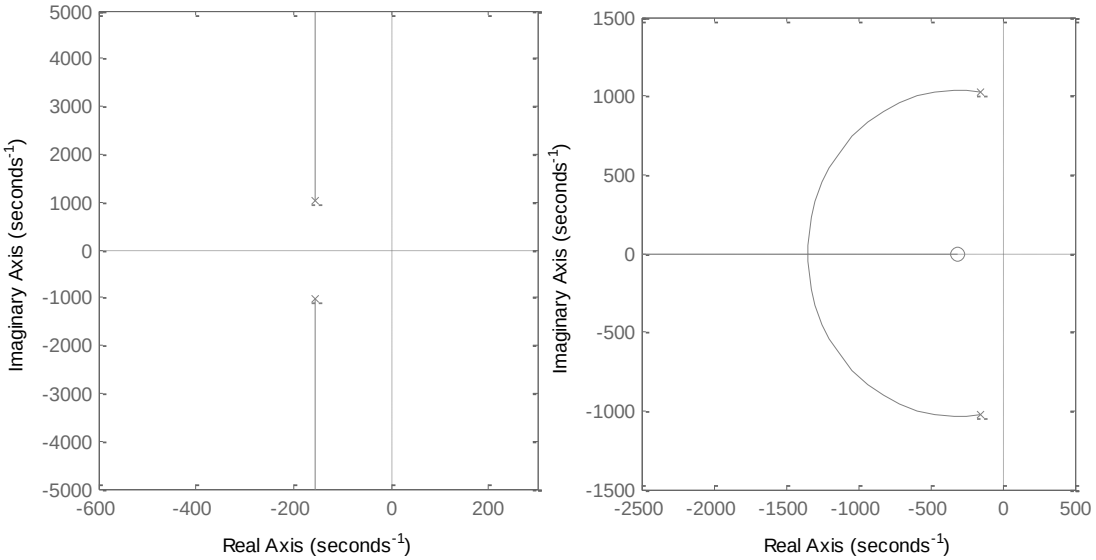

Figure 4-6. zeros and poles diagram (stationary model).

Current Capacitor Feedback

Current-capacitor information can be added to the open-loop Transfer function including current-capacitor feedback into (4.6). This mathematical expression is found to be

$$V_{o_{OL}} = G_{vo_{OL}}(s)V_o^* - G_{io_{OL}}(s)I_o \quad , \tag{4.10}$$

where

$$G_{vo_{OL}}(s) = \frac{K_{inv}}{LCS^2+RCS+1+K_{inv}CS} \tag{4.11}$$

and

$$G_{io_{OL}}(s) = \frac{(R+LS)}{LCS^2+RCS+1+K_{inv}CS} \quad . \tag{4.12}$$

Figure 4-7 shows pole-zero diagram of inverter model when current capacitor feedback is taken into account. This graph shows that introduction of current capacitor in the control loop shifts the poles of the system closer to origin. Moreover, since reference signal is not a constant signal it is important to know the plant frequency response. This behavior can be seen in Figure 4-8.

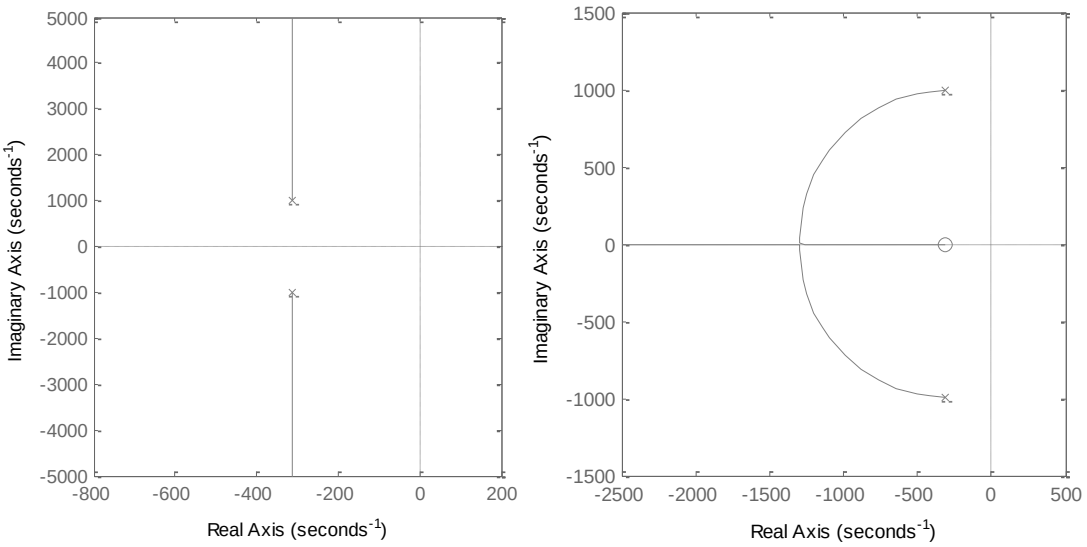

Figure 4-7. Stationary zeros and poles diagram.

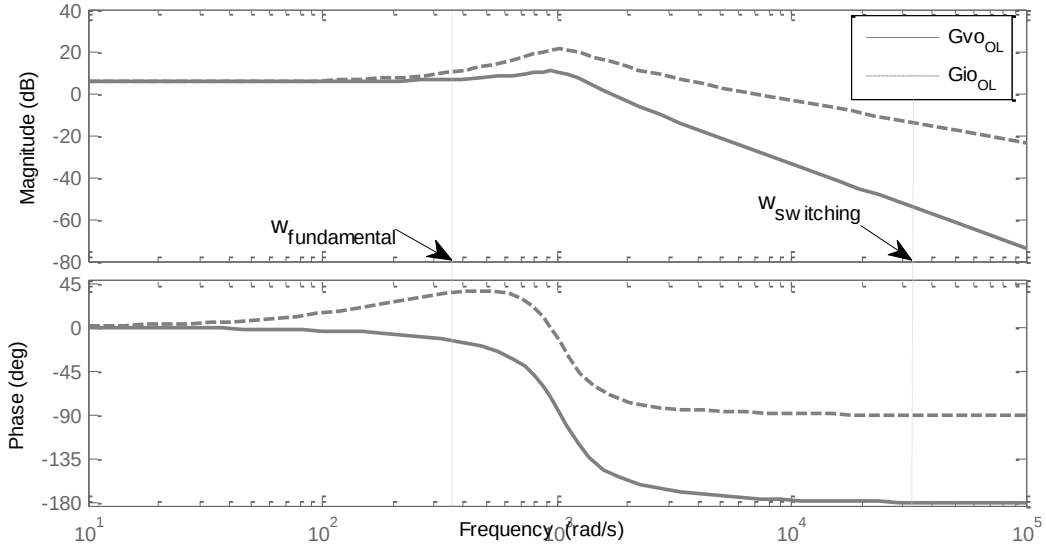

Figure 4-8. Stationary frequency behavior (open-loop), a) output voltage, b) load current disturbance.

Figure 4-9b shows the inverter dynamic behavior from an input step change, when there is no load connected. Figure 4-10c shows the inverter dynamic behavior when a load is connected into steady-state system. This dynamic behavior shows that the plant has a positive gain and also that the output voltage presents magnitude decrease when the load is connected.

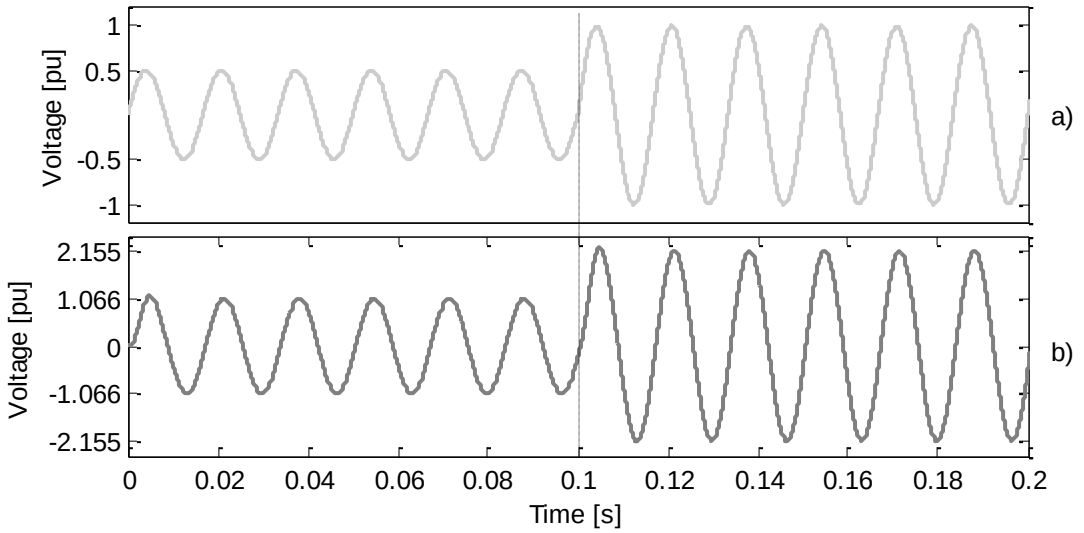

Figure 4-9. Stationary dynamic behavior, input step (open-loop), a) input step, b) model output.

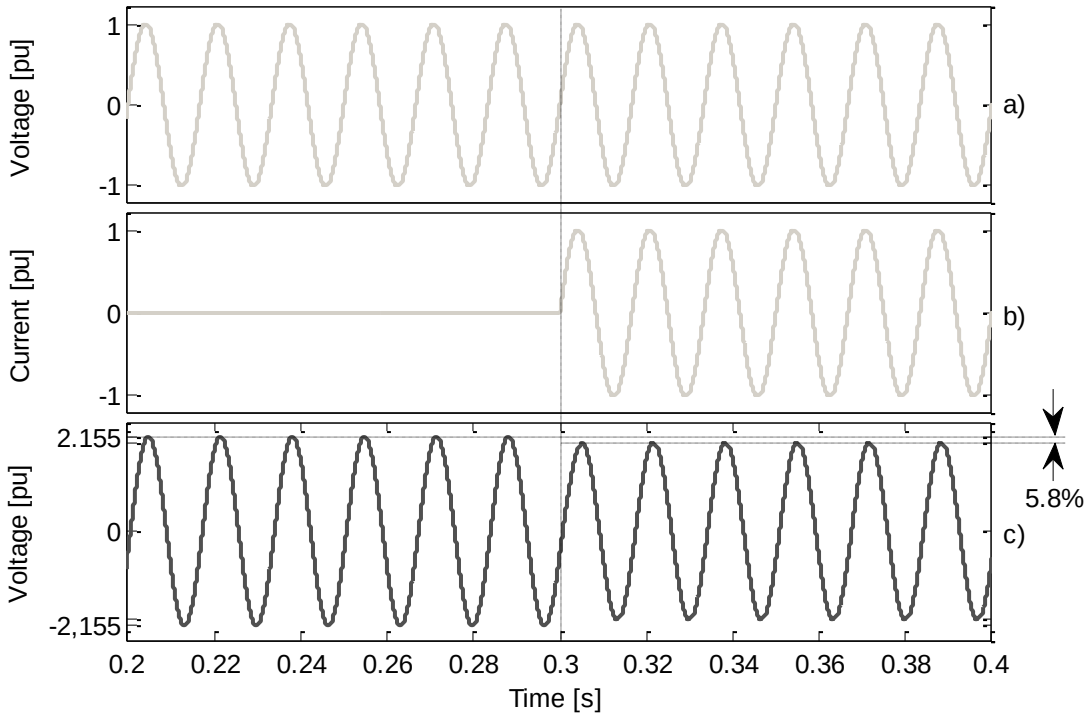

Figure 4-10. Stationary dynamic behavior, disturbance step (open-loop), a) input, b) disturbance step, c) model output.

Figure 4-9 and Figure 4-10 shows the qualitative behavior of the plant. Nevertheless it is possible to express the model of the plant (4.10) in the canonical representation, which allows to find some quantitative characteristics such as system gain (4.13), damping ratio (4.14), natural frequency of system (4.15), disturbance gain (4.16) and zero cutoff frequency introduced by disturbance (4.17). The mathematical expressions are found to be:

$$K_{V_o} = \frac{1}{LC} K_{inv} \quad , \tag{4.13}$$

$$\zeta = \frac{R_L}{2L\sqrt{\frac{1}{LC}}} \quad , \tag{4.14}$$

$$\omega_n = \sqrt{\frac{1}{LC}} \quad , \tag{4.15}$$

$$K_{I_o} = R_L \tag{4.16}$$

and

$$\omega_b = \frac{R_L}{L} \quad . \tag{4.17}$$

It is important to highlight that the inverter and disturbance gain vary respectively to their frequencies. However information presented in (4.13) and (4.16) are important because they allow the identification of the system parameters that are related to said gain values. But also is important to note that impact of disturbance in open loop is proportional to the inductor-resistance value.

4.2.2. Controller Parameters

Unlike Chapter 3, this chapter does not propose the calculation of the controller parameters. Instead, information presented by the authors in [43] who demonstrated a relationship between the parameters of a synchronous PI controller and a stationary P+Resonant controller will be used, i.e. k_p and k_i values used in this chapter correspond to those calculated in section 3.2.3.

4.2.3. Close loop behavior

Fundamental-Frequency Voltage Control

Information presented in Section 4.2.1, allow us to understand dynamic and frequency behavior of the plant. However it is important to evaluate the impact of closed-loop system in output voltage behavior. Closed-loop mathematical model of the plant, including fundamental-frequency controller is found to be

$$V_{o_{CL}} = G_{vo_{CL}}(s) V_o^* - G_{io_{CL}}(s) I_o \quad , \tag{4.18}$$

where

$$G_{vo_{CL}}(s) = \frac{K_{inv}\left(K_p S^2 + 2K_i S + K_p \omega^2\right)}{CLS^4 + \left(K_{inv} + R\right)CS^3 + \left(1 + K_{inv}k_p + CL\omega^2\right)S^2 + \left(2k_i K_{inv} + CK_{inv}\omega^2 + CR\omega^2\right)S + \omega^2 + K_{inv}k_p\omega^2} \quad (4.19)$$

and

$$G_{io_{CL}}(s) = \frac{(R + LS)(S^2 + \omega^2)}{CLS^4 + \left(K_{inv} + R\right)CS^3 + \left(1 + K_{inv}k_p + CL\omega^2\right)S^2 + \left(2k_i K_{inv} + CK_{inv}\omega^2 + CR\omega^2\right)S + \omega^2 + K_{inv}k_p\omega^2} \quad . \quad (4.20)$$

Figure 4-11 shows root locus of the controlled plant. In this diagram it can be observed that a pair of complex conjugated poles were introduced by controller. The effect of the aforementioned poles are shown in Figure 4-12, where a gain value of the controlled plant at controller resonance-frequency equals 1.

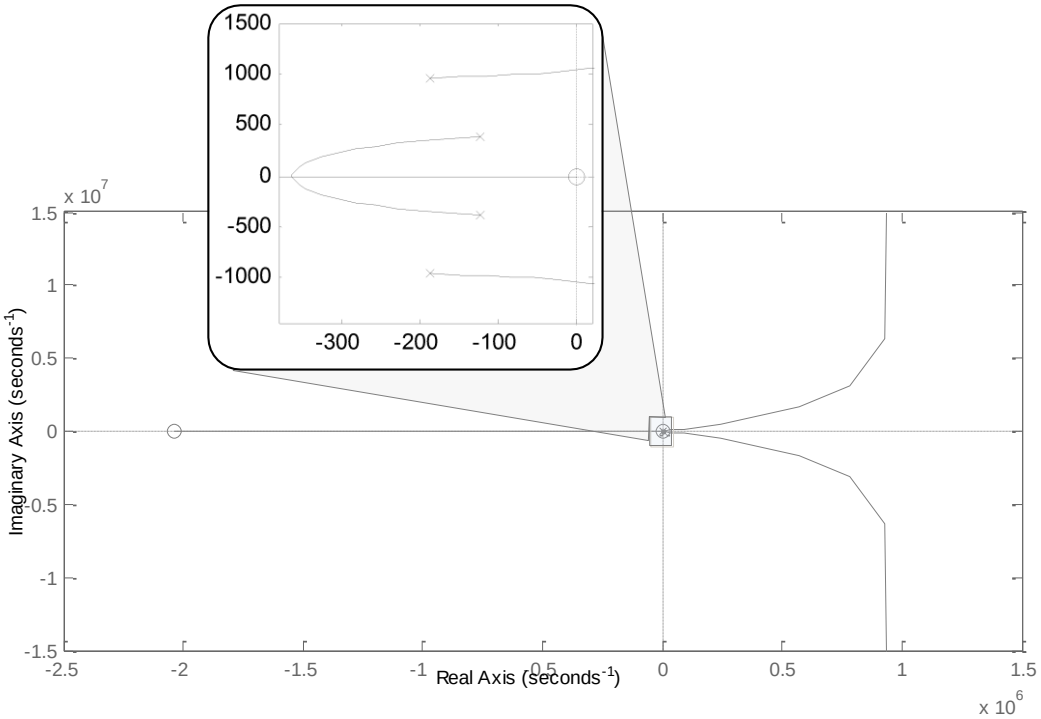

Figure 4-11. .Stationary control root locus diagram.

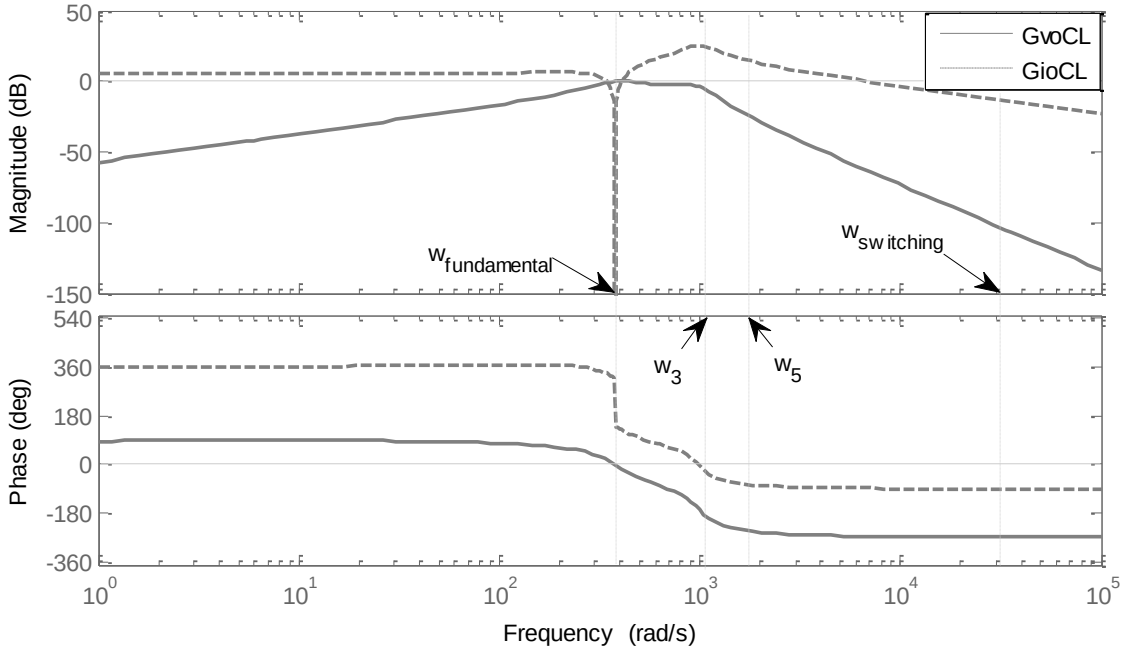

Figure 4-12. Stationary control bode diagram.

Fundamental-frequency voltage control also has an effect on the transfer function of the disturbance (4.20). This is called by some authors as "system stiffness" [5] [6], i.e. it is possible to determine the robustness of inverter voltage control by observing the dynamic behavior in disturbance transfer function.|

Harmonic Voltage Compensation

Effect of series and parallel harmonics compensation described in section 4.1 are represented in block diagram of Figure 4-13. Resonant 5th harmonic compensator was added in parallel to the fundamental-frequency control. A resonant 3rd harmonic compensator was added in series to controlled plant, as described in section 3.1.2. However, to facilitate the mathematical analysis, the following simplifications were considered:

- Only HC action will be considered on "parallel HC" block.
- HC series will be considered in its alpha-beta reference. This assumption doesn´t affect analysis as demonstrated in Appendix C, dynamic information between stationary references axes "*abc*" and "*αβ*" is the same.
- Gains of HC will be considered as "1" for theoretical analysis. Its values will be both adjusted in simulation and prototype experiments.

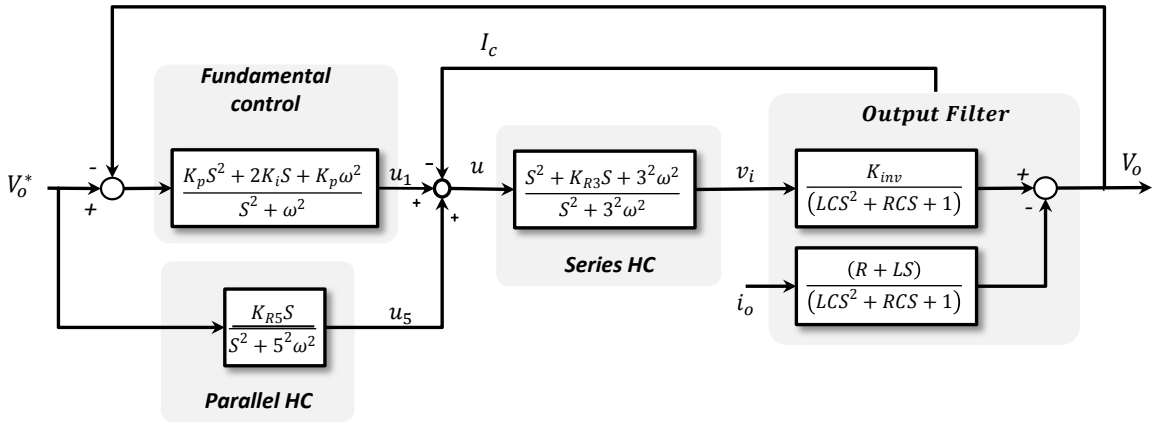

Figure 4-13. Fundamental control and harmonic compensation high level bloc diagram.

Using information of Figure 4-13 and the theoretical assumptions presented above the mathematical model is found to be

$$V_{o_{CL}} = G_{vo}(s)V_o^* - G_{io}(s)I_o \quad , \tag{4.21}$$

where:

$$G_{vo}(s) = \frac{num_{Vo}}{den_{Vo}} \quad , \tag{4.22}$$

$$num_{Vo} = K_{inv}\left(K_pS^6 + \left(2K_i + k_pK_{r3}\right)S^5 + \left(35k_p\omega^2 + 2k_ik\_r3\right)S^4 + \left(68k_i + 26k_pk_{r3}\right)\omega^2S^3 + \left(259k_p\omega^2 + 50k_ik_{r3}\right)\omega^2S^2 + \left(450k_i + 25k_pK_{r3}\right)\omega^4S + \left(225k_p\omega^6\right)\right) \quad , \tag{4.23}$$

$$den_{Vo} = LCS^8 + (k_{inv} + Rl)CS^7 + \left(35CL\omega^2 + K_{inv}k_p + CK_{inv}k_{r3} + 1\right)S^6 + \left(2k_i - k_{r5} + k_pk_{r3} + 35C\omega^2 + \frac{35CR\omega^2}{K_{inv}}\right)K_{inv}S^5 + \left(35\omega^2 + 2K_{inv}k_ik_{r3} - K_{inv}k_{r3}k_{r5} + 259CL\omega^4 + 35K_{inv}k_p\omega^2 + 26CK_{inv}k_{r3}\omega^2\right)S^4 + \left(259C\omega^2 + \frac{259CR\omega^2}{K_{inv}} + 68k_i - 10k_{r5} + 26k_pk_{r3}\right)K_{inv}\omega^2S^3 + \left(259\omega^4 + 225CL\omega^6 + 259K_{inv}k_p\omega^4 + 25CK_{inv}k_{r3}\omega^4 + 50K_{inv}k_ik_{r3}\omega^2 - K_{inv}k_{r3}k_{r5}\omega^2\right)S^2 + \left(225CK_{inv}\omega^6 + 225CR\omega^6 + 450K_{inv}k_i\omega^4 - 9K_{inv}k_{r5}\,\omega^4 + 25K_{inv}k_pk_{r3}\omega^4\right)S + \left(225\omega^6 + 225K_{inv}k_p\omega^6\right) \quad , \tag{4.24}$$

$$G_{io}(s) = \frac{num_{Io}}{den_{Io}} \quad , \tag{4.25}$$

$$num_{Io} = LS^7 + RS^6 + 35L\omega^2S^5 + 35R\omega^2S^4 + 259L\omega^4S^3 + 259R\omega^4S^2 + 225L\omega^6S + 225R\omega^6 \quad , \tag{4.26}$$

and

$$den_{Io} = den_{Vo} \quad . \tag{4.27}$$

Figure 4-14 shows the root locus diagram of the controlled system. This graph exhibits two pairs of pure complex conjugate poles. Giving the system a resonance characteristic at those specifics frequencies. In addition, these new poles and zeros do not significantly alter the root locus shown in Figure 4-11.

The effect introduced by both HC is highlighted in Figure 4-15. The series compensator (3ω) ensures a controlled system gain for this frequency, reducing unbalance load effects mentioned in Chapter 2. While the parallel compensator (5ω) has a strong selective attenuation or rejection for this specific frequency.

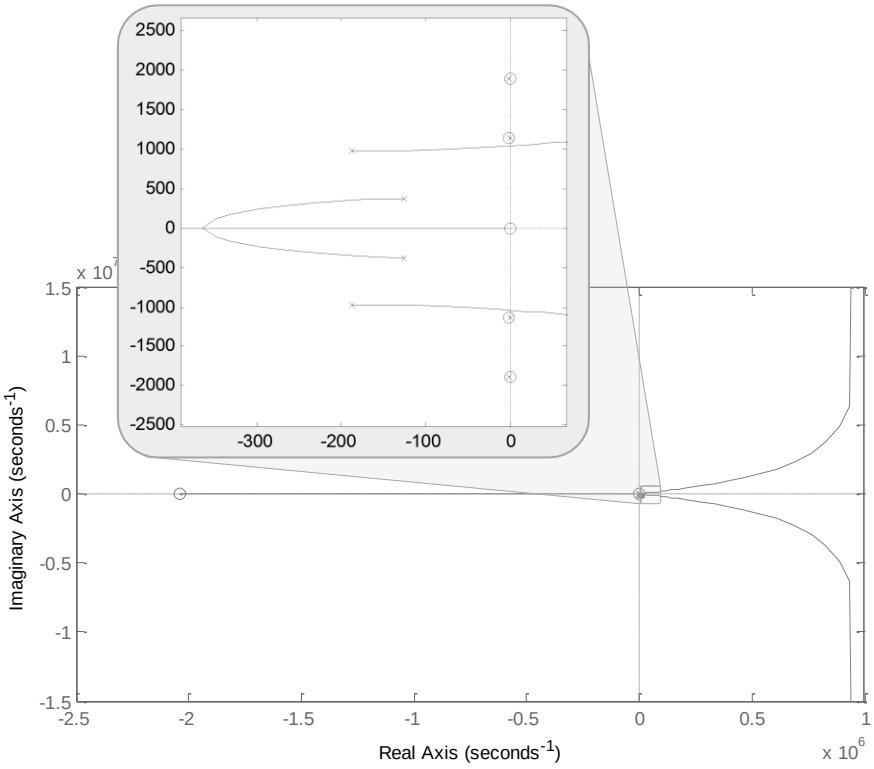

Figure 4-14. Root locus (stationary control+harmonic compensation).

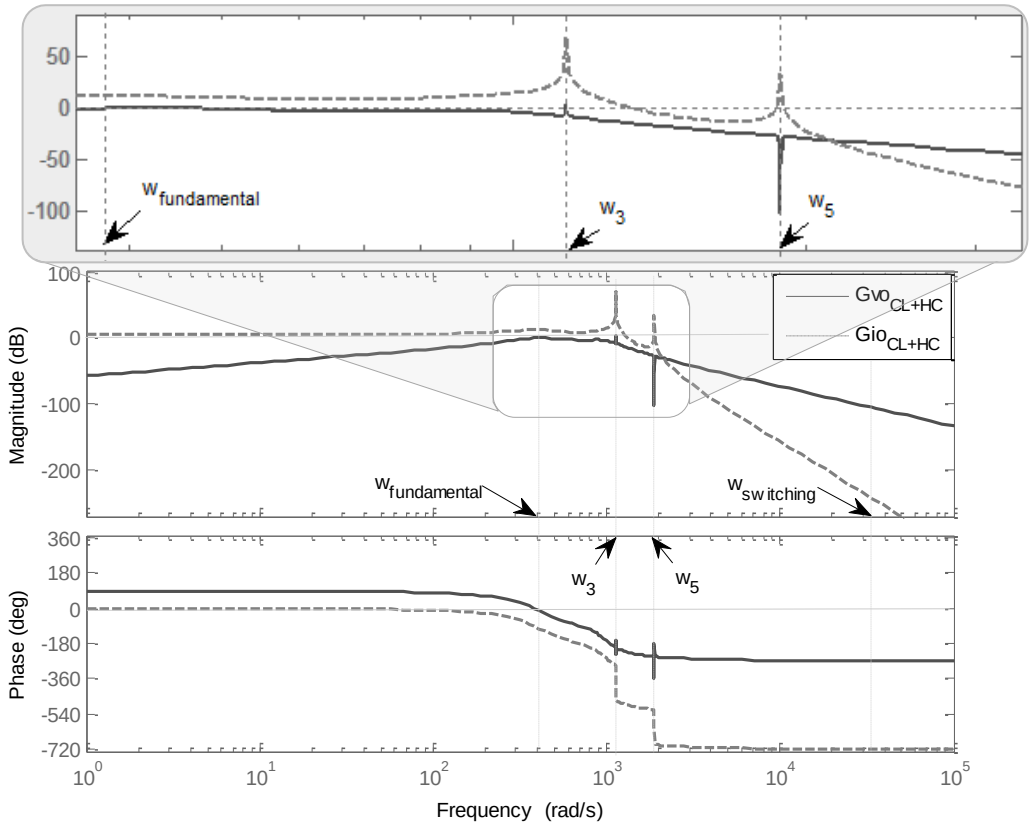

Figure 4-15. bode diagram (stationary control+harmonic compensation).

4.3. Simulation Results

As Chapter 3, PSCAD was the selected tool to perform simulations and verifying theoretical analysis. Simulated circuit is shown in Figure 3-14. Controller-parameters and harmonic-compensators gains are shown in Table 3-2.

Continuous Time Domain

The fundamental-frequency controllers and HC were implemented using second-order transfer functions. Simulator Integration period was set 97 times faster than controller sample time.

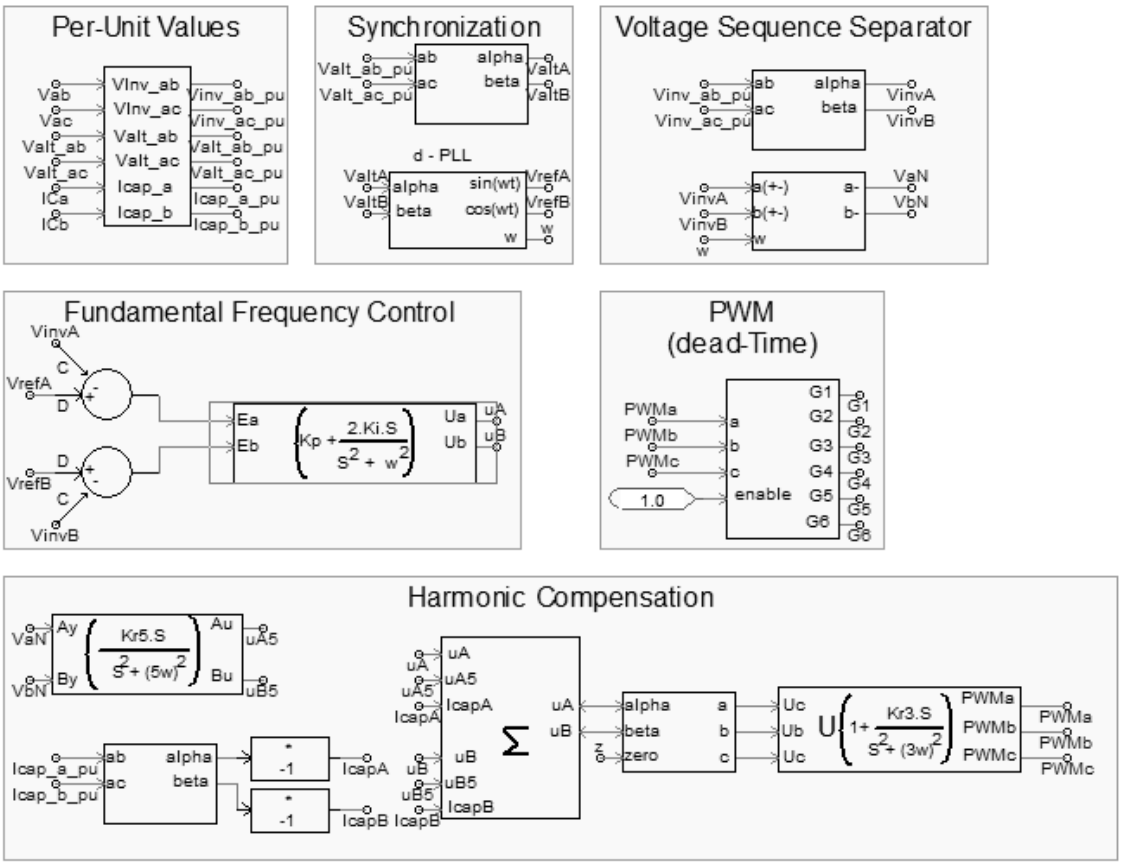

Figure 4-16. Simulated stationary voltage control using PSCAD functional blocks.

Figure 4-17 shows the dynamic behavior of output voltage vector (3.22) with a connection and disconnection of the three phase load. The proposed control strategy achieves rejecting load-disturbance within limits of time and magnitude.

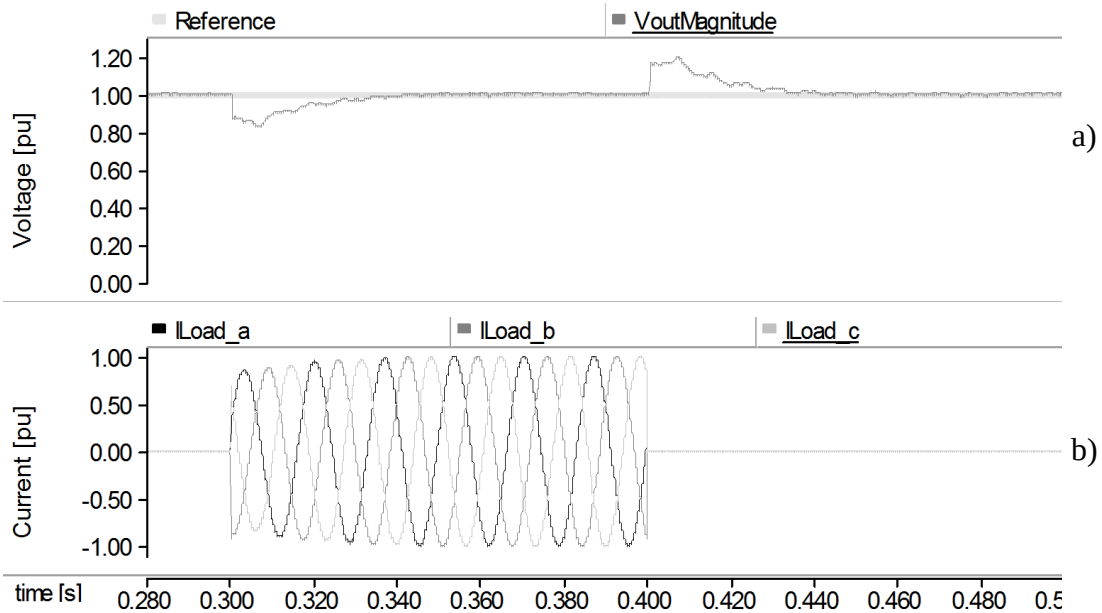

Figure 4-17. Stationary voltage control response on connection and disconnection of a three-phase linear load (simulation), a) reference and output voltage, b) load currents.

The unbalanced load behavior is shown in Figure 4-18, where a two-phase load is connected to the system and the proposed control scheme successfully eliminates the negative sequence component. While at the same time it presents zero steady-state error.

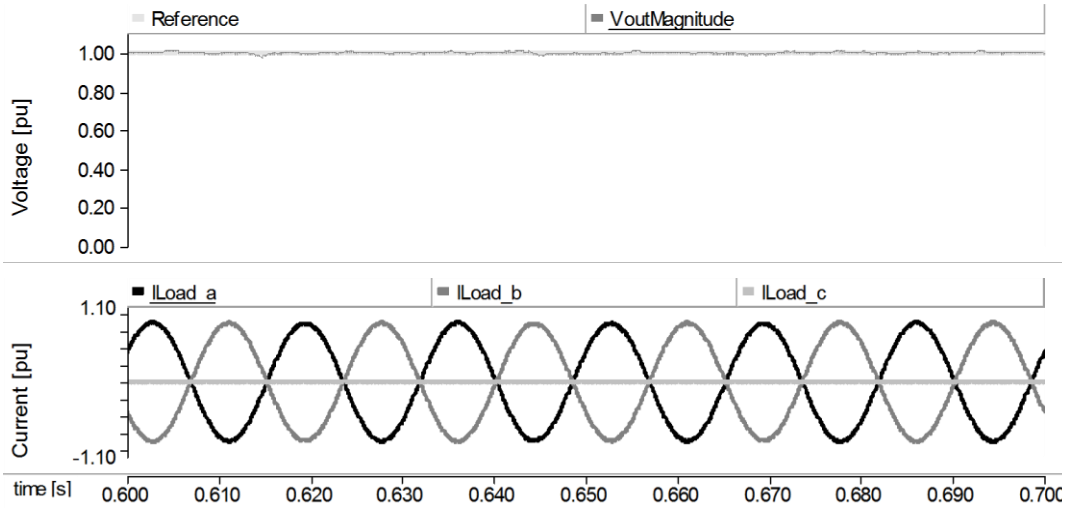

Figure 4-18. Stationary voltage control response with unbalanced load (simulation), a) reference and output voltage, b) load currents.

Discrete Time Domain

The implementation of the proposed control system in digital form was performed using discrete approximation methods using backward and forward Euler. It was also used the simulation scheme proposed in section 3.3.2. Where, code written in C language is shared by simulation and DSP.

As can be seen on Figure 4-19a resonant voltage control with the stationary reference axes alpha-beta, successfully achieved tracking reference despite connection of any type of load.

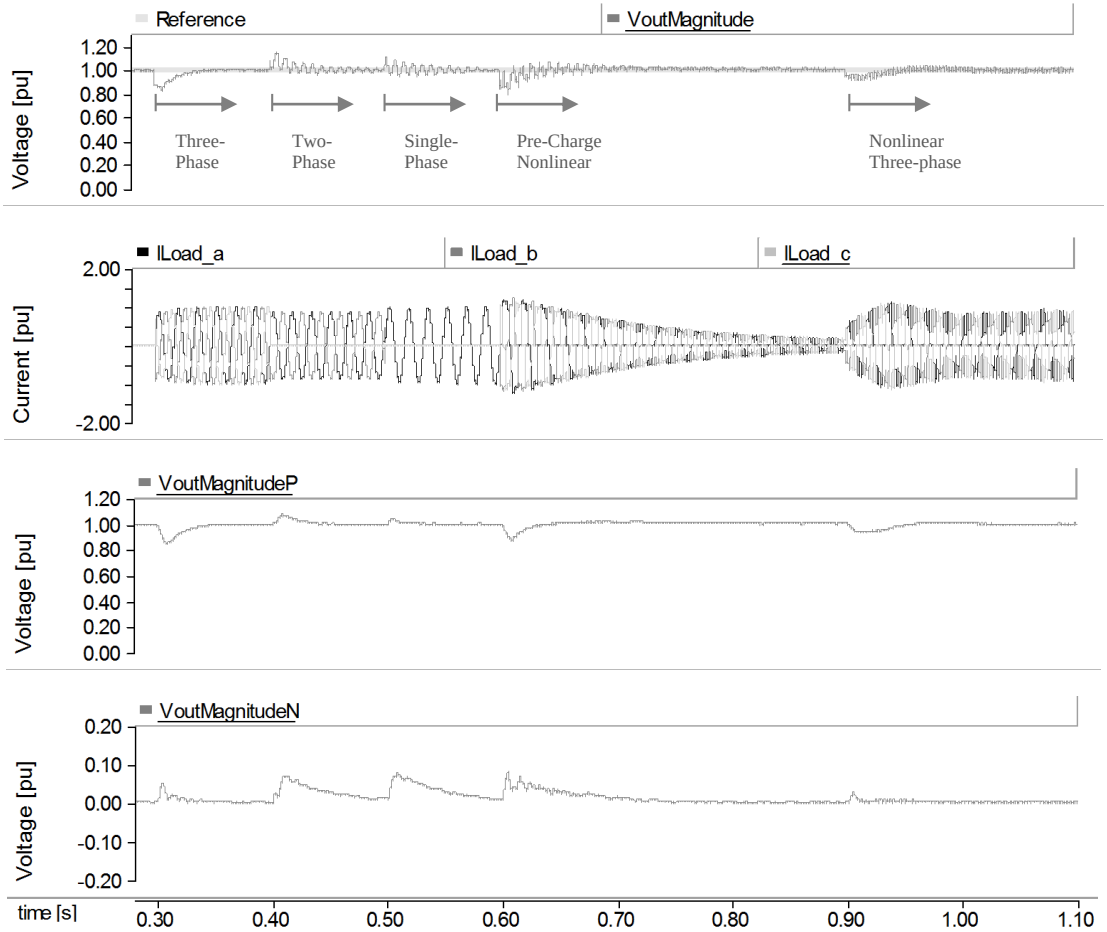

Figure 4-19. Three-phase inverter instantaneous behavior with stationary voltage control (simulation), a) Output voltage, b) Load current, c) Positive sequence output voltage, d) Negative sequence output voltage.

The frequency behavior of the controlled system can be observed in Figure 4-20, where harmonic spectrum for each of the simulated loads is presented. Transient behavior of harmonic compensation on connection of each type of load is presented by Figure 4-21. It should be noted that even in the worst case scenario, simulation of proposed control strategy is able to maintain value of each harmonic within the limits set by standards such as IEEE and IEC.

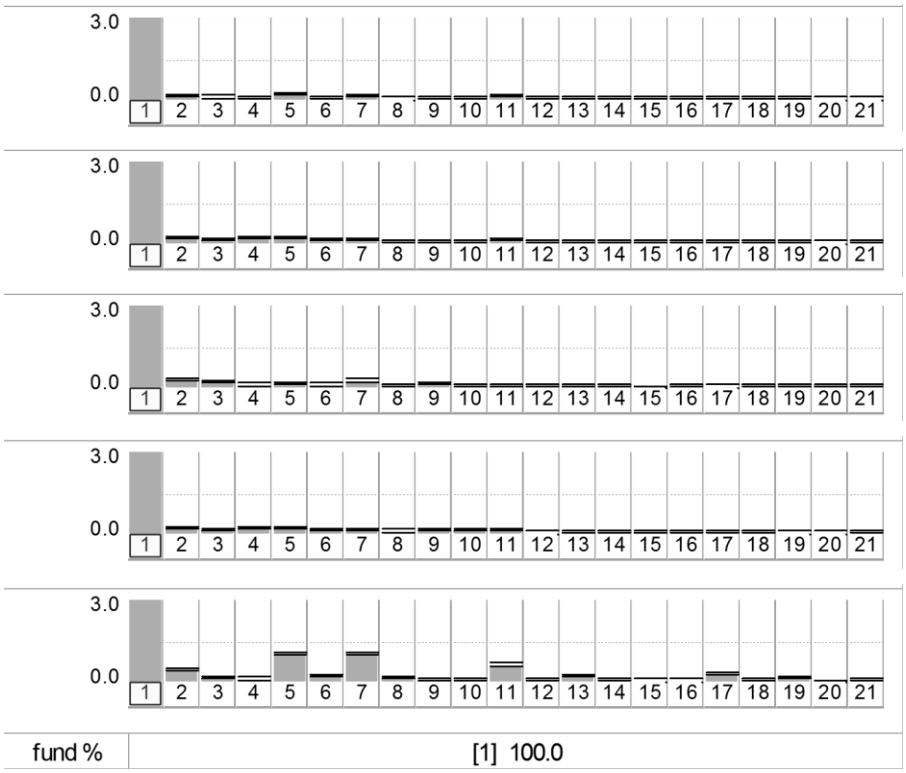

Figure 4-20. Output voltage with stationary voltage control harmonic spectrum (simulation), a) none-Load, b) Three-phase linear load, c) Two-phase linear load, d) single-phase linear load, e) Three-phase none-linear load.

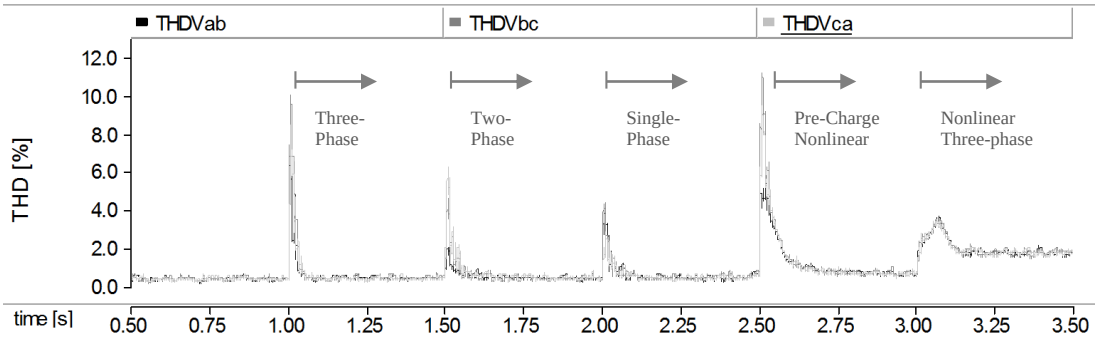

Figure 4-21. Transient response harmonic compensators (simulated stationary voltage control), output voltage THD.

4.4. Experimental Confirmation

The same experimental validation scenario presented in section 3.5 will be used. A summary of the main features of prototype are presented in Table 3-3.

Figure 4-22 shows the dynamic response of the proposed voltage control when a change is made to reference signal. In this condition, controlled system behaves without overshoot and settling time of approximately 40ms. It presents a similar behavior to the design parameters specified in section 3.2.3. This result validates relationship between parameters of synchronous PI controllers and P + Resonant shown in [47], i.e. using the calculated values from the synchronous PI controller it is possible to obtain a desired dynamic output in stationary P+Resonant controller.

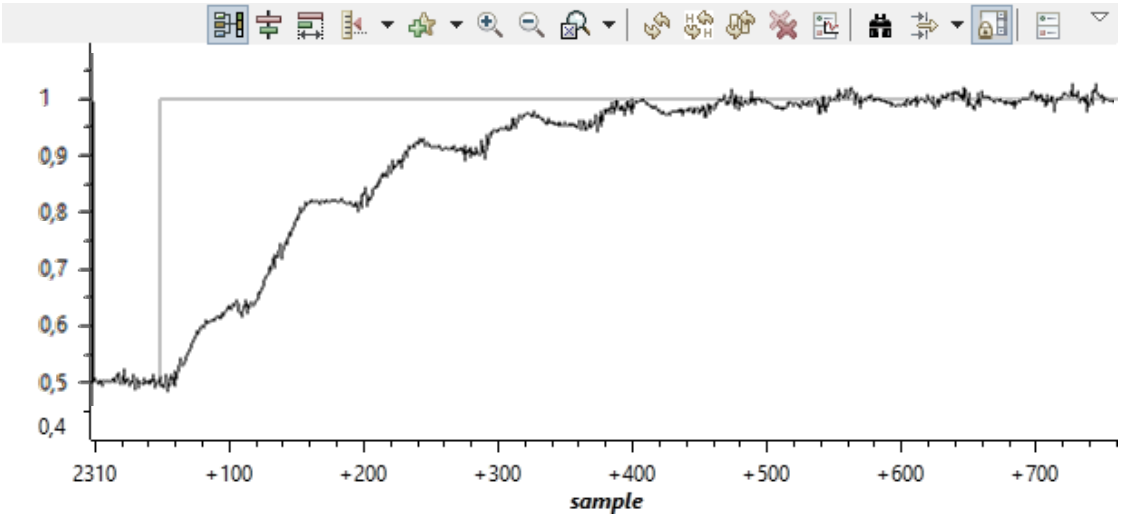

Figure 4-22. Stationary voltage control response on reference step.

Disturbance rejection of the proposed control topology can be seen on connection and disconnection of a three-phase linear load as shown in Figure 4-23a and Figure 4-23b respectively. In addition, this type of load presents an interesting challenge for a control scheme from the point of view of a disturbance. Since the inverter requires nominal power with almost instantaneous dynamics (ignoring small inductances of wires and resistors). The proposed controller can eliminate effect of disturbance, showing same dynamics observed at reference exchange (Figure 4-22). This result validates theoretical analysis shown in (4.20).

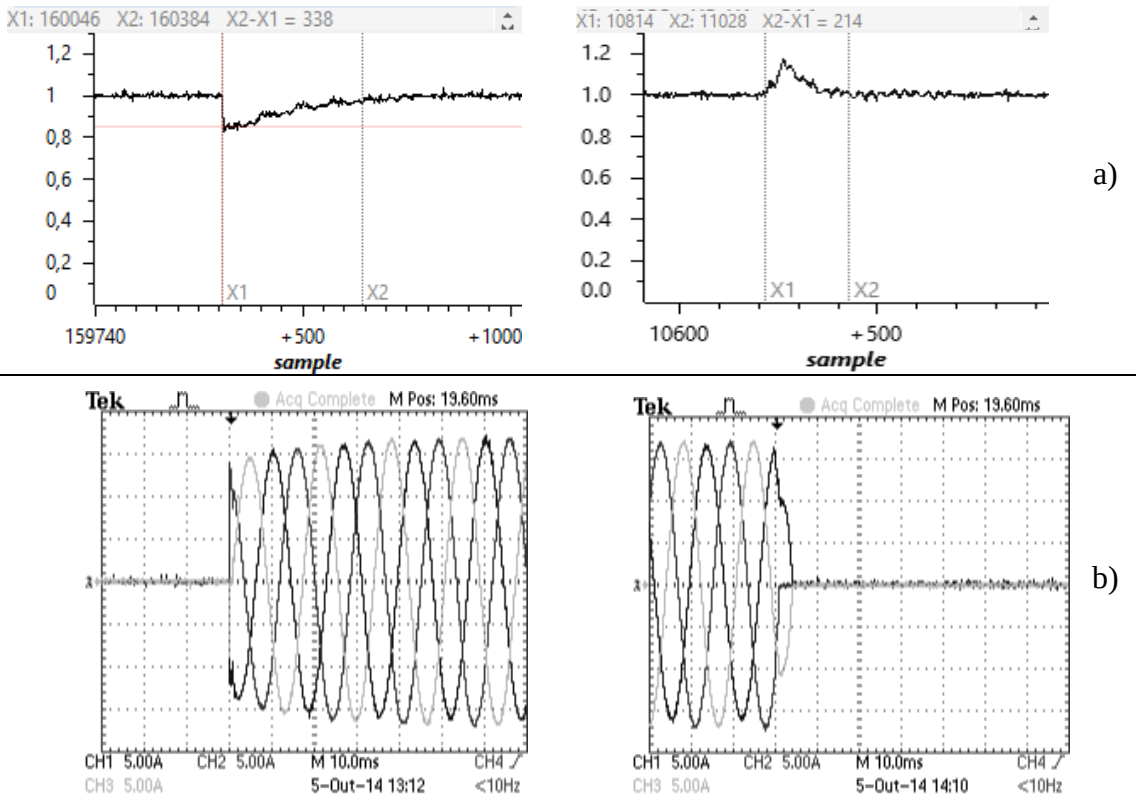

Figure 4-23. Stationary voltage control response on connection and disconnection of a three-phase linear load, a) output voltage magnitude, b) load currents.

Performance of the proposed control voltage with unbalanced loads is shown in Figure 4-24. Where the magnitude vector of output voltage shows a minimum variation and does not exhibit oscillatory behavior of 2ω. Which means the controller effectively eliminates the negative-sequence component introduced by unbalanced loads. In addition, output voltage vectors a, b, c are shifted 120° with only a ±1° error.

Figure 4-25 shows the performance of the proposed control strategy under nonlinear loads. Figure 4-25a shows output-voltage steady state, under a highly distorted current form demanded by the load Figure 4-25b.

Figure 4-25c shows harmonic spectra of inverter output voltage. Total harmonic distortion factor (THD) is 1.8%, which is within the allowed margin of 5% restricts by IEEE and IEC standards.

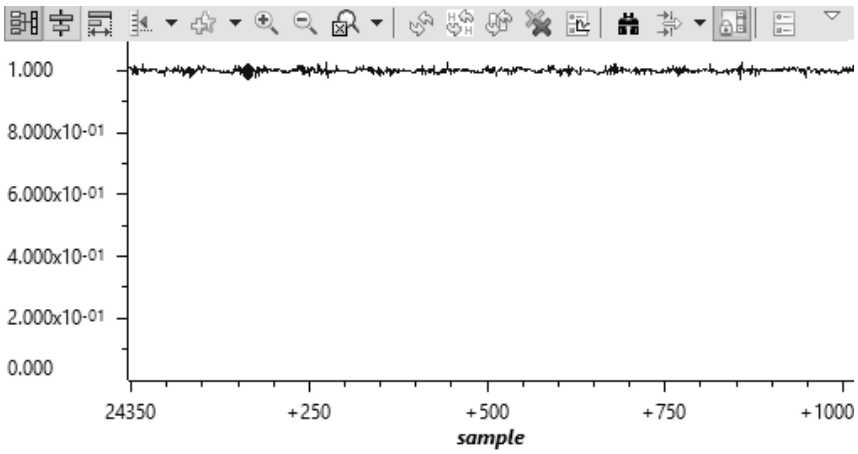

a)

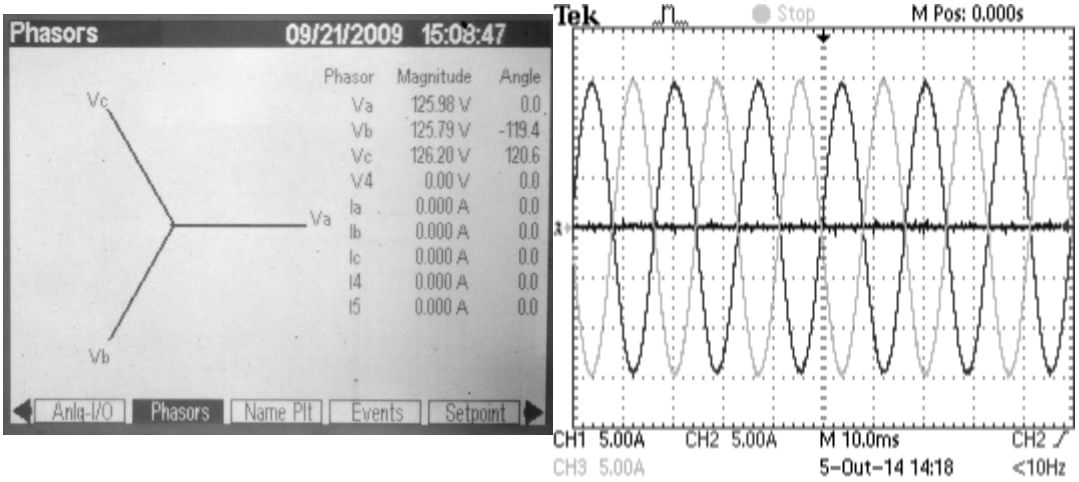

b) c)

Figure 4-24. Stationary voltage control with unbalance linear load, a) output voltage magnitude, b) output voltage phasor diagram, c) load currents.

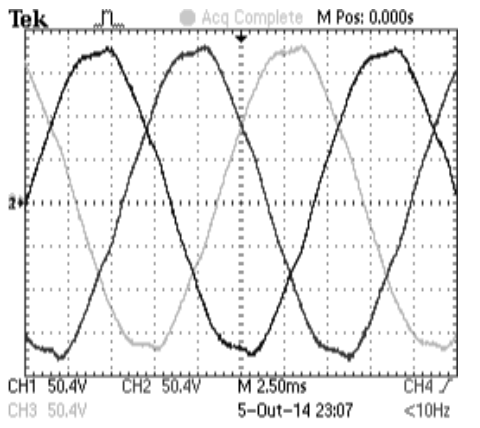

a)

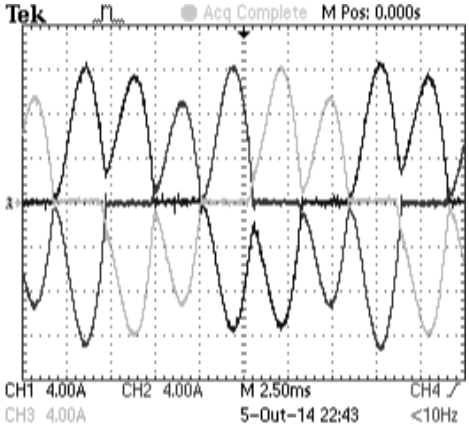

a)

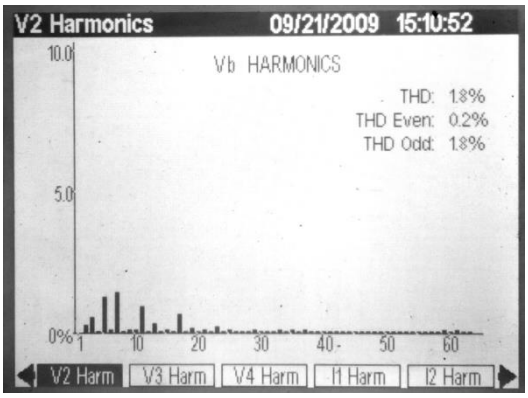

c)

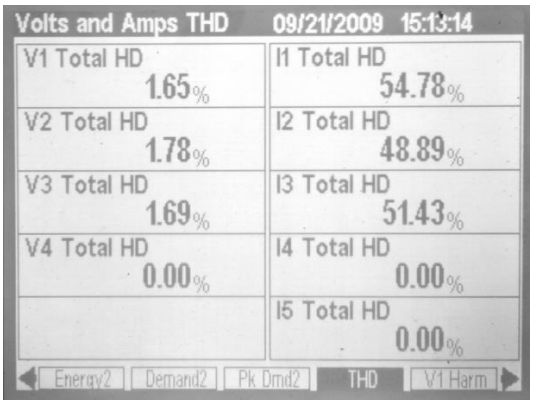

d)

Figure 4-25. Stationary voltage control with none-linear load, a) output voltage, b) load currents, c) voltage harmonic spectrum. d) Voltage and current THD.

4.5. Partial conclusions

- Inverter output voltage remains balanced in spite of the connection of an extremely unbalanced load.
- HC blocks in the proposed topology gets harmonic magnitudes significantly below from requirements imposed by IEC and IEEE standards.
- The dynamic behavior exhibited in the simulation and experiments, validates theoretical assumptions and mathematical models introduced in this chapter.
- P+Resonant controller was able to obtain similar dynamic results compared to theoretical calculations. Thus using values of k_p and k_i calculated for

synchronous PI controller, i.e. no overshoot, with a 21.8% error in the settling time.

- Voltage control based on P+Resonant controllers can handle both positive and negative-sequences components, without any sequence separator scheme.

Chapter 5 - Performance Comparison between Stationary and Synchronous Voltage Controllers

In this chapter, it will be performed a comparison between voltage control topologies presented in Chapters 3 and 4. It will be compared temporal and frequency behavior under different types of loads, using only experimental results of both control strategies. Study results presented in this chapter, allows to identify which is the most suitable strategy implementing a controller output voltage of a three-phase UPS inverter.

5.1. Comparison of Experimental Results

5.1.1. Transients response

To compare transient response of the controlled plant it will be evaluated the system reaction to a change in reference signal when there is no load connected to inverter. In this comparison, experimental results shown in chapter 3 and 4 were performed using the same values of k_p, k_i, k_{r3} and k_{r5}.

To compare three-phase results it will be used vector magnitudes of output voltages (3.22). These quantities were measured internally in DSP and data were exported for post-treatment in MATLAB.

Result are shown in Figure 5-1 where it can be observed that synchronous-voltage controller is 0.5x faster under reference changes compared to stationary-voltage controller and applied to three phase UPS inverters.

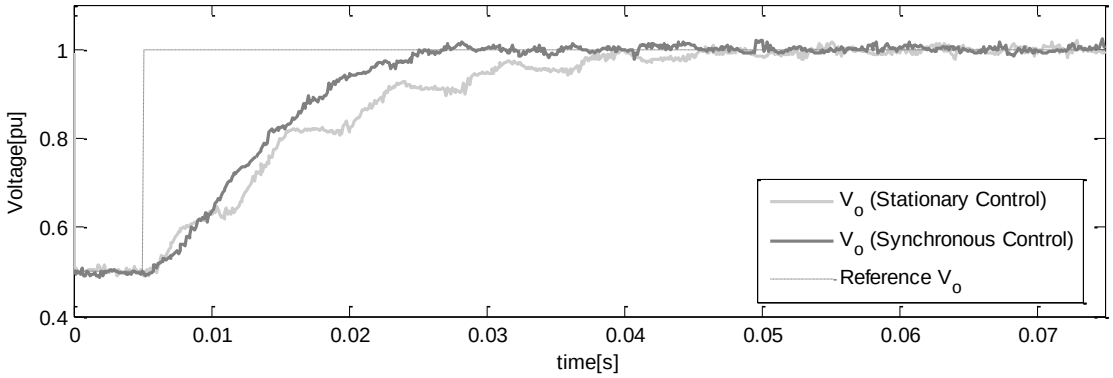

Figure 5-1. reference step comparison (experimental results).

Step response in reference signal represents a major information of system dynamics. In case of UPS output-voltage control, usually the reference is a constant value. Therefore is important to compare controller's behavior under disturbance exerted by load connection and disconnection. The result of this comparison is presented below.

Disturbance rejection

This comparison was performed when a three phase linear load is connected or disconnected from inverter's output. Since, it represents to system, an instantaneous rated power demand. Result is shown in Figure 5-2, this graph shows that stationary topology presents a better performance, i.e. on connection/disconnection it shows a lower voltage

sag/drop. Although, both topologies shows the same dynamics. It is also possible to see that both control topologies are within IEC limits.

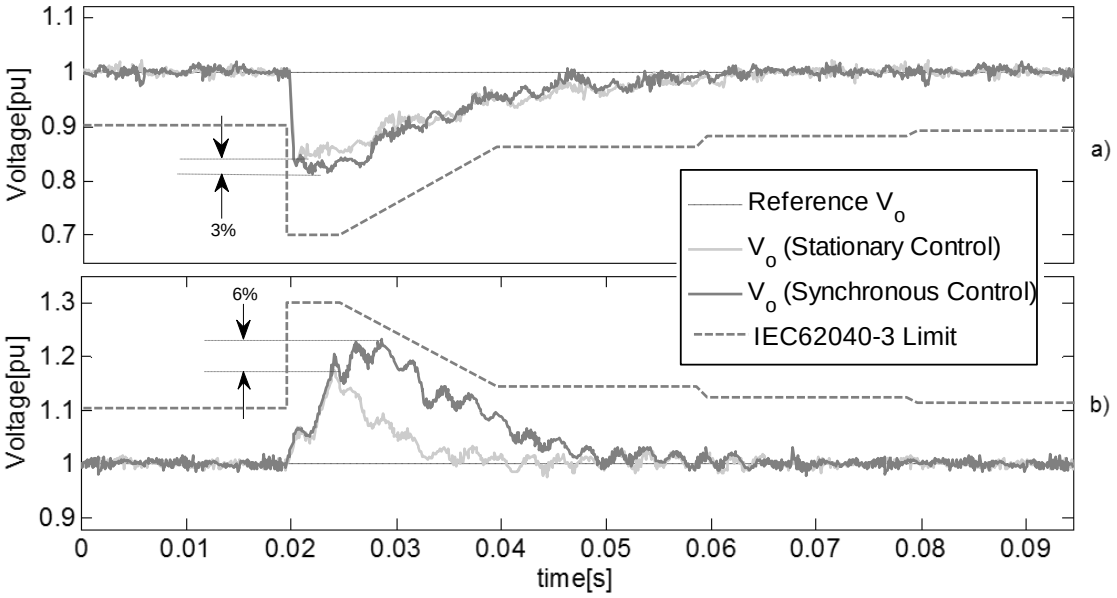

Figure 5-2. Disturbance rejection comparison (experimental results), a) load conection, b) load disconection.

5.1.2. Behavior with Unbalanced Loads

Performance evaluation of unbalanced load was made using a two phase linear load. Since this load demands more than 60% of inverter rated power and also represents a huge imbalance to system.

In Chapters 3 and 4, both control topologies successfully achieve removing negative-sequence component introduced by unbalanced load. As shown in Figure 5-3 both inverter output-voltage achieves tracking the reference without second harmonic fluctuations. However, a detailed analysis of output-voltage signal shows that stationary topology decreases 33% the high frequency variations around the reference point, i.e. stationary controller presents higher attenuation at high frequency variations.

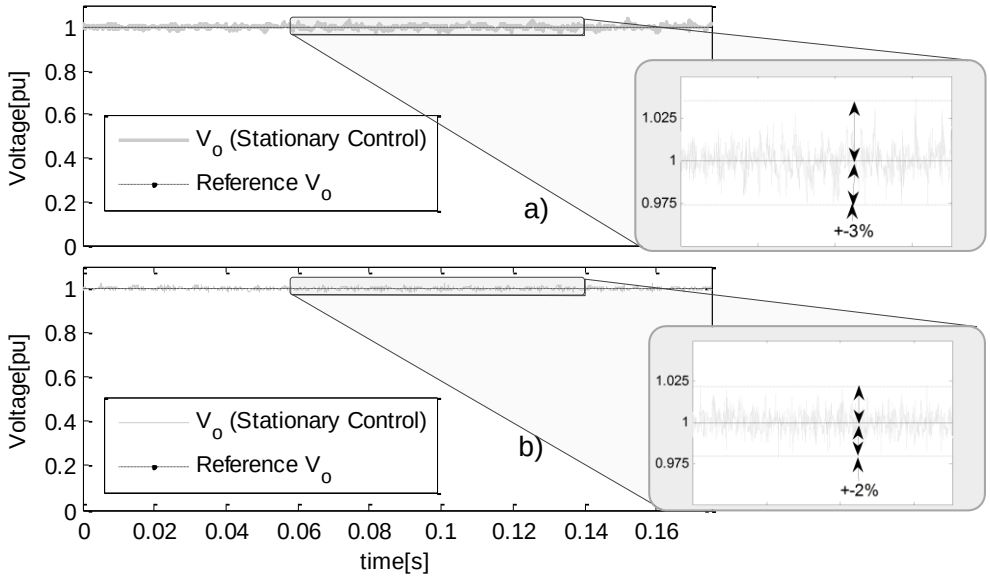

Figure 5-3. Temporal Comparison with unbalanced load (experimental results), a) synchronous voltage control, b) stationary voltage control.

5.1.3. Behavior with Nonlinear Loads

Frequency behaviors of proposed topologies compared in the frequency spectrum are shown in Figure 5-4. This figure shows that stationary scheme presents a harmonic content lower than exhibited by the synchronous one, especially in the 2nd, 3rd and 7th harmonics, which can be quantitatively compared using THD value of output voltage. Table 5-1 shows that synchronous voltage control presents a THD 44% higher compared to stationary voltage control.

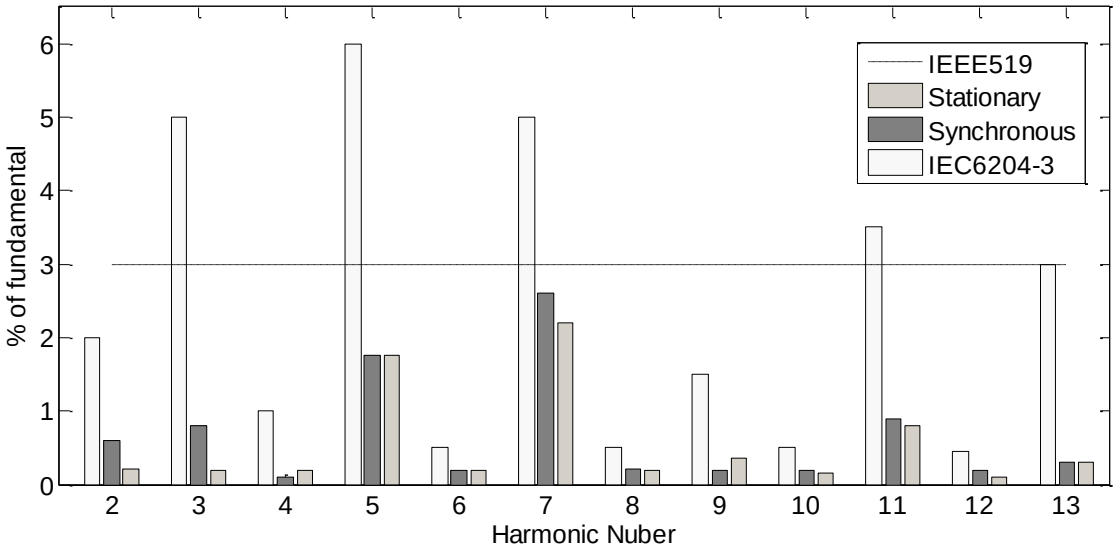

Figure 5-4. Frequency comparison for unbalanced linear load (experimental results)

Table 5-1. Inverter output voltage THD.

Control Topology	Output Voltage THD [%]
Stationary	1.8
Synchronous	2.6

5.1.4. Computational Effort

Comparing detailed block diagrams of both proposed strategies Figure 3-2 and Figure 4-5, there is a significant reduce on the number of elementary blocks in case of stationary scheme. Figure 5-5 shows how this complexity decrease the processing time. In this case, synchronous topology is 1,84x more processor demanding.

This is a very important factor to consider developing a UPS. Since mentioned in Chapter 2, inverter control represents only a portion of total UPS control. Therefore, processing time becomes a very important criterion to ensure the entire control structure can be implemented within the DSP sampling period.

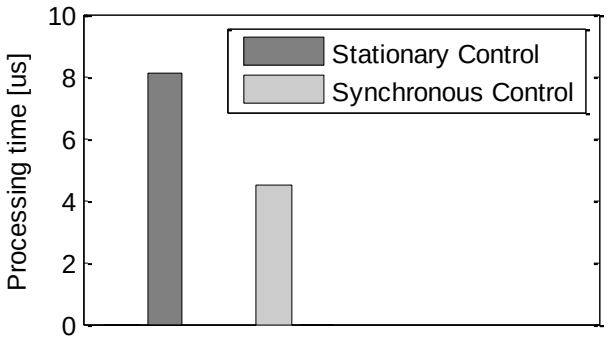

Figure 5-5. Processing time.

5.2. Partial conclusions

- Proposed synchronous control strategy presents a better behavior to changes in the reference signal, being able to stabilize the system 1.5x faster than the stationary Control strategy, at the same time presents a lower oscillation in the transient part.
- The proposed stationary control strategy showed a better ability to reject disturbances exerted by load connection and disconnection.

- Both proposed control strategies, successfully manage to eliminate the negative-sequence component when an extremely unbalanced load is connected to the output of the three phase inverter.
- In steady state, stationary control strategy presents a behavior with less harmonic pollution of high frequencies, reducing up to 30% the content of high frequency noise in the output voltage of the inverter.
- In presence of nonlinear loads the stationary controller has a better performance, showing a THD 44% lower than strategy presented by synchronous control.
- Processing time demanded by stationary strategy is 44% lower than synchronous strategy.
- Based on obtained results and requirements for controlling three-phase UPS inverter, it may be concluded that proposed stationary control strategy presents the best performance.

Chapter 6 - General Conclusion

This chapter presents a summary of major contributions of this document and some suggestions for development of future work.

6.1. Conclusions

- IEEE519/IEC62040-3 standards and the PETROBRAS technical norm N-567 were analyzed in order to obtain control requirements for UPS inverters. These transient and frequency constrictions provided the necessary criteria for controller calculations with the proposed methodology.
- It was presented a review of voltage control schemes applied to UPS inverters. Thus allowing to identify main features of control proposal found in the state of art.
- The dynamic performance of the fundamental frequency controller, shows a high accuracy between simulation and experimental results, thus allowing to use the same gains calculated by the theoretical analysis. On the other hand, performance of the harmonic compensator presents several differences between the gain values used in simulation and experimental prototype. Nevertheless, the methodology proposed in this work allows such differences, due to the proposed online adjustment process.
- Dynamic behavior exhibited in simulation and experiments, validates theoretical assumptions and mathematical models introduced in this work. This also validates the proposed methodology to calculate the parameters of fundamental-frequency controller.
- Based on experimental results presented in chapter 5 and the requirements for controlling three-phase UPS inverter presented in chapter 2, it may be concluded that proposed stationary control strategy presented in chapter 4, presents a superior performance in comparison with synchronous control strategy presented in chapter 3, i.e. it presents a lower THD (44% lower), the high frequency noise was reduced to 30% and the processing time was reduced to 44%. It also shows a better ability to reject disturbances exerted by the connection and disconnection of loads.
- Despites of the load type connected into the UPS inverter, the harmonic Compensator scheme presented in this work gets the harmonic magnitudes significantly below from requirements imposed by the IEC and IEEE standards.
- This study presents a new control strategy for voltage control of UPS inverter. It was able to achieve high performance behavior without need of high gains of

controller parameter, i.e. controlled system isn't close to unstable region as demonstrated in chapter 4.

6.2. Future Research

The gain value of resonant harmonic compensation reported large differences within simulation and experimental values. It's encouraged to pursuit a methodology to calculate not just controller parameters as presented in this document, but HC parameters as well. In addition, as reported in chapter 4, there are some facilities for theoretical analysis where all control blocks are referenced to same mathematical plane.

This document encouraged to evaluate the dynamic impact due to sequence-separator in "parallel harmonic compensator" block and maybe deploying alternatives options demanding lower computational cost.

Control strategies shown in this study were based on solving the problems caused by different types of loads. However, using mathematical modeling presented in Chapter 4 is possible to create a control topology based on the minimization of system stiffness (4.12) while ensuring zero steady-state error.

Control based on optimization of internal model can open a new line of research. Where not only controller parameters are calculated but, simultaneously optimized physical parameters of inverter. Looking for suitable performance, reduced size, weight and cost.

References

[1] J. Caicedo, T. Brasil y M. Aredes, «Synchronous Voltage Control for Three-phase UPS Inverter,» de *International Conference and Exhibition on Power Electronics, Intelligent Motion, Renewable Energy and Energy Management*, 2014.

[2] *Uninterruptible Power Systems (UPS)—Part 3: Method of Specifying the Performance and Test Requirements*, First Edition 1999-03, International Standard IEC 62040-3.

[3] M. Niroomand y H. Karshenas, «Review and comparison of control methods for uninterruptible power supplies,» de *Power Electronic \& Drive Systems \& Technologies Conference (PEDSTC), 2010 1st*, 2010.

[4] B. Tamyurek, «A High-Performance SPWM Controller for Three-Phase UPS Systems Operating Under Highly Nonlinear Loads,» *Power Electronics, IEEE Transactions on*, vol. 28, nº 8, pp. 3689-3701, 2013.

[5] M. Ryan, W. Brumsickle y R. Lorenz, «Control topology options for single-phase UPS inverters,» *Industry Applications, IEEE Transactions on*, vol. 33, nº 2, pp. 493-501, 1997.

[6] P. C. Loh, M. Newman, D. Zmood y D. Holmes, «A comparative analysis of multiloop voltage regulation strategies for single and three-phase UPS systems,» *Power Electronics, IEEE Transactions on*, vol. 18, nº 5, pp. 1176-1185, 2003.

[7] P. Mattavelli, «Synchronous-frame harmonic control for high-performance AC power supplies,» *Industry Applications, IEEE Transactions on*, vol. 37, nº 3, pp. 864-872, 2001.

[8] P. Cortes, M. Kazmierkowski, R. Kennel, D. Quevedo y J. Rodriguez, «Predictive Control in Power Electronics and Drives,» *Industrial Electronics, IEEE Transactions on*, vol. 55, nº 12, pp. 4312-4324, 2008.

[9] P. Mattavelli, «An improved deadbeat control for UPS using disturbance observers,» *Industrial Electronics, IEEE Transactions on*, vol. 52, nº 1, pp. 206-212, 2005.

[10] M. Niroomand y H. Karshenas, «Hybrid learning control strategy for three-phase uninterruptible power supply,» *Power Electronics, IET*, vol. 4, nº 7, pp. 799-807, 2011.

[11] P. Cortes, G. Ortiz, J. Yuz, J. Rodriguez, S. Vazquez y L. Franquelo, «Model Predictive Control of an Inverter With Output LC Filter for UPS Applications,» *Industrial Electronics, IEEE Transactions on*, vol. 56, nº 6, pp. 1875-1883, 2009.

[12] C. Rech, H. Pinheiro, H. Grundling, H. Hey y J. Pinheiro, «Comparison of digital control techniques with repetitive integral action for low cost PWM inverters,» *Power Electronics, IEEE Transactions on,* vol. 18, nº 1, pp. 401-410, 2003.

[13] F. Botteron y H. Pinheiro, «A Three-Phase UPS That Complies With the Standard IEC 62040-3,» *Industrial Electronics, IEEE Transactions on,* vol. 54, nº 4, pp. 2120-2136, 2007.

[14] C. Rech, H. Pinheiro, H. Grundling, H. Hey y J. Pinheiro, «A modified discrete control law for UPS applications,» *Power Electronics, IEEE Transactions on,* vol. 18, nº 5, pp. 1138-1145, 2003.

[15] L. Michels, H. Pinheiro y H. Grundling, «Design of plug-in repetitive controllers for single-phase PWM inverters,» de *Industry Applications Conference, 2004. 39th IAS Annual Meeting. Conference Record of the 2004 IEEE*, 2004.

[16] Y.-Y. Tzou, R.-S. Ou, S.-L. Jung y M.-Y. Chang, «High-performance programmable AC power source with low harmonic distortion using DSP-based repetitive control technique,» *Power Electronics, IEEE Transactions on,* vol. 12, nº 4, pp. 715-725, 1997.

[17] Y.-Y. Tzou, S.-L. Jung y H.-C. Yeh, «Adaptive repetitive control of PWM inverters for very low THD AC-voltage regulation with unknown loads,» *Power Electronics, IEEE Transactions on,* vol. 14, nº 5, pp. 973-981, 1999.

[18] H. Deng, R. Oruganti y D. Srinivasan, «Analysis and Design of Iterative Learning Control Strategies for UPS Inverters,» *Industrial Electronics, IEEE Transactions on,* vol. 54, nº 3, pp. 1739-1751, 2007.

[19] X. Sun, M. H. L. Chow, F. H. F. Leung, D. Xu, Y. Wang y Y. S. Lee, «Analogue implementation of a neural network controller for UPS inverter applications,» *Power Electronics, IEEE Transactions on,* vol. 17, nº 3, pp. 305-313, 2002.

[20] H. Deng, R. Oruganti y D. Srinivasan, «High-performance Control of UPS Inverters Using a B-Spline Network,» de *Power Electronics Specialists Conference, 2005. PESC '05. IEEE 36th*, 2005.

[21] T. Radwan, «On the Use of Neuro-Fuzzy to Control a Three-Phase Uninterruptible Power Supply,» de *Industrial Electronics, 2006 IEEE International Symposium on*, 2006.

[22] S. Muthu y J. Kim, «Discrete-time sliding mode control for output voltage regulation of three-phase voltage source inverters,» de *Applied Power Electronics Conference and Exposition, 1998. APEC '98. Conference Proceedings 1998., Thirteenth Annual*, 1998.

[23] S. Ribas, V. Montagner, H. Pinheiro y R. C. L. F. Oliveira, «Discrete-time H(inf) control of PWM inverters: Experimental results complying with IEC 62040-3,» de *Circuits and Systems (ISCAS), 2011 IEEE International Symposium on*, 2011.

[24] P. Rodriguez, J. Pou, J. Bergas, J. Candela, R. Burgos y D. Boroyevich, «Decoupled Double Synchronous Reference Frame PLL for Power Converters Control,» *Power Electronics, IEEE Transactions on,* vol. 22, nº 2, pp. 584-592, 2007.

[25] J. A. Suul, «Control of Grid Integrated Voltage Source Converters under Unbalanced Conditions,» 2012.

[26] P. Rodriguez, A. Luna, I. Candela, R. Mujal, R. Teodorescu y F. Blaabjerg, «Multiresonant Frequency-Locked Loop for Grid Synchronization of Power Converters Under Distorted Grid Conditions,» *Industrial Electronics, IEEE Transactions on,* vol. 58, nº 1, pp. 127-138, 2011.

[27] D. Siemaszko, «Double frame control and power compensation for power converters connected to weak networks with disturbances,» de *Power Electronics and Applications (EPE), 2013 15th European Conference on*, 2013.

[28] Y. Suh, V. Tijeras y T. Lipo, «A nonlinear control of the instantaneous power in dq synchronous frame for PWM AC/DC converter under generalized unbalanced operating conditions,» de *Industry Applications Conference, 2002. 37th IAS Annual Meeting. Conference Record of the*, 2002.

[29] M. Reyes, P. Rodriguez, S. Vazquez, A. Luna, R. Teodorescu y J. Carrasco, «Enhanced Decoupled Double Synchronous Reference Frame Current Controller for Unbalanced Grid-Voltage Conditions,» *Power Electronics, IEEE Transactions on,* vol. 27, nº 9, pp. 3934-3943, 2012.

[30] Y. Liang, «A new time domain positive and negative sequence component decomposition algorithm,» de *Power Engineering Society General Meeting, 2003, IEEE*, 2003.

[31] A. Kulka, «Sensorless Digital Control of Grid Connected Three Phase Converters for Renewable Sources,» 2009.

[32] W. V. Lyon, Applications of the method of symmetrical components, McGraw-Hill book company, 1937.

[33] P. Rodriguez, R. Teodorescu, I. Candela, A. Timbus, M. Liserre y F. Blaabjerg, «New Positive-sequence Voltage Detector for Grid Synchronization of Power Converters under Faulty Grid Conditions,» de *Power Electronics Specialists Conference, 2006. PESC '06. 37th IEEE*, 2006.

[34] L. R. Limongi, R. Bojoi, C. Pica, F. Profumo y A. Tenconi, «Analysis and Comparison of Phase Locked Loop Techniques for Grid Utility Applications,» de *Power Conversion Conference - Nagoya, 2007. PCC '07*, 2007.

[35] L. Rolim, D. da Costa y M. Aredes, «Analysis and Software Implementation of a Robust Synchronizing PLL Circuit Based on the pq Theory,» *Industrial Electronics, IEEE Transactions on,* vol. 53, nº 6, pp. 1919-1926, 2006.

[36] R. Teodorescu, F. Blaabjerg, U. Borup y M. Liserre, «A new control structure for grid-connected LCL PV inverters with zero steady-state error and selective

harmonic compensation,» de *Applied Power Electronics Conference and Exposition, 2004. APEC '04. Nineteenth Annual IEEE*, 2004.

[37] J. Guerrero, «Connecting renewable energy sources into the smartgrid,» de *Industrial Electronics (ISIE), 2011 IEEE International Symposium on*, 2011.

[38] A. Timbus, M. Ciobotaru, R. Teodorescu y F. Blaabjerg, «Adaptive resonant controller for grid-connected converters in distributed power generation systems,» de *Applied Power Electronics Conference and Exposition, 2006. APEC '06. Twenty-First Annual IEEE*, 2006.

[39] M. Liserre, R. Teodorescu y F. Blaabjerg, «Multiple harmonics control for three-phase grid converter systems with the use of PI-RES current controller in a rotating frame,» *Power Electronics, IEEE Transactions on*, vol. 21, nº 3, pp. 836-841, 2006.

[40] A. G. Yepes, «Digital Resonant Current Controllers for Voltage Source Converters,» 2011.

[41] R. Teodorescu, F. Blaabjerg, M. Liserre y P. Loh, «Proportional-resonant controllers and filters for grid-connected voltage-source converters,» *Electric Power Applications, IEE Proceedings*, vol. 153, nº 5, pp. 750-762, 2006.

[42] K. Ogata y Y. Yang, Modern control engineering, 3 ed., Prentice-Hall Englewood Cliffs, 1999, pp. 57-133.

[43] D.-E. Kim y D.-C. Lee, «Inverter Output Voltage Control of Three-Phase UPS Systems Using Feedback Linearization,» de *Industrial Electronics Society, 2007. IECON 2007. 33rd Annual Conference of the IEEE*, 2007.

[44] D. Zmood y D. Holmes, «Stationary frame current regulation of PWM inverters with zero steady state error,» de *Power Electronics Specialists Conference, 1999. PESC 99. 30th Annual IEEE*, 1999.

[45] S. Fukuda y T. Yoda, «A novel current-tracking method for active filters based on a sinusoidal internal model [for PWM invertors],» *Industry Applications, IEEE Transactions on*, vol. 37, nº 3, pp. 888-895, 2001.

[46] X. Yuan, W. Merk, H. Stemmler y J. Allmeling, «Stationary-frame generalized integrators for current control of active power filters with zero steady-state error for current harmonics of concern under unbalanced and distorted operating conditions,» *Industry Applications, IEEE Transactions on*, vol. 38, nº 2, pp. 523-532, 2002.

[47] Y. Sato, T. Ishizuka, K. Nezu y T. Kataoka, «A new control strategy for voltage type PWM rectifiers to realise zero steady-state control error in input current,» de *Industry Applications Conference, 1997. Thirty-Second IAS Annual Meeting, IAS '97., Conference Record of the 1997 IEEE*, 1997.

[48] D. Zmood, D. Holmes y G. Bode, «Frequency-domain analysis of three-phase linear current regulators,» *Industry Applications, IEEE Transactions on,* vol. 37, nº 2, pp. 601-610, 2001.

[49] D. Zmood y D. Holmes, «Stationary frame current regulation of PWM inverters with zero steady-state error,» *Power Electronics, IEEE Transactions on,* vol. 18, nº 3, pp. 814-822, 2003.

Appendix A. Fundamental Concepts

This appendix displays mathematics postulations of the Clarke and Park transformations used in this work.

A1. Stationary Alpha-Beta Reference Plane (Clarke´s transformation)

Figure A-1, shows the representation of non-normalized Clarke transform used in this work.

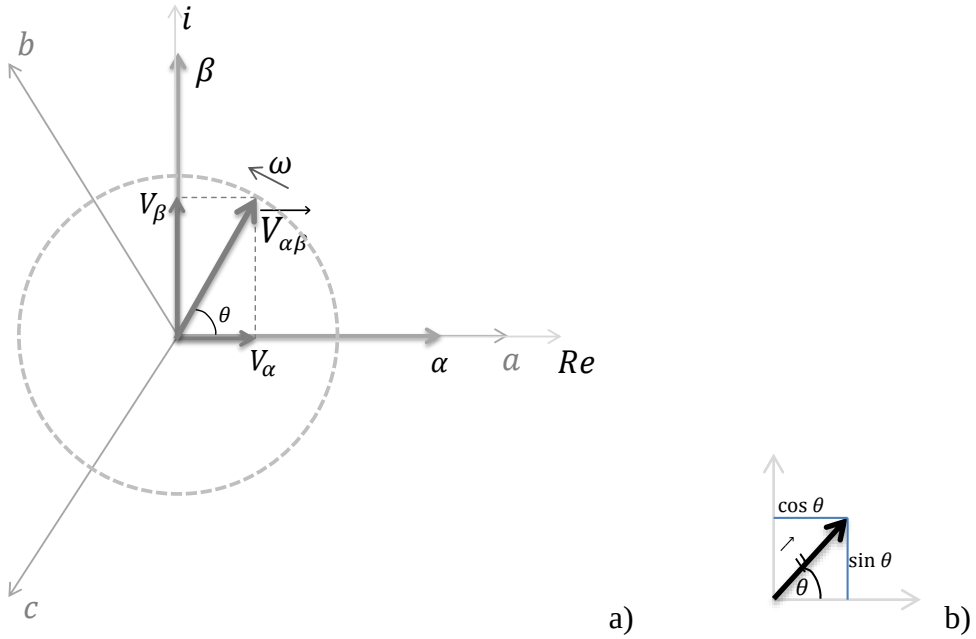

a) b)

Figure A-1. Alpha-Beta Reference Plane, a) vector definition, b) vector projections.

Given a system defined by

$$\begin{bmatrix} V_a \\ V_b \\ V_c \end{bmatrix} = \begin{bmatrix} V_a \sin(\omega t) \\ V_b \sin\left(\omega t - \frac{2\pi}{3}\right) \\ V_c \sin\left(\omega t + \frac{2\pi}{3}\right) \end{bmatrix} , \qquad \text{(A.1)}$$

and projecting the axes "abc" on alpha-beta axes as shown in Figure A-1, the Clarke transformation matrix is found to be

$$\begin{bmatrix} V_\alpha \\ V_\beta \\ V_0 \end{bmatrix} = \frac{2}{3} \begin{bmatrix} 1 & -1/2 & -1/2 \\ 0 & \sqrt{3}/2 & -\sqrt{3}/2 \\ 1/2 & 1/2 & 1/2 \end{bmatrix} \begin{bmatrix} V_a \\ V_b \\ V_c \end{bmatrix} . \qquad \text{(A.2)}$$

In the case of three wire balanced system the transformation matrix can be simplified as

$$\begin{bmatrix} V_\alpha \\ V_\beta \end{bmatrix} = \frac{2}{3} \begin{bmatrix} 1 & -1/2 & -1/2 \\ 0 & \sqrt{3}/2 & -\sqrt{3}/2 \end{bmatrix} \begin{bmatrix} V_a \\ V_b \\ V_c \end{bmatrix} . \qquad \text{(A.3)}$$

Clarke´s Inverse Transformation

Using transformation matrix (A.2) and calculating its inverse matrix, it is possible to find the “abc" axes from information provided by axes “alpha-beta”. This expression is given by

$$\begin{bmatrix} V_a \\ V_b \\ V_c \end{bmatrix} = \begin{bmatrix} 1 & 0 & 1 \\ -1/2 & \sqrt{3}/2 & 1 \\ -1/2 & -\sqrt{3}/2 & 1 \end{bmatrix} \begin{bmatrix} V_\alpha \\ V_\beta \\ V_0 \end{bmatrix} . \qquad \text{(A.4)}$$

A2. Synchronous d-q Reference Plane (Park transformation)

Figure A-2 shows the convention adopted in this work for representation of Park transform.

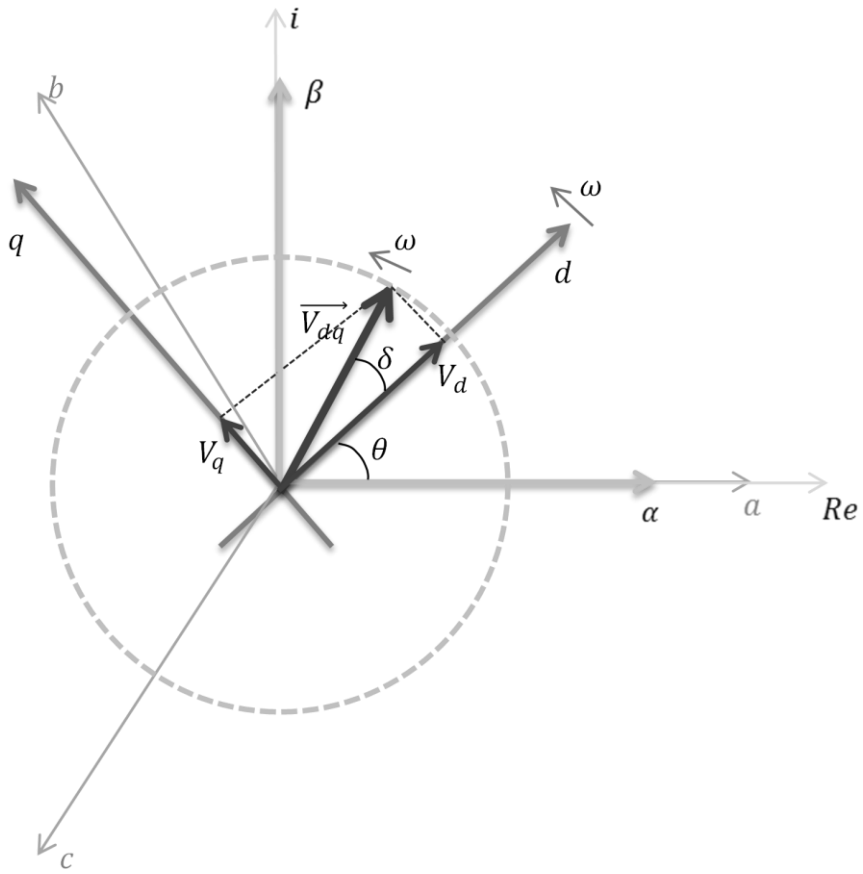

Figure A-2. d-q Reference Plane.

Defining alpha-beta and dq vector as

$$\overrightarrow{V_{\alpha\beta}} = V_\alpha + jV_\beta \quad , \tag{A.5}$$

And

$$\overrightarrow{V_{dq}} = V_d + jV_q \quad , \tag{A.6}$$

it is possible to define vector $\overrightarrow{V_{dq}}$ as a θ rotation of vector $\overrightarrow{V_{\alpha\beta}}$ in the ω direction, this expression is found to be

$$\overrightarrow{V_{dq}} = \left(V_\alpha + jV_\beta\right)e^{-j\theta} \tag{A.7}$$

where,

$$e^{-j\theta} = cos\theta - jsin\theta \quad . \tag{A.8}$$

Using definitions of "dq" vector 0 and (A.7), the relationship between vector $\overrightarrow{V_{\alpha\beta}}$ and $\overrightarrow{V_{dq}}$ is given by

$$\begin{gathered} V_d + jV_q = \left(V_\alpha + jV_\beta\right)e^{-j\theta} \\ V_d + jV_q = V_\alpha cos\theta - jV_\alpha sin\theta + jV_\beta cos\theta + V_\beta sin\theta \quad . \end{gathered} \tag{A.9}$$

Grouping similar terms direct Park transformation is found to be

$$\begin{bmatrix} \boldsymbol{V_d} \\ \boldsymbol{V_q} \end{bmatrix} = \begin{bmatrix} \boldsymbol{cos\theta} & \boldsymbol{sin\theta} \\ \boldsymbol{-sin\theta} & \boldsymbol{cos\theta} \end{bmatrix} \begin{bmatrix} \boldsymbol{V_\alpha} \\ \boldsymbol{V_\beta} \end{bmatrix} \quad . \tag{A.10}$$

Inverse Park transformation

It is possible to define the $\overrightarrow{V_{\alpha\beta}}$ vector as a θ rotation of the $\overrightarrow{V_{dq}}$ vector in opposite direction of ω, this expression is given by

$$\overrightarrow{V_{\alpha\beta}} = \left(V_d + jV_q\right)e^{j\theta} \tag{A.11}$$

Where,

$$e^{j\theta} = cos\theta + jsin\theta \quad . \tag{A.12}$$

Using definitions of vector alpha-beta (A.5) and (A.11) is possible to find a direct relationship between $\overrightarrow{V_{dq}}$ and $\overrightarrow{V_{\alpha\beta}}$ vectors as

$$V_\alpha + jV_\beta = \left(V_d + jV_q\right)e^{j\theta}$$
$$V_\alpha + jV_\beta = V_d cos\theta + jV_d sin\theta + jV_q cos\theta - V_q sin\theta \quad . \tag{A.13}$$

Grouping similar terms of expression above, it possible to find that inverse Park transformation is given by

$$\begin{bmatrix} \boldsymbol{V_\alpha} \\ \boldsymbol{V_\beta} \end{bmatrix} = \begin{bmatrix} \boldsymbol{cos\theta} & \boldsymbol{-sin\theta} \\ \boldsymbol{sin\theta} & \boldsymbol{cos\theta} \end{bmatrix} \begin{bmatrix} \boldsymbol{V_d} \\ \boldsymbol{V_q} \end{bmatrix} \quad . \tag{A.14}$$

Appendix B. Mathematical Development of Expressions of Chapters 3

.

This appendix displays detailed development of mathematical expressions presented in chapter 3.

B1. Temporal Dynamic in "*abc*" stationary reference plane

Voltage and current analysis in one phase of the inverter is found to be

$$v_{in} = v_{RLn} + v_{Ln} + v_{on} \tag{B.1}$$

and

$$i_n = i_{cn} + i_{on} \tag{B.2}$$

where, "n" represents $\{a, b, c\}$ phases. Moreover, capacitor current and inductor voltage is given by

$$v_{Ln} = L\frac{di_{in}}{dt} \tag{B.3}$$

Using Ohm's law, voltage on inductor resistance is given by:

$$v_{cn} = C\frac{dv_{on}}{dt} \;\; v_{RLn} = i_n R_L \; . \tag{B.4}$$

Using Ohm's law, voltage on inductor resistance is given by

$$v_{RLn} = i_n R_L \quad , \tag{B.5}$$

thus replacing resistance inductor voltage (B.4) and inductor voltage (B.3) on the voltages analysis (B.1) we obtain that

$$\begin{gathered} v_{in} = i_n R_L + L\frac{di_n}{dt} + v_{on} \\ v_{in} = R_L(i_{cn} + i_{on}) + L\frac{d}{dt}(i_{cn} + i_{on}) + v_{on} \quad . \end{gathered} \tag{B.6}$$

Replacing capacitor current 0 in (B.6) we obtain (B.7) which represented temporal dynamics of synthesized inverter output voltage in "abc" phases.

$$v_{in} = R_L\left(C\frac{dv_{on}}{dt} + i_{on}\right) + L\frac{d}{dt}\left(C\frac{dv_{on}}{dt} + i_{on}\right) + v_{on}$$

$$v_{in} = R_L C\frac{dv_{on}}{dt} + R_L i_{on} + LC\frac{d^2 v_{on}}{dt^2} + L\frac{di_{on}}{dt} + v_{on}$$

$$\boldsymbol{v_{in} = LC\frac{d^2 v_{on}}{dt^2} + R_L C\frac{dv_{on}}{dt} + v_{on} + L\frac{di_{on}}{dt} + R_L i_{on}} \qquad \text{(B.7)}$$

B2. Temporal Dynamic in "*d-q*" Synchronous Reference Plane

Positive Sequence Component

As presented in Appendix C1, the system in alpha-beta reference axis can be defined as a vector in dq synchronous reference axis as

$$\overrightarrow{v_{dq}}_{+} = \left(v_{\alpha+} + jv_{\beta+}\right)e^{-j\theta} \qquad \text{(B.8)}$$

and

$$\overrightarrow{i_{dq}}_{+} = \left(i_{\alpha+} + ji_{\beta+}\right)e^{-j\theta} \qquad \text{(B.9)}$$

Taking the analysis of positive-sequence voltage in alpha and beta axis (C.7) and (C.8) respectively, and replacing in to the positive sequence vector definition (B.8). It is possible to find dynamic response of voltage vector in synchronous reference axis, this is given by

$$\overrightarrow{v_{idq}}_{+} = \left\{\left(LC\frac{d^2 v_{o\alpha+}}{dt^2} + R_L C\frac{dv_{o\alpha+}}{dt} + v_{o\alpha+} + L\frac{di_{o\alpha+}}{dt} + R_L i_{\alpha+}\right) + j\left(LC\frac{d^2 v_{o\beta+}}{dt^2} + R_L C\frac{dv_{o\beta+}}{dt} + v_{o\beta+} + L\frac{di_{o\beta+}}{dt} + R_L i_{\beta+}\right)\right\}e^{-j\theta}$$

$$\overrightarrow{v_{idq}}_{+} = LC\frac{d^2}{dt^2}\left(v_{o\alpha+} + jv_{o\beta+}\right)e^{-j\theta} + R_L C\frac{d}{dt}\left(v_{o\alpha+} + jv_{o\beta+}\right)e^{-j\theta} + \left(v_{o\alpha+} + jv_{o\beta+}\right)e^{-j\theta} + L\frac{d}{dt}\left(i_{o\alpha+} + ji_{o\beta+}\right)e^{-j\theta} + R_L\left(i_{o\alpha+} + ji_{o\beta+}\right)e^{-j\theta} \quad . \qquad \text{(B.10)}$$

Zero order terms of (B.10) can be defined by (B.8) and (B.9), while (B.15), (B.17) and (B.19) resolve the terms of first and second order. Procedure for finding these expressions will be presented below.

By deriving definition of voltage vector in dq (B.8) we obtain

$$\frac{d\overrightarrow{v_{odq+}}}{dt} = \frac{d}{dt}\left[\left(v_{o\alpha+} + jv_{o\beta+}\right)e^{-j\theta}\right]$$

$$\frac{d\overrightarrow{v_{odq+}}}{dt} = \frac{dv_{o\alpha+}}{dt}e^{-j\theta} - v_{o\alpha+}e^{-j\theta}j\frac{d\theta}{dt} + j\frac{dv_{o\beta+}}{dt}e^{-j\theta} - jv_{o\beta+}e^{-j\theta}j\frac{d\theta}{dt}$$

.

As $\frac{d\theta}{dt} = \omega$, then

$$\frac{d\overrightarrow{v_{odq+}}}{dt} = \frac{d\left(v_{o\alpha_+}+jv_{o\beta_+}\right)}{dt}e^{-j\theta} - j\omega v_{o\alpha_+}e^{-j\theta} + \omega v_{o\beta_+}e^{-j\theta} \quad . \qquad \text{(B.11)}$$

Based on definition of vector dq (B.8) and (B.9) we can express

$$(\alpha + j\beta)e^{-i\theta} = (d + jq) \quad .$$

Using Euler's identity:

$$\alpha\cos\theta - i\alpha\sin\theta + \beta\sin\theta + j\beta\cos\theta = (d + jq) \qquad \text{(B.12)}$$

Associating α with d and β whit q in (B.12) is obtained

$$\alpha(\cos\theta - j\sin\theta) = d$$

$$\mathbf{d = \alpha e^{-j\theta}} \quad , \qquad \text{(B.13)}$$

and

$$\beta(\sin\theta + j\cos\theta) = jq$$

$$\boldsymbol{q = \beta e^{-j\theta}} \qquad \text{(B.14)}$$

Substituting expressions for d and q components (B.13), (B.14) into (B.11) we can obtain the voltage of first order equation in (B.10),

$$\frac{d\overrightarrow{v_{odq+}}}{dt} = \frac{d\left(v_{o\alpha+}+jv_{o\beta+}\right)}{dt}e^{-j\theta} - j\omega v_{od_+} + \omega v_{oq_+}$$

$$\boldsymbol{\frac{d\left(v_{o\alpha+}+jv_{o\beta+}\right)}{dt}e^{-j\theta} = \frac{d\overrightarrow{v_{odq+}}}{dt} + j\omega v_{od_+} - \omega v_{oq_+}} \quad . \qquad \text{(B.15)}$$

Similarly as voltage analysis, current can be also performed, i.e., deriving current vector defining in dq (B.9) we obtain

$$\frac{d\overrightarrow{i_{odq+}}}{dt} = \frac{d}{dt}\left[\left(i_{o\alpha+} + ji_{o\beta+}\right)e^{-j\theta}\right]$$

$$\frac{d\overrightarrow{i_{odq+}}}{dt} = \frac{di_{o\alpha+}}{dt}e^{-j\theta} - i_{o\alpha+}e^{-j\theta}j\frac{d\theta}{dt} + j\frac{di_{o\beta+}}{dt}e^{-j\theta} - ji_{o\beta+}e^{-j\theta}j\frac{d\theta}{dt} \ .$$

As $\frac{d\theta}{dt} = \omega$, then

$$\frac{d\overrightarrow{i_{odq+}}}{dt} = \frac{d\left(i_{o\alpha_+} + ji_{o\beta_+}\right)}{dt}e^{-j\theta} - j\omega i_{o\alpha_+}e^{-j\theta} + \omega i_{o\beta_+}e^{-j\theta} \quad . \qquad \text{(B.16)}$$

Substituting expressions for d and q components (B.13), (B.14) into (B.16), we can obtain the voltage of first order equation in (B.10)

$$\frac{d\overrightarrow{i_{odq+}}}{dt} = \frac{d\left(i_{o\alpha+} + ji_{o\beta+}\right)}{dt}e^{-j\theta} - j\omega i_{od_+} + \omega i_{oq_+}$$

$$\boldsymbol{\frac{d\left(i_{o\alpha+} + ji_{o\beta+}\right)}{dt}e^{-j\theta} = \frac{d\overrightarrow{i_{odq+}}}{dt} + j\omega i_{od_+} - \omega i_{oq_+}} \quad . \qquad \text{(B.17)}$$

To find the second order term of equation (B.10) can be based on the definition of second derivative of voltage vector dq (B.8),

$$\frac{d^2\overrightarrow{v_{odq_+}}}{dt^2} = \frac{d^2}{dt^2}\left[\left(v_{o\alpha_+} + jv_{o\beta_+}\right)e^{-j\theta}\right]$$

$$\frac{d^2\overrightarrow{v_{odq+}}}{dt^2} = \frac{d}{dt}\left\{\frac{d}{dt}\left[\left(v_{o\alpha+} + jv_{o\beta+}\right)e^{-j\theta}\right]\right\}$$

$$\frac{d^2\overrightarrow{v_{odq+}}}{dt^2} = \frac{d}{dt}\left(\frac{dv_{o\alpha+}}{dt}e^{-j\theta} - j\omega v_{o\alpha+}e^{-j\theta} + j\frac{dv_{o\beta+}}{dt}e^{-j\theta} + \omega v_{o\beta+}e^{-j\theta}\right)$$

$$\frac{d^2\overrightarrow{v_{odq+}}}{dt^2} = \frac{d^2v_{o\alpha+}}{dt^2}e^{-j\theta} + j\frac{d^2v_{o\beta+}}{dt^2}e^{-j\theta} - j2\omega\frac{dv_{o\alpha+}}{dt}e^{-j\theta} + 2\omega\frac{dv_{o\beta+}}{dt}e^{-j\theta} - \omega^2 v_{o\alpha+}e^{-j\theta} - j\omega^2 v_{o\beta+}e^{-j\theta}$$

$$\frac{d^2\overrightarrow{v_{odq+}}}{dt^2} = \frac{d^2\left(v_{o\alpha_+} + jv_{\beta_+}\right)}{dt^2}e^{-j\theta} - j2\omega\frac{dv_{o\alpha+}}{dt}e^{-j\theta} + 2\omega\frac{dv_{o\beta+}}{dt}e^{-j\theta} - \omega^2 v_{o\alpha+}e^{-j\theta} - j\omega^2 v_{o\beta+}e^{-j\theta} \quad . \qquad \text{(B.18)}$$

As can be seen from equation (B.18), it contains second-order term in equation (B.10). Isolating the second order term it is possible to find

$$\frac{d^2(v_{o\alpha+}-jv_{\beta+})}{dt^2}e^{-j\theta} = \frac{d^2\overrightarrow{v_{odq+}}}{dt^2} + j2\omega\frac{dv_{o\alpha+}}{dt}e^{-j\theta} - 2\omega\frac{dv_{o\beta+}}{dt}e^{-j\theta} + \omega^2\overrightarrow{v_{odq+}} \quad \text{(B.19)}$$

Using definitions of the voltage terms with zero, first and second order, equations (B.8), (B.15) and (B.19) respectively, as well as definitions of current with zero and first-order, equations (B.9) and (B.17) respectively, and replacing temporary definition of voltage inverter dq (B.10) we obtain

$$\overrightarrow{v_{\imath dq}}_+ = LC\left(\frac{d^2\overrightarrow{v_{odq+}}}{dt^2} + j2\omega\frac{dv_{o\alpha+}}{dt}e^{-j\theta} - 2\omega\frac{dv_{o\beta+}}{dt}e^{-j\theta} + \omega^2\overrightarrow{v_{odq+}}\right) + R_LC\left(\frac{d\overrightarrow{v_{odq+}}}{dt} + j\omega v_{od+} - \omega v_{oq+}\right) + \overrightarrow{v_{odq+}} + L\left(\frac{d\overrightarrow{\imath_{odq+}}}{dt} + j\omega i_{od_+} - \omega i_{oq_+}\right) + R_L\overrightarrow{\imath_{dq}}_+$$

$$\overrightarrow{v_{\imath dq}}_+ = LC\frac{d^2\overrightarrow{v_{odq+}}}{dt^2} + R_LC\frac{d\overrightarrow{v_{odq+}}}{dt} + \overrightarrow{v_{odq+}} + \omega^2LC\overrightarrow{v_{odq+}} + j2\omega LC\frac{dv_{o\alpha+}}{dt}e^{-j\theta} - 2\omega LC\frac{dv_{o\beta+}}{dt}e^{-j\theta} + j\omega R_LCv_{od+} - \omega R_LCv_{oq+} + L\frac{d\overrightarrow{\imath_{odq+}}}{dt} + j\omega Li_{od_+} - \omega Li_{oq_+} + R_L\overrightarrow{\imath_{dq}}_+ \quad \text{(B.20)}$$

Equation (B.20) has two terms of first-order (alpha and beta components of the inverter output-voltage vector), these terms can be found by deriving definition of d component (B.13) and q component (B.14).

$$\frac{dv_{od+}}{dt} = \frac{d}{dt}\left(v_{o\alpha+}e^{-j\theta}\right)$$

$$\frac{dv_{od+}}{dt} = \frac{dv_{o\alpha+}}{dt}e^{-j\theta} - j\omega v_{o\alpha+}e^{-j\theta}$$

Using definition of d-component, (B.13)

$$\frac{dv_{o\alpha+}}{dt}e^{j\theta} = \frac{dv_{od+}}{dt} + j\omega v_{od+} \quad . \quad \text{(B.21)}$$

Also is possible to deriving (B.14), obtaining

$$\frac{dv_{oq+}}{dt} = \frac{d}{dt}\left(v_{o\beta+}e^{-j\theta}\right)$$

$$\frac{dv_{oq+}}{dt} = \frac{dv_{o\beta+}}{dt}e^{j\theta} - j\omega v_{o\beta+}e^{-j\theta} \quad .$$

Using definition of q-component, (B.14)

$$\frac{dv_{o\beta+}}{dt}e^{j\theta} = \frac{dv_{oq+}}{dt} + j\omega v_{oq+} \quad . \tag{B.22}$$

Replacing (B.21) and (B.22) into (B.20) can be found

$$\begin{aligned}\overrightarrow{v_{\imath dq}}_{+} = LC\frac{d^2\overrightarrow{v_{odq+}}}{dt^2} + R_L C\frac{d\overrightarrow{v_{odq+}}}{dt} + \overrightarrow{v_{odq+}} + \omega^2 LC\overrightarrow{v_{odq+}} + \\ j2\omega LC\left(\frac{dv_{od+}}{dt} + j\omega v_{od+}\right) - 2\omega LC\left(\frac{dv_{oq+}}{dt} + j\omega v_{oq+}\right) + \\ j\omega R_L C v_{od+} - \omega R_L C v_{oq+} + L\frac{d\overrightarrow{\imath_{odq+}}}{dt} + j\omega L i_{od_+} - \\ \omega L i_{oq_+} + R_L\overrightarrow{\imath_{dq}}_{+} \quad ,\end{aligned}$$

$$\begin{aligned}\overrightarrow{v_{\imath dq}}_{+} = LC\frac{d^2\overrightarrow{v_{odq+}}}{dt^2} + R_L C\frac{d\overrightarrow{v_{odq+}}}{dt} + (1+\omega^2 LC)\overrightarrow{v_{odq+}} + \\ j2\omega LC\frac{dv_{od+}}{dt} - j2\omega^2 LC v_{oq+} + j\omega R_L C v_{od+} - 2\omega LC\frac{dv_{oq+}}{dt} - \\ 2\omega^2 LC v_{od+} - \omega R_L C v_{oq+} + L\frac{d\overrightarrow{\imath_{odq+}}}{dt} + j\omega L i_{od_+} - \omega L i_{oq_+} + \\ R_L\overrightarrow{\imath_{dq}}_{+} \quad .\end{aligned} \tag{B.23}$$

Finally, as $\left(\overrightarrow{v_{dq}} = v_d - jv_q\right)$ and $\left(\overrightarrow{\imath_{dq}} = i_d - ji_q\right)$, then it is possible to associate the component "d" with the real terms, and "q" component with the imaginary terms of equation (B.23). Thus, in order to obtain the temporal representation of the positive sequence voltages in the reference axes d and q, equations (B.24) and 0 respectively. These temporal representations are found to be

$$\begin{aligned}\boldsymbol{v_{id+} = LC\frac{d^2 v_{od_+}}{dt^2} + R_L C\frac{dv_{od_+}}{dt} + (1-\omega^2 LC)v_{od_+} +} \\ \boldsymbol{L\frac{di_{od_+}}{dt} + R_L i_{od_+} - 2\omega LC\frac{dv_{oq_+}}{dt} - \omega R_L C v_{oq_+} -} \\ \boldsymbol{\omega L i_{oq_+} \quad ,}\end{aligned} \tag{B.24}$$

and

$$\begin{aligned}\boldsymbol{v_{iq+} = LC\frac{d^2 v_{oq+}}{dt^2} + R_L C\frac{dv_{oq+}}{dt} + (1-\omega^2 LC)v_{oq+} +} \\ \boldsymbol{L\frac{di_{oq+}}{dt} + R_L i_{oq+} + 2\omega LC\frac{dv_{od+}}{dt} + \omega R_L C v_{od+} + \omega L i_{od_+} \quad .}\end{aligned} \tag{B.25}$$

Negative Sequence Component

The negative sequence component in the synchronous reference axis can be found following the same procedure of the positive component presented in last section. But, it has to be applied the definition of d-q voltage vector expressed in (B.26) and the definition of d-q current vector expressed in (B.27). The result of this procedure is shown in (B.28) and 0, in which the system dynamics is the same as the positive component, only the sign of the coupling between both phases is inverted. The expressions mentioned above are found to be

$$\overrightarrow{v_{dq\_}} = \left(v_{\alpha-} + jv_{\beta-}\right)e^{j\theta} \quad , \tag{B.26}$$

$$\overrightarrow{i_{dq\_}} = \left(i_{\alpha-} + ji_{\beta-}\right)e^{j\theta} \quad , \tag{B.27}$$

$$\begin{aligned} \boldsymbol{v_{id-}} = \boldsymbol{LC}\frac{\boldsymbol{d^2v_{od\_}}}{\boldsymbol{dt^2}} + \boldsymbol{R_LC}\frac{\boldsymbol{dv_{od\_}}}{\boldsymbol{dt}} + (\boldsymbol{1-\omega^2LC})\boldsymbol{v_{od\_}} + \boldsymbol{L}\frac{\boldsymbol{di_{od-}}}{\boldsymbol{dt}} + \\ \boldsymbol{R_Li_{od\_}} + \boldsymbol{2\omega LC}\frac{\boldsymbol{dv_{oq\_}}}{\boldsymbol{dt}} + \boldsymbol{\omega R_LCv_{oq\_}} + \boldsymbol{\omega Li_{oq\_}} \quad , \end{aligned} \tag{B.28}$$

and

$$\begin{aligned} \boldsymbol{v_{iq\_}} = \boldsymbol{LC}\frac{\boldsymbol{d^2v_{oq\_}}}{\boldsymbol{dt^2}} + \boldsymbol{R_LC}\frac{\boldsymbol{dv_{oq\_}}}{\boldsymbol{dt}} + (\boldsymbol{1-\omega^2LC})\boldsymbol{v_{oq\_}} + \boldsymbol{L}\frac{\boldsymbol{di_{oq\_}}}{\boldsymbol{dt}} + \\ \boldsymbol{R_Li_{oq\_}} - \boldsymbol{2\omega LC}\frac{\boldsymbol{dv_{od\_}}}{\boldsymbol{dt}} - \boldsymbol{\omega R_LCv_{od\_}} - \boldsymbol{\omega Li_{od\_}} \quad . \end{aligned} \tag{B.29}$$

B3. Synchronous Mathematical Model with Capacitor Current feedback

Taking the temporal dynamics of the voltage analysis in d and q reference axes, (B.24) and 0 respectively, and ignoring the coupling between axes, it can be found

$$v_{in} = LC\frac{d^2v_{on}}{dt^2} + R_LC\frac{dv_{on}}{dt} + (1-\omega^2LC)v_{on} + L\frac{di_{on}}{dt} + R_Li_{on} \quad . \tag{B.30}$$

where $n = \{d_+ \quad q_+ \quad d_- \quad q_-\}$.

Then, expressing (B.30) in the Laplace domain it can be found

$$V_i = LCS^2V_o + R_LCSV_o + (1-\omega^2LC)V_0 + LSI_{on} + R_LI_{on} \quad . \tag{B.31}$$

Now, considering the capacitor current feedback, the converter gain and the transformer turns ratio, "I_c", "K_{inv}", "K_{trans}" respectively, we can express

$$V_i = (U - I_c)K_{inv} \quad , \tag{B.32}$$

where "U", is the system input which comes from the controller effort and "I_c", represents the capacitor current in dq.reference axes. In addition, defining

$$K_{inv} = K_o K_{trans} \quad , \tag{B.33}$$

using the definition of current in the capacitor 0 and substituting in (B.32), it can be found

$$V_i = (U - CSV_o)K_{inv} \quad . \tag{B.34}$$

Substituting (B.34) into (B.31), we can obtain the transfer function that describes the three phase inverter in dq reference axes, this transfer function is found to be

$$K_{inv}(U - CSV_o) = \big(LCS^2 + R_L CS + (1 - \omega^2 LC)\big)V_0 + (LS + R_L)I_{on} \ ,$$

$$V_o = \frac{K_{inv}}{\left(LCS^2 + (R_L + K_o)CS + (1 - \omega^2 LC)\right)} U - \frac{(LS + R_L)}{\left(LCS^2 + (R_L + K_o)CS + (1 - \omega^2 LC)\right)} I_{on} \quad . \tag{B.35}$$

Then, it is possible to express (B.35) as

$$\boldsymbol{G(s) = G_{Vo}(s) - G_{Io}(s)} \quad , \tag{B.36}$$

Where,

$$\boldsymbol{G_{Vo}(s) = \frac{V_o}{U} = \frac{K_{inv}}{LCS^2 + (R_L + K_o)CS + (1 - \omega^2 LC)}} \quad , \tag{B.37}$$

and

$$\boldsymbol{G_{Io}(s) = \frac{V_o}{I_o} = \frac{LS + R_L}{LCS^2 + (R_L + K_o)CS + (1 - \omega^2 LC)}} \quad . \tag{B.38}$$

Appendix C. Mathematical Development of Expressions of Chapter 4

This appendix displays detailed development of mathematical expressions presented in chapter 4.

C1. Temporal Dynamic in "*alpha-beta*" stationary reference plane

Using none- normalized Clarke transformation to voltage alpha axis, it can be found

$$v_\alpha = \frac{2}{3}\left(v_a - \frac{1}{2}v_b - \frac{1}{2}v_c\right) \quad . \tag{C.1}$$

Replacing the dynamic expression of voltage in the reference axes "abc" (B.7), into the transformation of Clarke for "alpha" axis (C.1), it is possible to obtain

$$v_{i\alpha} = \frac{2}{3}\left(\left(LC\frac{d^2v_{oa}}{dt^2} + R_LC\frac{dv_{oa}}{dt} + v_{oa} + L\frac{di_{oa}}{dt} + R_Li_{oa}\right) - \frac{1}{2}\left(LC\frac{d^2v_{ob}}{dt^2} + R_LC\frac{dv_{ob}}{dt} + v_{ob} + L\frac{di_{ob}}{dt} + R_Li_b\right) - \frac{1}{2}\left(LC\frac{d^2v_{oc}}{dt^2} + R_LC\frac{dv_{oc}}{dt} + v_{oc} + L\frac{di_{oc}}{dt} + R_Li_{oc}\right)\right) \quad ,$$

$$v_{i\alpha} = LC\frac{d^2}{dt^2}\left[\frac{2}{3}\left(v_a - \frac{1}{2}v_b - \frac{1}{2}v_c\right)\right] + R_LC\frac{d}{dt}\left[\frac{2}{3}\left(v_a - \frac{1}{2}v_b - \frac{1}{2}v_c\right)\right] + \left[\frac{2}{3}\left(v_a - \frac{1}{2}v_b - \frac{1}{2}v_c\right) + L\frac{d}{dt}\left(i_a - \frac{1}{2}i_b - \frac{1}{2}i_c\right) + R_L\left(i_a - \frac{1}{2}i_b - \frac{1}{2}i_c\right)\right].$$

Using the definition (C.1), it is possible to find the temporal response of the inverter voltage in the reference alpha axis. This expression is found to be

$$\boldsymbol{v_{i\alpha} = LC\frac{d^2v_{o\alpha}}{dt^2} + R_LC\frac{dv_{o\alpha}}{dt} + v_{o\alpha} + L\frac{di_{o\alpha}}{dt} + R_Li_{o\alpha}} \quad . \tag{C.2}$$

Moreover, using the non-normalized Clarke transformation to beta axis

$$v_\beta = \frac{2}{3}\left(\frac{\sqrt{3}}{2}v_b - \frac{\sqrt{3}}{2}v_c\right) \quad , \tag{C.3}$$

taking the dynamics of the output voltage (B.7) and substituting in (C.3), it can be found

$$v_{i\beta} = \frac{2}{3}\left(\frac{\sqrt{3}}{2}\left(LC\frac{d^2v_{ob}}{dt^2} + R_LC\frac{dv_{ob}}{dt} + v_{ob} + L\frac{di_{ob}}{dt} + R_Li_b\right) - \frac{\sqrt{3}}{2}\left(LC\frac{d^2v_{oc}}{dt^2} + R_LC\frac{dv_{oc}}{dt} + v_{oc} + L\frac{di_{oc}}{dt} + R_Li_{oc}\right)\right) \quad ,$$

$$v_{i\beta} = LC\frac{d^2}{dt^2}\left[\frac{2}{3}\left(\frac{\sqrt{3}}{2}v_b - \frac{\sqrt{3}}{2}v_c\right)\right] + R_L C\frac{d}{dt}\left[\frac{2}{3}\left(\frac{\sqrt{3}}{2}v_b - \frac{\sqrt{3}}{2}v_c\right)\right] + \left[\frac{2}{3}\left(\frac{\sqrt{3}}{2}v_b - \frac{\sqrt{3}}{2}v_c\right)\right] + L\frac{d}{dt}\left[\frac{2}{3}\left(\frac{\sqrt{3}}{2}i_b - \frac{\sqrt{3}}{2}i_c\right)\right] + R_L\left[\frac{2}{3}\left(\frac{\sqrt{3}}{2}i_b - \frac{\sqrt{3}}{2}i_c\right)\right].$$

Using the definition (C.3), the temporal analysis of the inverter voltage reference axis beta is found to be

$$\boldsymbol{v_{i\beta} = LC\frac{d^2v_{o\beta}}{dt^2} + R_L C\frac{dv_{o\beta}}{dt} + v_{o\beta} + L\frac{di_{o\beta}}{dt} + R_L i_\beta} \quad . \tag{C.4}$$

Positive Sequence Component

Using the method of symmetrical components in the time domain, it is possible to find the positive sequence alpha-beta as

$$\alpha_+ = \frac{1}{2}(\alpha - q\beta) = \frac{1}{2}(\alpha + j\beta) \quad , \tag{C.5}$$

$$\beta_+ = \frac{1}{2}(q\alpha + \beta) = \frac{1}{2}(-j\alpha + \beta) \quad , \tag{C.6}$$

where, $q = e^{-j\frac{\pi}{2}} = -j$. Replacing the definition alpha voltage (C.2) in the expression of positive component (C.5) it can be found

$$v_{i\alpha_+} = \frac{1}{2}\left(\left(LC\frac{d^2v_{o\alpha}}{dt^2} + R_L C\frac{dv_{o\alpha}}{dt} + v_{o\alpha} + L\frac{di_{o\alpha}}{dt} + R_L i_{o\alpha}\right) + j\left(LC\frac{d^2v_{o\beta}}{dt^2} + R_L C\frac{dv_{o\beta}}{dt} + v_{o\beta} + L\frac{di_{o\beta}}{dt} + R_L i_\beta\right)\right) \quad ,$$

$$v_{i\alpha_+} = LC\frac{d^2}{dt^2}\left[\frac{1}{2}\left(v_{o\alpha} + jv_{o\beta}\right)\right] + R_L C\frac{d}{dt}\left[\frac{1}{2}\left(v_{o\alpha} + jv_{o\beta}\right)\right] + \frac{1}{2}\left(v_{o\alpha} + jv_{o\beta}\right) + L\frac{d}{dt}\left[\frac{1}{2}\left(i_{o\alpha} + ji_{o\beta}\right)\right] + R_L\left[\frac{1}{2}\left(i_{o\alpha} + ji_{o\beta}\right)\right] \quad .$$

Using the definition of positive component for alpha expressed in (C.5), it can be found the positive sequence component to the analysis of voltage inverter in the alpha reference axis, and this expression is given by

$$\boldsymbol{v_{i\alpha_+} = LC\frac{d^2v_{o\alpha_+}}{dt^2} + R_L C\frac{dv_{o\alpha_+}}{dt} + v_{o\alpha_+} + L\frac{di_{o\alpha_+}}{dt} + R_L i_{\alpha_+}} \quad . \tag{C.7}$$

Moreover, replacing the voltage definition beta (C.4), in the expression of positive component (C.6) it can be found

$$v_{i\beta_+} = \frac{1}{2}\Bigg(-j\left(LC\frac{d^2v_{o\alpha}}{dt^2} + R_LC\frac{dv_{o\alpha}}{dt} + v_{o\alpha} + L\frac{di_{o\alpha}}{dt} + R_Li_\alpha\right) + \left(LC\frac{d^2v_{o\beta}}{dt^2} + R_LC\frac{dv_{o\beta}}{dt} + v_{o\beta} + L\frac{di_{o\beta}}{dt} + R_Li_\beta\right)\Bigg) \quad ,$$

$$v_{i\beta_+} = LC\frac{d^2}{dt^2}\left[\frac{1}{2}\left(-jv_{o\alpha} + v_{o\beta}\right)\right] + R_LC\frac{d}{dt}\left[\frac{1}{2}\left(-jv_{o\alpha} + v_{o\beta}\right)\right] + \frac{1}{2}\left(-jv_{o\alpha} + v_{o\beta}\right) + L\frac{d}{dt}\left[\frac{1}{2}\left(-ji_{o\alpha} + i_{o\beta}\right)\right] + R_L\left[\frac{1}{2}\left(-ji_{o\alpha} + i_{o\beta}\right)\right] \quad .$$

Using the definition of positive component for alpha expressed in (C.6), it can be found the positive sequence component of inverter voltage in the alpha reference axis, and this expression is given by

$$\boldsymbol{v_{i\beta_+} = LC\frac{d^2v_{o\beta_+}}{dt^2} + R_LC\frac{dv_{o\beta_+}}{dt} + v_{o\beta_+} + L\frac{di_{o\beta_+}}{dt} + R_Li_{\beta_+}} \quad . \qquad \text{(C.8)}$$

Negative Sequence Component

Using the method of symmetrical components in the time domain, it is possible to find the negative sequence alpha-beta as:

$$\alpha_- = \frac{1}{2}(\alpha + q\beta) = \frac{1}{2}(\alpha - j\beta) \quad , \qquad \text{(C.9)}$$

$$\beta_- = \frac{1}{2}(-q\alpha + \beta) = \frac{1}{2}(j\alpha + \beta) \quad , \qquad \text{(C.10)}$$

where, $q = e^{-j\frac{\pi}{2}} = -j$. Replacing the definition of alpha voltage (C.10) in the expression of negative component (C.9) it can be found

$$v_{i\alpha_-} = \frac{1}{2}\Bigg(\left(LC\frac{d^2v_{o\alpha}}{dt^2} + R_LC\frac{dv_{o\alpha}}{dt} + v_{o\alpha} + L\frac{di_{o\alpha}}{dt} + R_Li_\alpha\right) - j\left(LC\frac{d^2v_{o\beta}}{dt^2} + R_LC\frac{dv_{o\beta}}{dt} + v_{o\beta} + L\frac{di_{o\beta}}{dt} + R_Li_\beta\right)\Bigg) \quad ,$$

$$v_{i\alpha_-} = LC\frac{d^2}{dt^2}\left[\frac{1}{2}\left(v_{o\alpha} - jv_{o\beta}\right)\right] + R_LC\frac{d}{dt}\left[\frac{1}{2}\left(v_{o\alpha} - jv_{o\beta}\right)\right] + \frac{1}{2}\left(v_{o\alpha} - jv_{o\beta}\right) + L\frac{d}{dt}\left[\frac{1}{2}\left(i_{o\alpha} - ji_{o\beta}\right)\right] + R_L\left[\frac{1}{2}\left(i_{o\alpha} - ji_{o\beta}\right)\right] \quad .$$

Using (C.9) it can be found the expression that defines the negative sequence component to the inverter voltage in the alpha reference axis. This expression is given by

$$\boldsymbol{v_{i\alpha_-} = LC\frac{d^2v_{o\alpha_-}}{dt^2} + R_LC\frac{dv_{o\alpha_-}}{dt} + v_{o\alpha_-} + L\frac{di_{o\alpha_-}}{dt} + R_Li_{\alpha_-}} \quad . \qquad \text{(C.11)}$$

Replacing the voltage beta definition (C.8) in the expression of negative component (C.10) it can be found

$$v_{i\beta\_} = \frac{1}{2}\left(j\left(LC\frac{d^2v_{o\alpha}}{dt^2} + R_LC\frac{dv_{o\alpha}}{dt} + v_{o\alpha} + L\frac{di_{o\alpha}}{dt} + R_Li_\alpha\right) + \left(LC\frac{d^2v_{o\beta}}{dt^2} + R_LC\frac{dv_{o\beta}}{dt} + v_{o\beta} + L\frac{di_{o\beta}}{dt} + R_Li_\beta\right)\right) ,$$

$$v_{i\beta\_} = LC\frac{d^2}{dt^2}\left[\frac{1}{2}\left(jv_{o\alpha} + v_{o\beta}\right)\right] + R_LC\frac{d}{dt}\left[\frac{1}{2}\left(jv_{o\alpha} + v_{o\beta}\right)\right] + \frac{1}{2}\left(jv_{o\alpha} + v_{o\beta}\right) + L\frac{d}{dt}\left[\frac{1}{2}\left(ji_{o\alpha} + i_{o\beta}\right)\right] + R_L\left[\frac{1}{2}\left(ji_{o\alpha} + i_{o\beta}\right)\right] .$$

Using equation (C.10), it can be found the expression that defines the negative sequence component to the inverter voltage in beta reference axis, this expression is given by

$$\boldsymbol{V_{i\beta\_} = LC\frac{d^2V_{o\beta\_}}{dt^2} + R_LC\frac{dV_{o\beta\_}}{dt} + V_{o\beta\_} + L\frac{di_{o\beta\_}}{dt} + R_Li_{\beta\_}} \quad \text{(C.12)}$$

C2. Stationary Mathematical Model

Taking the temporal dynamics of the voltage analysis in the inverter on α and β reference axes, equations (C.7), (C.8), (C.11) and (C.12) we obtain:

$$v_{in} = LC\frac{d^2v_{on}}{dt^2} + R_LC\frac{dv_{on}}{dt} + v_{on} + L\frac{di_{on}}{dt} + R_Li_{on} \quad \text{(C.13)}$$

Where $n = \{\alpha_+ \quad \beta_+ \quad \alpha_- \quad \beta_-\}$

Expressing the dynamic equation of the output voltage (C.13) in the Laplace domain:

$$V_i = LCS^2V_o + R_LCSV_o + V_0 + LSI_{on} + R_LI_{on} \quad \text{(C.14)}$$

Grouping similar terms and taking into account the gain presented by the inverter we find the mathematical model of inverter in the alpha-beta reference axes:

$$V_o = G_{vo}(s)V_o^* - G_{io}(s)I_o \quad \text{(C.15)}$$

Where:

$$G_{vo}(s) = \frac{K_{inv}}{(LCS^2 + RCS + 1)} \quad \text{(C.16)}$$

$$G_{io}(s) = \frac{(R + LS)}{(LCS^2 + RCS + 1)} \quad \text{(C.17)}$$

C.2.1. Open-loop Dynamic Equations.

Expressing the mathematical model (C.15) in the canonical form we obtain:

$$V_o = G_{vo_{can}}(s)V_o^* - G_{io_{can}}(s)I_o \tag{C.18}$$

Where:

$$G_{vo_{can}}(s) = \frac{\left(\frac{1}{LC}\right)K_{inv}}{\left(S^2 + \frac{RS}{L} + \frac{1}{LC}\right)} \tag{C.19}$$

$$G_{io_{can}}(s) = \frac{\left(\frac{1}{C}\right)\left(S + \frac{R}{L}\right)}{\left(S^2 + \frac{RS}{L} + \frac{1}{LC}\right)} \tag{C.20}$$

It is possible to factor the denominator of the expressions (C.19) and (C.20) using the general equation for a square polynomial factorization.

$$-P_{1,2} = \frac{-b \pm \sqrt{b^2 - 4ac}}{2a} \tag{C.21}$$

Using (C.21) we find the expression that shows the location of the poles of the model according to the value of the inverter parameters.

$$P_{1,2} = \frac{R}{2L} \mp \sqrt{\left(\frac{R}{2L}\right)^2 - \frac{1}{LC}} \tag{C.22}$$

Rewriting the canonical model (C.18) we obtain the factored system:

$$V_o = \frac{K_{vi}}{(S + P_1)(S + P_2)}V_i - \frac{K_{io}(S + Z_1)}{(S + P_1)(S + P_2)}I_o$$

Where:

$P_1 = \frac{R}{2L} - \sqrt{\left(\frac{R}{2L}\right)^2 - \frac{1}{LC}}$; $\quad K_{io} = \frac{1}{C}$ $\quad Z_1 = \frac{R}{L}$; $\quad K_{vi} = \frac{1}{LC}K_{inv}$

$P_2 = \frac{R}{2L} + \sqrt{\left(\frac{R}{2L}\right)^2 - \frac{1}{LC}}$;

Comparing the expression of the output voltage with respect to the reference (C.19) with the general canonical form of a second order system, we obtain:

$$\frac{V_o}{U} = \frac{\frac{K_{inv}}{LC}}{\left(S^2 + \frac{R_L}{L}S + \frac{1}{LC}\right)} = \frac{K_{V_o}\omega_n^2}{(S^2 + 2\zeta\omega_n + {\omega_n}^2)} \quad \text{(C.23)}$$

Is possible using the above expression identify dynamic characteristic parameter of the inverter output voltage with respect to the reference voltage

$${\omega_n}^2 = \frac{1}{LC} \qquad 2\zeta\omega_n = \frac{R_L}{L} \qquad K_{V_o}\omega_n^2 = \frac{K_{inv}}{LC}$$

$$\boldsymbol{\omega_n = \sqrt{\frac{1}{LC}}} \qquad \boldsymbol{\zeta = \frac{R_L}{2L\sqrt{\frac{1}{LC}}}} \qquad \boldsymbol{K_{V_o} = K_{inv}}$$

Comparing the system (C.20) with the general canonical form of a second order system and general canonical form of a finite zero, we obtain

$$\frac{I_o}{U} = \frac{\left(\frac{1}{LC}\right)(R_L)\left(\frac{S}{\left(\frac{R_L}{L}\right)} + 1\right)}{\left(S^2 + \frac{R_L C}{LC}S + \left(\frac{1}{LC}\right)\right)} = \frac{K_{I_o}\omega_n^2\left(\frac{S}{\omega_b} + 1\right)}{(S^2 + 2\zeta\omega_n + {\omega_n}^2)} \quad \text{(C.24)}$$

Is possible using the above expression identify characteristic dynamic parameter of the inverter output voltage with respect to the disturbance of the load current

$$K_{I_o}\omega_n^2 = \frac{R_L}{LC} \qquad \boldsymbol{\omega_b = \frac{R_L}{L}}$$

$$\boldsymbol{K_{I_o} = R_L}$$

C.2.2. Capacitor Current feedback + stationary voltage control (open-loop)

The objective of this section is to find the function equivalent to the model presented by the Figure C-1.

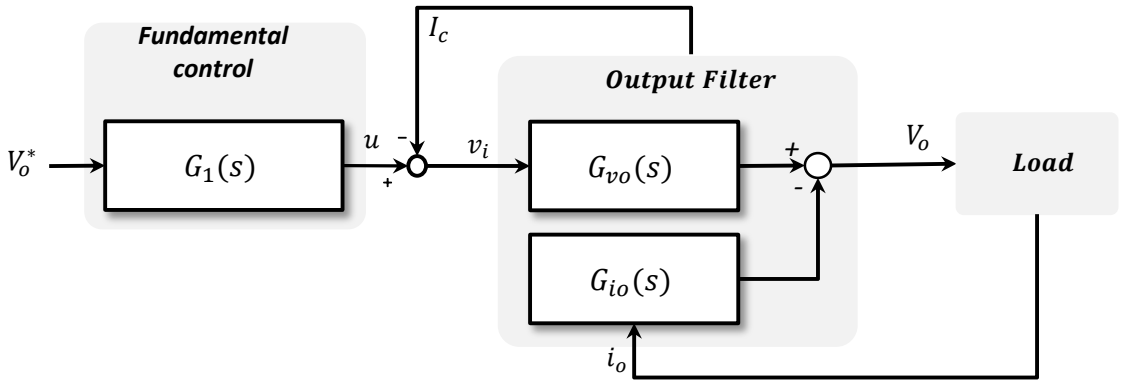

Figure C-1. stationary mathematical (openLoop) model high level bloc diagram.

Considering the P+Resonant controller and the capacitor current feedback within the input voltage expression:

$$V_i = V_o^* G_1 - I_c \tag{C.25}$$

The capacitor current in Laplace-domain can be expressed as a function of capacitor voltage:

$$I_c = CSV_o \tag{C.26}$$

Replacing the capacitor current (C.26) in the expression of voltage (C.25) we obtain

$$V_i = V_o^* G_1 - CSV_o \tag{C.27}$$

Replacing the voltage expression (C.27) in the output filter model of Figure C-1 we get:

$$V_o = \frac{K_{inv}}{(LCS^2 + RCS + 1)}(V_o^* G_1 - CSV_o) - \frac{(R + LS)}{(LCS^2 + RCS + 1)} I_o$$

$$V_o = \frac{K_{inv} G_1}{(LCS^2 + RCS + 1)} V_o^* - \frac{K_{inv} CS}{(LCS^2 + RCS + 1)} V_o - \frac{(R + LS)}{(LCS^2 + RCS + 1)} I_o$$

$$\left(\frac{LCS^2 + RCS + 1 + K_{inv} CS}{(LCS^2 + RCS + 1)}\right) V_o = \frac{K_{inv} G_2}{(LCS^2 + RCS + 1)} V_o^* - \frac{(R + LS)}{(LCS^2 + RCS + 1)} I_o$$

$$\boldsymbol{V_o = \frac{K_{inv}G_2}{LCS^2 + RCS + 1 + K_{inv}CS}V_o^* - \frac{(R + LS)}{LCS^2 + RCS + 1 + K_{inv}CS}I_o} \qquad \text{(C.28)}$$

For V_o^*:

$$V_o = \frac{K_{inv}G_2}{LCS^2 + RCS + 1 + K_{inv}CS}V_o^*$$

$$\boldsymbol{\frac{V_o}{V_o^*} = \frac{K_{inv}(K_pS^2 + 2K_iS + K_p\omega^2)}{(S^2 + \omega^2)(LCS^2 + RCS + K_{inv}CS + 1)}} \qquad \text{(C.29)}$$

For I_o:

$$V_o = \frac{(R + LS)}{LCS^2 + RCS + 1 + K_{inv}CS}I_o$$

$$\boldsymbol{\frac{V_o}{I_o} = -\frac{(R + LS)}{LCS^2 + RCS + 1 + K_{inv}CS}} \qquad \text{(C.30)}$$

C.2.3. Current capacitor feedback + stationary voltage control (close-loop)

The objective of this section is to find the function equivalent to the model presented by Figure C-2.

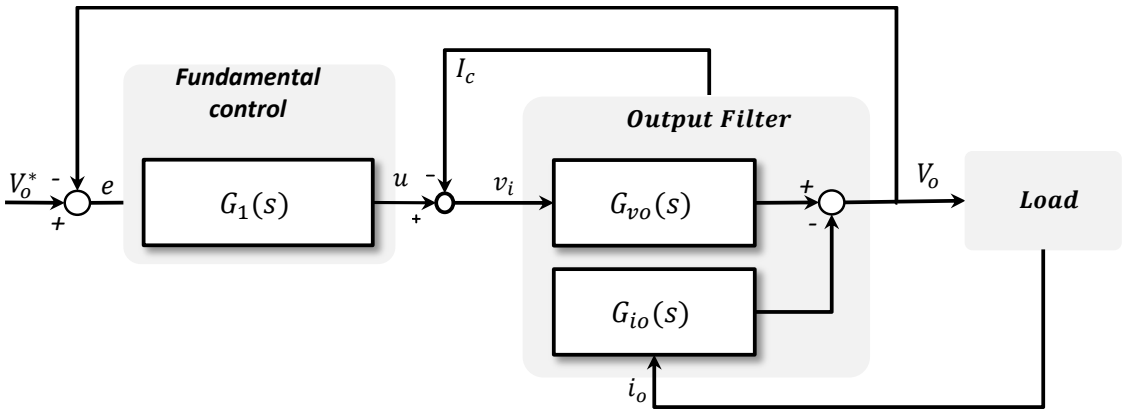

Figure C-2. stationary mathematical (closeLoop) model high level bloc diagram.

Considering the P+Resonant controller, the capacitor current feedback and the output voltage feedback within the input voltage expression

$$V_i = (V_o^* - V_o)G_1 - I_c \tag{C.31}$$

Replacing the capacitor current (C.26) in the expression of voltage (C.31) we obtain

$$V_i = (V_o^* - V_o)G_1 - CSv_o \tag{C.32}$$

Replacing the voltage expression (C.32) in the output filter model of Figure C-2 we get:

$$V_o = \frac{K_{inv}}{(LCS^2 + RCS + 1)}\left((V_o^* - V_o)G_1 - CSv_o\right) - \frac{(R + LS)}{(LCS^2 + RCS + 1)}I_o$$

$$(LCS^2 + RCS + CSK_{inv} + 1 + G_1K_{inv})V_o = K_{inv}G_1V_o^* - (R + LS)I_o$$

$$\boldsymbol{V_o = \frac{K_{inv}G_1}{(LCS^2 + RCS + CSK_{inv} + G_1K_{inv} + 1)}V_o^* - \frac{(R + LS)}{(LCS^2 + RCS + CSK_{inv} + G_1K_{inv} + 1)}I_o} \tag{C.33}$$

Where:

$$G_1 = \frac{K_pS^2 + 2K_iS + K_p\omega^2}{S^2 + \omega^2} \tag{C.34}$$

Replacing the transfer function of the resonant controller (C.34) in the transfer function of the closed loop system (C.33):

For $\boldsymbol{V_o^*}$

$$\frac{V_o}{V_o^*} = \frac{K_{inv}\frac{K_pS^2+2K_iS+K_p\omega^2}{S^2+\omega^2}}{\left(LCS^2 + RCS + CSK_{inv} + \frac{K_pS^2+2K_iS+K_p\omega^2}{S^2+\omega^2}K_{inv} + 1\right)}$$

$$\frac{V_o}{V_o^*} = G_{vo_{CL}}(s) = \frac{num_{vo_{CL}}(s)}{den_{vo_{CL}}(s)} \tag{C.35}$$

Where:

$$num_{vo_{CL}}(s) = \boldsymbol{K_{inv}\left(K_pS^2 + 2K_iS + K_p\omega^2\right)} \tag{C.36}$$

$$den_{vo_{CL}}(s) = \boldsymbol{CLS^4 + (K_{inv} + R)CS^3 + \left(1 + K_{inv}k_p + CL\omega^2\right)S^2} + \boldsymbol{(2k_iK_{inv} + CK_{inv}\omega^2 + CR\omega^2)S + \omega^2 + K_{inv}k_p\omega^2} \quad \text{(C.37)}$$

For I_o

$$\frac{V_o}{I_o} = \frac{(R + LS)}{(LCS^2 + RCS + CSK_{inv} + G_2K_{inv} + 1)} I_o$$

$$\frac{V_o}{I_o} = G_{io_{CL}}(s) = \frac{num_{io_{CL}}(s)}{den_{io_{CL}}(s)} \quad \text{(C.38)}$$

Where:

$$num_{io_{CL}}(s) = (R + LS)(S^2 + \omega^2) \quad \textit{(C.39)}$$

$$den_{io_{CL}}(s) = CLS^4 + (K_{inv} + R)CS^3 + \left(1 + K_{inv}k_p + CL\omega^2\right)S^2 + (2k_iK_{inv} + CK_{inv}\omega^2 + CR\omega^2)S + \omega^2 + K_{inv}k_p\omega^2 \quad \text{(C.40)}$$

C.2.4. Current capacitor feedback + stationary voltage control + Harmonic Compensators (close-loop)

The objective of this section is to find the function equivalent to the model presented by Figure C-3.

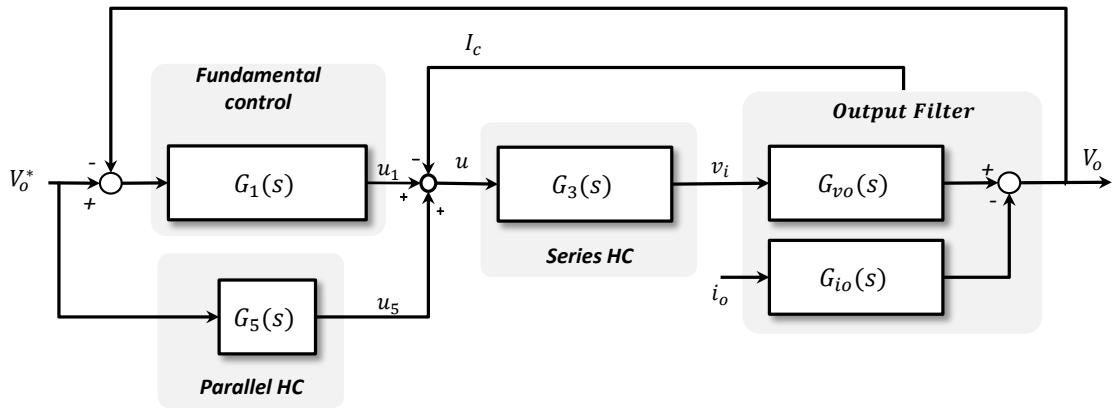

Figure C-3. stationary with harmonics (closeLoop) high level bloc diagram.

Considering the P+Resonant controller, the capacitor current feedback, the output voltage feedback and the harmonic compensators within the input voltage expression

$$V_i = \big((V_o^* - V_o)G_1 + V_o G_5 - I_c\big)G_3 \tag{C.41}$$

Replacing the capacitor current (C.26) in the expression of voltage (C.41):

$$V_i = \big((V_o^* - V_o)G_1 + V_o G_5 - CSv_o\big)G_3 \tag{C.42}$$

Replacing the voltage expression (C.42) in the output filter model of Figure C-3 we get:

$$V_o = \frac{K_{inv}}{(LCS^2 + RCS + 1)}\Big(\big((V_o^* - V_o)G_1 + V_o G_5 - CSv_o\big)G_3\Big) - \frac{(R + LS)}{(LCS^2 + RCS + 1)} I_o$$

$$V_o = \frac{K_{inv}G_1G_3}{(LCS^2 + RCS + CSK_{inv}G_3 - G_5K_{inv}G_3 + G_1K_{inv}G_3 + 1)} V_o^* - \frac{(R + LS)}{(LCS^2 + RCS + CSK_{inv}G_3 - G_5K_{inv}G_3 + G_1K_{inv}G_3 + 1)} I_o \tag{C.43}$$

Where:

$$G_3 = \frac{S^2 + K_{R3}S + 3^2\omega^2}{S^2 + 3^2\omega^2} \tag{C.44}$$

$$G_5 = \frac{K_{R5}S}{S^2 + 5^2\omega^2} \tag{C.45}$$

Replacing the transfer function (C.34), (C.44) and (C.45) in the transfer function of the closed loop system (C.43):

For V_o^*

$$\frac{V_o}{V_o^*} = G_{vo_{CL}}(s) = \frac{num_{Vo}(s)}{den_o(s)} \tag{C.46}$$

Where:

$$num_{Vo}(s) = K_{inv}\Big(K_pS^6 + \big(2K_i + k_pK_{r3}\big)S^5 + \big(35k_p\omega^2 + 2k_ik\_r3\big)S^4 + \big(68k_i + 26k_pk_{r3}\big)\omega^2S^3 + \big(259k_p\omega^2 + 50k_ik_{r3}\big)\omega^2S^2 + \big(450k_i + 25k_pK_{r3}\big)\omega^4S + \big(225k_p\omega^6\big)\Big) \quad \text{(C.47)}$$

$$den_{Vo}(s) = LCS^8 + (k_{inv} + Rl)CS^7 + \big(35CL\omega^2 + K_{inv}k_p + CK_{inv}k_{r3} + 1\big)S^6 + \Big(2k_i - k_{r5} + k_pk_{r3} + 35C\omega^2 + \frac{35CR\omega^2}{K_{inv}}\Big)K_{inv}S^5 + \big(35\omega^2 + 2K_{inv}k_ik_{r3} - K_{inv}k_{r3}k_{r5} + 259CL\omega^4 + 35K_{inv}k_p\omega^2 + 26CK_{inv}k_{r3}\omega^2\big)S^4 + \Big(259C\omega^2 + \frac{259CR\omega^2}{K_{inv}} + 68k_i - 10k_{r5} + 26k_pk_{r3}\Big)K_{inv}\omega^2S^3 + \big(259\omega^4 + 225CL\omega^6 + 259K_{inv}k_p\omega^4 + 25CK_{inv}k_{r3}\omega^4 + 50K_{inv}k_ik_{r3}\omega^2 - K_{inv}k_{r3}k_{r5}\omega^2\big)S^2 + \big(225CK_{inv}\omega^6 + 225CR\omega^6 + 450K_{inv}k_i\omega^4 - 9K_{inv}k_{r5}\,\omega^4 + 25K_{inv}k_pk_{r3}\omega^4\big)S + \big(225\omega^6 + 225K_{inv}k_p\omega^6\big) \quad \text{(C.48)}$$

For I_o

$$\frac{V_o}{I_o} = G_{io}(s) = \frac{num_{Io}(s)}{den_{Io}(s)} \quad \text{(C.49)}$$

Where:

$$num_{Io}(s) = LS^7 + RS^6 + 35L\omega^2S^5 + 35R\omega^2S^4 + 259L\omega^4S^3 + 259R\omega^4S^2 + 225L\omega^6S + 225R\omega^6 \quad \text{(C.50)}$$

$$den_{Io}(s) = den_{Vo} \quad \text{(C.51)}$$